CREATING LONG-RANGE HYDROPHOBIC FORCES BY COADSORPTION OF IONIC AND NEUTRAL SURFACTANTS

by

Ravishankar S.A.

Dissertation submitted to the Faculty of the

Virginia Polytechnic Institute and State University

in partial fulfillment of the requirements for the degree of

Doctor of Philosophy

in

Materials Engineering Science

APPROVED:

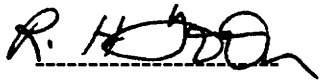

Dr. Roe-Hoan Yoon (chairman)

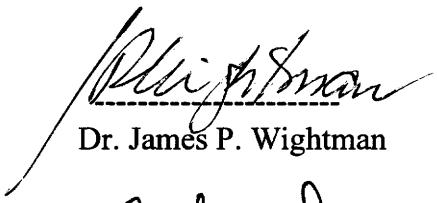

Dr. James P. Wightman

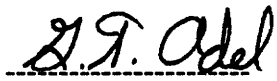

Dr. Gregory T. Adel

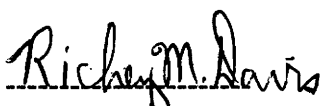

Dr. Richey M. Davis

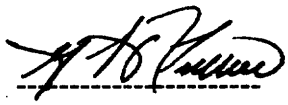

Dr. Gerald H. Luttrell

May, 1995

Blackburg, Virginia

CREATING LONG-RANGE HYDROPHOBIC FORCES BY COADSORPTION OF IONIC AND NEUTRAL SURFACTANTS

by

Ravishankar S.A.

Chairman: Dr. Roe-Hoan Yoon
Materials Engineering Science

ABSTRACT

A Mark IV surface force apparatus was used to measure surface forces between mica surfaces in dodecylamine hydrogenchloride (DAHCl) solutions at pH 5.7 in the presence and absence of long-chain alcohols. With DAHCl alone, only "short-range" hydrophobic forces were observed with decay lengths of 1.2-1.4 nm. In the presence of octanol, long range hydrophobic forces were observed with decay lengths in the range of 2.0-6.8 nm. In the presence of dodecanol, the decay length became as large as 9.0 nm, which represents the strongest ever recorded hydrophobic force with soluble single-chain surfactants. The appearance of the long-range hydrophobic forces in the presence of neutral surfactants can be attributed to the coadsorption mechanism, in which neutral surfactant molecules adsorb along with dodecylammonium (DAH^+) ions on mica to form close-packed monolayers.

Long-range hydrophobic forces were also measured between mica surfaces in DAHCl solutions at pH 9.5, at which considerable amount of neutral amine (DA) is produced as a result of hydrolysis. The force measurements exhibit long-range hydrophobic forces with decay length of 5.5 nm. Appearance of the long-range hydrophobic force at this pH can be attributed to the coadsorption of DA and DAH^+ on mica. The pH where the long-range hydrophobic force appears corresponds to the pH of maximum flotation of quartz, which suggests that long-range hydrophobic force may be required for good flotation.

The force measurements conducted at 10.1 show that phase-separated amine is formed on the mica surface at a 50-times lower concentration than for the bulk precipitation. Above this concentration, the mica surfaces do not jump into contact with each other, suggesting that the phase-separated amine renders the surface hydrophilic. Furthermore, the force measurements conducted at pH 10.1 show repulsive steric forces, which become stronger with increasing DAHCl concentration. The adhesion force between mica surfaces becomes zero when surface precipitation occurs, while water contact angle is less sensitive.

Hydrophobic force increases sharply when advancing water contact angle (θ_a) is greater than 90°, which may be attributed to the formation of domains of close-packed monolayers of hydrocarbon chains. The domains may acquire large dipole moments, which correlate with those of the opposing surface to give rise to long-range hydrophobic forces. Alternatively, microscopic cavitation may occur on the domain, whose

microscopic contact angle may be greater than 90° to satisfy the thermodynamic requirement for cavitation

ACKNOWLEDGMENTS

I am deeply grateful to my advisor, Dr. Roe-Hoan Yoon, for his valuable guidance, uncountable suggestions and criticisms, constant inspiration and support through out this work.

Special thanks to Dr. Yakov I. Rabinovich for helpful discussions. Thanks are also due to Dr. David A. Guzonas for teaching me the direct force measurement technique and Dr. Zhenghe Xu for helping me out in setting up the surface force laboratory. I would like to thank my other committee members Dr. James P. Wightman, Dr. Richey M. Davis, Dr. Greg T. Adel, Dr. Gerald H. Luttrell and for their constructive comments.

The financial support of the U.S. Department of Energy (Contract DE-AC22-90PC90174) is gratefully acknowledged.

Special appreciation is given to surface force group B. Suha Aksoy, Vivek Subramanian, and Darrin H. Flinn for their assistance, friendship and support. Very special thanks are due to Keith Kutz, Alisa Alls, Roy Hill and Marchel Doerr for being extremely supportive and helpful.

I would like to extend my thanks to Wayne Slusser and Jim Overfelt for their technical assistance. I would also like to thank to Neeraj Mendiratta, Rajesh Pazhianur and all other graduate students at Holden Hall and Plantation road laboratory for their friendship and company when I work during late hours.

Last, but not the least, I would like to express my sincere appreciation to the two most important people, my wife Shobana and my daughter Akshaya, for their immense understanding, unconditional love and support.

TABLE OF CONTENTS

CHAPTER 1 INTRODUCTION 1

1.1 General 1

1.2 Literature review 5

1.2.1 Hydrophobic interaction 5

1.2.2 Direct measurement of hydrophobic forces 6

1.2.3 Hydrophobic force 11

1.2.3.1 Short-and long-range hydrophobic forces 11

1.2.3.2 Origin of hydrophobic force 13

1.2.3.3 Effect of electrolytes 18

1.2.3.4 Effect of temperature 19

1.2.3.5 Effect of dissolved gases 20

1.2.3.6 Effect of solvent 21

1.2.3.7 Interaction between hydrophilic and hydrophobic surfaces 21

1.2.4 Extended DLVO theory 22

1.2.5 Hydrophobic force measurements for amine surfactant systems 23

1.2.6 Amine flotation 27

1.2.6.1 Coadsorption 27

1.2.6.2 Contact angle and flotation 29

1.3 Research Objectives 30

1.4 Report Organization 31

1.5 References 33

CHAPTER 2 EFFECT OF OCTANOL ON THE LONG-RANGE HYDROPHOBIC FORCES BETWEEN DODECYLAMINE-COATED MICA SURFACES

2.1 Introduction 43

2.2 Experimental 47

2.2.1 Materials 47

2.2.2 Surface Forces Measurements 48

2.2.3 Contact Angle Measurements 49

2.2.4 Flotation Experiments 50

2.3 Results 50

2.3.1 Direct Force Measurements 50

2.3.2 Contact Angle Measurements 63

2.3.3 Flotation Results 65

2.4 Discussion 67

2.5 Conclusions 81

2.6 References 83

CHAPTER 3 LONG-RANGE HYDROPHOBIC FORCES BETWEEN DODECYLAMINE-COATED MICA SURFACES IN THE PRESENCE OF DODECANOL

3.1 Introduction 88

3.2 Experimental 93

3.2.1 Materials 93

3.2.2 Surface Forces Measurements 93

3.2.3 Contact Angle Measurements 95

3.3 Results 95

3.3.1 Direct Force Measurements 95

3.3.2 Advancing and Receding Angles 118

3.4 Discussion 119

3.5 Summary and Conclusions 136

3.6 References 138

CHAPTER 4 EFFECT OF pH ON THE HYDROPHOBIC FORCES BETWEEN DODECYLAMINE-COATED MICA SURFACES

4.1 Introduction 143

4.2 Experimental 147

4.2.1 Materials 147

4.2.2 Surface Forces Measurements 147

4.2.3 Contact Angle Measurements 148

4.3 Results 149

4.4 Discussion 166

4.5 Conclusions 176

4.6 References 178

CHAPTER 5 SUMMARY AND CONCLUSIONS 182

CHAPTER 6 RECOMMENDATIONS FOR FUTURE RESEARCH 187

LIST OF FIGURES

Figure 1.1 Schematic diagram of surface force apparatus Mark IV. 7

Figure 1.2 Schematic diagram of modified atomic force microscopy. 10

Figure 1.3 D_2 vs. advancing angle (θ_a) plot for mica surfaces coated with DAHCl, DDOAB (hollow triangles), and ODTCS (filled circles) at pH 5.7. Note that the medium range hydrophobic decay lengths D_2 ≈3-10 nm are missing. 26

Figure 1.4 Correlation between contact angle, adsorption density, zeta-potential and flotation recovery of quartz (98). 28

Figure 2.1 *F/R* vs. *H* between mica surfaces in various DAHCl solutions at pH 5.7. The upper and lower dotted curves represent the constant charge and constant potential models, respectively, of the DLVO theory obtained using A_{131}=2.2x10^{-20} J, Ψ_o=-170 mV and κ^{-1}=96.0 nm for Nanopure water; -125 mV and 76.1 nm at 10^{-6} M DAHCl; and -35 mV and 68.0 nm at 5x10^{-6} M DAHCl. The arrows

represent the distance at which the two surfaces jump into contact due to attractive forces. 51

Figure 2.2 *F/R* vs. *H* between mica surfaces in 10^{-6} M DAHCl with and without ethanol at pH 5.7. The upper and lower curves represent the constant charge and constant potential models, respectively, of the DLVO theory obtained using A_{131}=2.2x10^{-20} J, Ψ_o=-125 mV and κ^{-1}=76.1 nm. The arrow shows the jump distance. 55

Figure 2.3 Effect of octanol on the *F/R* vs. *H* curves obtained with mica surfaces at pH 5.7. The upper and lower curves represent the constant charge and constant potential models, respectively, of the DLVO theory obtained using A_{131}=2.2x10^{-20} J, Ψ_o=-170 mV and κ^{-1}=96.0 nm. The arrow shows the jump distance. 56

Figure 2.4 *F/R* vs. *H* between mica surfaces in 10^{-6} M DAHCl solutions with varying amounts of octanol at pH 5.7. The upper and lower curves represent the constant charge and constant potential models, respectively, of the DLVO theory obtained using A_{131}=2.2x10^{-20} J, Ψ_o=-125 mV and κ^{-1}=76.1 nm without octanol; Ψ_o=-70 mV and κ^{-1}

^{1}=76.1 nm with 10^{-7} M octanol; and -70 mV and 76.1 nm at 10^{-6} M octanol. The arrows show the jump distance. 57

Figure 2.5 *F/R* vs. *H* between mica surfaces in $5x10^{-6}$ M DAHCl solutions with varying amounts of octanol at pH 5.7. The upper and lower curves represent the constant charge and constant potential models, respectively, of the DLVO theory obtained using A_{131}=$2.2x10^{-20}$ J, Ψ_o=-35 mV and κ^{-1}=68.0 nm without octanol; Ψ_o=0 mV at $5x10^{-7}$ M octanol; and Ψ_o=+45 and κ^{-1}=68 nm at $5x10^{-6}$ M octanol. The arrows show the jump distance. 58

Figure 2.6 *F/R* vs. *H* between mica surfaces at 10^{-5} M DAHCl and pH 5.7 with and without octanol. In the absence of octanol, Ψ_o becomes zero, but at 10^{-6} M octanol large repulsive force is observed, indicating a charge reversal; the force curve can be fitted with Ψ_o=+350 mV and κ^{-1}=43 nm. This repulsive force is larger than in Nanopure water, which can be fitted with Ψ_o=-170 mV and κ^{-1}=96 m. The arrows shows the jump distance. 61

Figure 2.7 *F/R* vs. *H* curves between mica surfaces in solutions containing both DAHCl and octanol at pH 5.7. At $5x10^{-6}$ M DAHCl and

$5x10^{-5}$ M octanol, large repulsive forces which cannot be explained by the Poisson-Boltzmann equation are observed; but the force measurement shows no hysteresis. At higher DAHCl and octanol concentrations, larger steric forces are observed and the measurements exhibit hysterisis; the hysteresis becomes more significant 24 hours after octanol addition. 62

Figure 2.8 Floatability of silica in DAHCl and octanol solutions at pH 5.7. 66

Figure 2.9 Schematic representation for the adsorption of DA^+ ions and octanol molecules on mica. 72

Figure 2.10 V_t vs. H between mica surfaces in $5x10^{-6}$ M of DAHCl and varying concentration of octanol at pH 5.7. The dotted and solid lines represent the classical and extended DLVO fits, respectively. The hydrophobic force parameters are as follows: C_1=-50 mN/m and D_1=1.4 nm at $5x10^{-6}$ M DAHCl; C_1=-50 mN/m, C_2=-0.5 mN/m, D_1=1.2 nm and D_2=6.8 nm at $5x10^{-6}$ M DAHCl and $5x10^{-7}$ M octanol; C_1=-50 mN/m, C_2=-0.5 mN/m, D_1=1.2 nm and D_2=4.0 nm at $5x10^{-6}$ M DAHCl and $5x10^{-6}$ M octanol. 77

Figure 2.11 Normalized force gradient vs. H between mica surfaces in $5x10^{-6}$ M DAHCl and $5x10^{-7}$ M octanol at pH 5.7. The squares represent the data obtained using the gradient method, while the circles represent the data obtained using the equilibrium method. The solid line represents an extended DLVO fit incorporating a double exponential function for the hydrophobic force (Eq. [8]): A_{131}=2.2x10^{-20} J, C_1=-40 mN/m, C_2=-0.5 mN/m, D_1=1.2 nm, and D_2=6.8 nm. The dashed line represents an extended DLVO fit with power law representing the hydrophobic force: K=-1.0x10^{-19} J. Also shown for comparison are the normalized force gradients for the nonretarded van der Waals force and for the mica surfaces coated with soluble (DAHCl and CTAB) and insoluble (DDOAB) surfactants. The soluble surfactants without octanol show only the short-range hydrophobic force. 80

Figure 3.1 F/R *vs.* H between mica surfaces with and without dodecanol solutions at pH 5.7. The upper and lower curves (dotted lines) represent the constant charge and constant potential models of the DLVO theory, respectively. The DLVO theoretical curves were obtained using A_{131}=2.2x10^{-20} J, Ψ_o=-170 mV and κ^{-1}=96.0 nm for Nanopure water and $5x10^{-5}$ M dodecanol. The arrows represent

the distance at which the two surfaces jump into contact due to attractive forces. 96

Figure 3.2 *F/R vs. H* between mica surfaces in 10^{-6} M DAHCl with and without ethanol at pH 5.7. The upper and lower curves (dotted lines) represent the constant charge and constant potential models, respectively, of the DLVO theory obtained using A_{131}=2.2x10^{-20} J, Ψ_o=-125 mV and κ^{-1}=76.1 nm. The arrow shows the jump distance. 98

Figure 3.3 *F/R vs. H* between mica surfaces in 10^{-6} M DAHCl solutions with varying amounts of dodecanol at pH 5.7. The upper and lower curves (dotted lines) represent the constant charge and constant potential models, respectively, of the DLVO theory obtained using A_{131}=2.2x10^{-20} J, Ψ_o=-125 mV and κ^{-1}=76.1 nm without dodecanol; Ψ_o=-70 mV and κ^{-1}=76.1 nm with 10^{-7} M dodecanol; and -70 mV and 76.1 nm at 10^{-6} M dodecanol. The arrows show the jump distance. 99

Figure 3.4 *F/R vs. H* between mica surfaces in 5x10^{-6} M DAHCl solutions with varying amounts of dodecanol at pH 5.7. The upper dotted

line (dotted line) represents the constant charge model of the DLVO theory obtained using A_{131}=2.2x10^{-20} J, Ψ_o=-35 mV and κ^{-1}=68.0 nm without dodecanol and the lower dotted line indicate the van der Waals force with Ψ_o=0 mV and A_{131}=2.2x10^{-20} J at 1x10^{-7} M and 5x10^{-6} M dodecanol. Note that the attractive forces measured in the presence of dodecanol is much stronger than the van der Waals forces, suggesting that there is long-range hydrophobic force. The arrows show the jump distance. 103

Figure 3.5 V_t *vs.* H between mica surfaces in 5x10^{-6} M of DAHCl and varying concentration of dodecanol at pH 5.7. The energy vs distance profiles are fitted using classical (solid lines) and extended DLVO theory including hydrophobic force described by double-exponential form (Eq. [2]; dotted lines) and power law function (Eq. [3]; dashed lines). The hydrophobic force parameters for the double exponential form are as follows: C_1=-50 mN/m and D_1=1.4 nm at 5x10^{-6} M DAHCl; C_1=-50 mN/m, C_2=-1.2 mN/m, D_1=1.2 nm and D_2=6.9 nm at 5x10^{-6} M DAHCl and 1x10^{-7} M dodecanol; C_1=-50 mN/m, C_2=-1.2 mN/m, D_1=1.2 nm and D_2=9.0 nm at 5x10^{-6} M DAHCl and 5x10^{-7} M dodecanol. The power law fitting

coefficients are found to be $1.5x10^{-19}$ and $3.3x10^{-19}$ J when the dodecanol concentrations are, respectively, $1x10^{-7}$ and $5x10^{-7}$ M. 106

Figure 3.6 Normalized force gradient vs. H between mica surfaces in $5x10^{-6}$ M DAHCl and $5x10^{-7}$ M dodecanol at pH 5.7. The solid line represents an extended DLVO fit incorporating a double-exponential function for the hydrophobic force (Eq. [9] and [12]): A_{131}=2.2x10^{-20} J, C_1=-45 mN/m, C_2=-1.2 mN/m, D_1=1.3 nm, and D_2=9.0 nm. The broken line represents an extended DLVO fit with power law representing the hydrophobic force (Eq. {9] and [13]): K=3.3x10^{-19} J. Shown for comparison are the normalized force gradients for the nonretarded van der Waals force (upper dashed line). Also indicated are the force gradients obtained with the mica surfaces coated with soluble DAHCl and CTAB (solid straight line) and the double exponential fit obtained for the force gradients data using insoluble (DDOAB) surfactants (lower dashed line) and DAHCl/octanol mixed monolayer (dotted line) (14). The DAHCl and dodecanol mixed monolayers show stronger hydrophobic forces compared to pure DAHCl/octanol mixed monolayers. 108

Figure 3.7 *F/R vs. H* between mica surfaces at $5x10^{-6}$ M DAHCl and $5x10^{-7}$ M dodecanol with and without 10^{-4} M KCl at pH 5.7. In the absence of KCl, the forces are net attractive with Ψ_o = 0 mV. In the presence of $1x10^{-4}$ M KCl, however, the attractive forces are reduced considerably and a weak repulsive force is observed. The dotted line represents the constant charge model of the DLVO fit with Ψ_o = 10 mV, κ^{-1}=33.3 nm and A_{131}=$2.2x10^{-20}$ J. The solid line represent the extended DLVO fit to the force curve in the presence of $1x10^{-4}$ M KCl using C_1=-10 mN/m, C_2=-0.35 mN/m, D_1=1.2 nm, and D_2=4.5 nm. The arrows shows the jump distance. Note that the jump distance in the presence of electrolyte is reduced considerably. 113

Figure 3.8 Normalized force gradient vs. *H* between mica surfaces in $5x10^{-6}$ M DAHCl, $5x10^{-7}$ M dodecanol, and $1x10^{-4}$ M KCl at pH 5.7 (triangles). The solid line represents an extended DLVO fit incorporating a double exponential function for the hydrophobic force (Eq. [9] and [13]): A_{131}=$2.2x10^{-20}$ J, C_1=-10 mN/m, C_2=-0.5 mN/m, D_1=1.1 nm, and D_2=4.5 nm. Also shown for comparison are the normalized force gradients for the nonretarded van der Waals force (dashed line) and for the DAHCl/dodecanol mixture

with double exponential fit (solid lines). The presence of electrolyte reduces the hydrophobic force. 115

Figure 3.9 *F/R vs. H* between mica surfaces in the presence of $5x10^{-6}$ M DAHCl and varying concentrations of dodecanol at pH 5.7. At $5x10^{-6}$ M DAHCl and $5x10^{-6}$ M dodecanol, electrical repulsive forces reappeared, indicating a charge reversal. The force curve can be fitted with Ψ_o=+90 mV and κ^{-1}=43 nm, C_1=-40 mN/m, C_2=-1.0 mN/m, D_1=1.2 nm, and D_2=2.5 nm.. With further increase in dodecanol to 10^{-5} M, large repulsive force which cannot be explained by the Poisson-Boltzman equation are observed. The force measurements showed hysteresis. The arrows shows the jump distance. 117

Figure 3.10 Long-range decay lengths D_2 *vs.* advancing angle (θ_a) plot obtained for DAHCl, DAHCl/octanol, DAHCl/dodecanol mixtures (squares) in the presence mica surfaces, DDOAB coated mica surfaces (triangles) and ODTCS coated silica (circles) at pH 5.7. Note that there is a sharp increase in the decay lengths D_2 from short- to long-range hydrophobic force when θ_a= 90°. 124

Figure 4.1. *F/R vs. H* between mica surfaces in various DAHCl solutions at pH 5.7. The upper and lower dotted curves represent the constant charge and constant potential models, respectively, of the DLVO theory obtained using A_{131}=2.2x10^{-20} J, Ψ_o=-170 mV and κ^{-1}=96.0 nm for Nanopure water; -125 mV and 76.1 nm at 10^{-6} M DAHCl; and -35 mV and 68.0 nm at 5x10^{-6} M DAHCl. The arrows represent the distance at which the two surfaces jump into contact due to attractive forces. 150

Figure 4.2. *F/R vs. H* between mica surfaces in 10^{-6} M DAHCl solutions at various pHs. The upper and lower dotted curves represent the constant charge and constant potential models, respectively, of the DLVO theory obtained using A_{131}=2.2x10^{-20} J, Ψ_o=-170 mV and κ^{-1}=96.0 nm for Nanopure water; -125 mV and 76.1 nm at 10^{-6} M DAHCl in pH range from 5.7 to 9.5; and -35 mV and 68.0 nm at 10^{-6} M DAHCl at pH 10.1. The arrows represent the distance at which the two surfaces jump into contact due to attractive forces. 153

Figure 4.3. *F/R vs. H* between mica surfaces in various DAHCl solutions at pH 10.1. The upper and lower dotted curves represent the constant charge model of the DLVO theory obtained using Ψ_o=-75 mV and

κ^{-1}=68.0 nm for 10^{-7} M and -35 mV and 68.1 nm at 10^{-6} , -20mV and 68.1 nm for $2x10^{-6}$ M DAHCl, and -10mV and 68.1 nm for $5x10^{-6}$ M. The theoretical DLVO curves include dispersion force calculated using A_{131}=2.2x10^{-20} J. The arrows represent the distance at which the two surfaces jump into contact due to attractive forces. The dashed lines are the extraneous repulsive forces that are stronger than the DLVO forces due to steric force created by the polymeric and surface precipitates. At $5x10^{-6}$ M DAHCl, the contact thickness is about 7 nm, suggesting a thick layer (3-4 nm) of surfactant on the mica surfaces. 155

Figure 4.4. *F/R vs. H* between mica surfaces in $3x10^{-6}$ M DAHCl solutions at pH 5.7 and 9.5. The upper and lower dotted curves represent the constant charge and constant potential models, respectively, of the DLVO theory obtained using A_{131}=2.2x10^{-20} J, Ψ_o=-75 mV and κ^{-1}=68.0 nm at $3x10^{-6}$ M DAHCl for pH 5.7 and 9.5. The arrows represent the distance at which the two surfaces jump into contact due to attractive forces. Note that the jump distance at pH 9.5 is larger than the that observed at pH 5.7. At pH 5.7, the data can be fitted only with a short-range hydrophobic force (Eq. 1) with D_0=1.2 nm. However, with the increase of pH from 5.7 to 9.5, it is

necessary the use of the double-exponential form [Eq. 2] with C_1=-40 mN/m, C_2=-0.5 mN/m, D_1=1.2 nm, and D_2=5.5 nm, suggesting the presence of long-range hydrophobic force. 158

Figure 4.5. The pull-off between mica surfaces in DAHCl solutions at varying pH. *F(0)/R* represents the pull-off force needed to separate the surfaces in contact. The adhesion force values denoted by squares and diamonds are measured in the present work at 10^{-6} and $3x10^{-6}$ M DAHCl solution, respectively. The shaded region are the measurements made by Rutland *et al.* (12) at 10^{-4} M of DAHCl. Note that the pull-off forces almost remain constant in the pH range from 5.7 to 9.5 and drops dramatically with further increase to 10.1. 160

Figure 4.6. The pull-off forces and contact angle data at different concentration of DAHCl solutions at pH 5.7. A point of inflection is obtained at p.c.r. (10^{-5} M DAHCl). A sharp decrease in adhesion force and contact angle above $3x10^{-3}$ M DAHCl concentration is due to micellar adsorption at the surface. 162

Figure 4.7. The pull-off forces and contact angle data at different concentration of DAHCl solutions at pH 10.1. The adhesion forces remain zero above $1x10^{-6}$ M DAHCl due to the adsorption of polymeric and surface precipitation species. The vertical dotted line indicates the various range of concentration in which polymeric preprecipitate, surface precipitates and bulk precipitates are formed. 164

Figure 4.8. Correlation between long-range hydrophobic force parameter (D_2) measured between mica surfaces in the presence of DAHCl, contact angles obtained on quartz in the presence of $4x10^{-5}$ M DAHCl, and flotability of quartz in the presence of $4x10^{-5}$ M DAHCl. An excellent correlation between the force measurements and the flotation data suggest that long-range hydrophobic forces may be required for good flotation. 173

LIST OF TABLES

Table 2.1. Results of surface force measurements with dodecylamine hydrochloride at pH 5.7. 53

Table 2.2. Results of surface force measurements with dodecylamine hydrochloride and octanol at pH 5.7. 59

Table 2.3. Results of advancing and receding angles. 64

Table 3.1. Results of surface force and contact angle measurements with dodecylamine hydrochloride in the presence of octanol and dodecanol at pH 5.7. 101

Table 4.1. Results of surface force and contact angle measurements with dodecylamine hydrochloride at pH 5.7. 151

Table 4.2. Results of surface force studies with dodecylamine hydrogenchloride at different pHs. 165

CHAPTER 1 INTRODUCTION

1.1 General

Fine particle technologies such as flotation are widely used by mineral industries for separating valuable minerals from waste materials. In froth flotation, air bubbles are introduced in an aqueous slurry of minerals to collect the selectively hydrophobized particles and remove them from the pulp (1). Since the introduction of froth flotation in mineral industry at the turn of the century, the technology continues to evolve and finds new applications in recycling, environmental remediation, food processing, *etc.* (2-4). Despite its widespread application, no comprehensive model based on first principles has yet been developed. The lack of such a model presents difficulty in the control, design, and optimization of various flotation processes (5).

Most of the early research efforts in flotation were concerned with the chemistry and mode of adsorption of the collectors, frothers, and other additives at the surface of minerals (6-8). Many investigators (9-11) studied the effects of particle size on flotation and found that the conventional flotation machines are effective only in a narrow particle size range, e.g., 10-100 mm, and that the flotation selectivity deteriorates rapidly with decreasing particle size (12). Hydrodynamic studies of bubble-particle interactions showed that the difficulty in floating fine particles is due to the low probability of bubble-

particle collision, while the problem of coarse particle flotation is caused by the high probability of bubble-particle detachment. Much attention has been paid in the last twenty years to improve the flotation of fine particles. Many models describing flotation processes show that the fine particle flotation can be improved by decreasing the bubble size (13-20) and/or increasing the energy dissipation (21), both of which are designed to improve the hydrodynamics of bubble-particle interaction. However, it is envisaged that the understanding the hydrodynamics of bubble-particle interaction alone is not sufficient to accurately model flotation processes and find ways of making appropriate improvements. Since the bubble-particle interaction is essentially a heterocoagulation process, it is necessary that surface forces be considered in modeling flotation.

When two macroscopic bodies interact with each other, they feel the presence of each other by way of surface forces when they are within a certain distance. According to the continuum theory, surface forces arise from the summation of all the interatomic (or intermolecular) forces over the entire surface areas of the interacting macroscopic bodies involved across an intervening medium. In classical colloid chemistry, two surface forces are considered, namely, the electrostatic force between two interacting electrical double layers and the London-van der Waals dispersion force. By considering these two surface forces, Derjaguin and Landau (22) and Verwey and Overbeek (23) independently developed a model for predicting the stability of lyophobic colloidal suspensions. Their theoretical treatment is generally referred to as DLVO theory, which is a landmark

accomplishment in colloid chemistry. The first attempt to model bubble-particle interactions using surface forces was made in 1961 by Derjaguin and Duhkin (24). They considered that a particle must pass through three distinct zones, i.e., hydrodynamic, diffusio-phoretic and wetting zones, around a bubble before adhesion can take place. Once the particle enters the wetting zone, it is subjected to three surface forces, namely van der Waals force, electrostatic force, and structural force. While the forces considered in the DLVO theory are based on the continuum theory, there may be surface forces of structural origin. However, these authors considered the structural force to be repulsive, which becomes zero when bubble-particle adhesion is to occur. In 1979, Derjaguin and Duhkin (25) again attempted modeling bubble-particle interactions using surface forces. However, the model considered only the DLVO forces, i.e., electrostatic and van der Waals forces. As a result, their model can explain the bubble-particle adhesion at the secondary minimum, which may be applicable only to inertialess fine particles.

More recently, Xu and Yoon (26,27) have studied the stability of hydrophobic particle suspensions, and have found that the DLVO theory is inadequate. Therefore, they developed an extended DLVO theory, which includes a term representing contributions from the hydrophobic force in addition to those from the electrostatic and van der Waals forces. The extended DLVO theory was also applied to describing bubble-particle interactions, in which the hydrophobic force is the only driving force for adhesion under most flotation conditions (28-31). In modeling bubble-particle

interactions using the extended DLVO theory, Yoon and his coworkers (30,31) assumed that the hydrophobic force operating between the surfaces of bubble and particle is of long-range and used a value of 10.6 nm as the decay length. In other cases, they back-calculated the hydrophobic force using the extended DLVO theory on the basis of the critical film rupture thickness measured experimentally. The decay length of the back-calculated hydrophobic force was 13.6 nm (28,29), which also suggested that bubble-particle interaction is controlled by long-range hydrophobic forces.

It is the purpose of the present work to directly measure hydrophobic forces using the surface force apparatus developed by Israelachivili (32). However, this apparatus has limitations in that the surface has to be molecularly smooth, transparent and isometric. Therefore, the measurements are conducted using freshly cleaved mica surfaces. The surfactant chosen for the study is dodecylammonium chloride, which is one of the most frequently used reagents for hydrophobizing minerals. The data obtained in the direct force measurements will be compared with the flotation and other surface chemistry data available in the literature. The results will be useful in determining the role of hydrophobic forces in flotation.

1.2 Literature Review

1.2.1 Hydrophobic interaction

The hydrophobic effect, or the attraction between small nonpolar solute molecules in aqueous solutions, is one of the most important phenomena in driving the self-assembly of amphiphilic molecules into micelles, vesicles and bilayers (33-35). It also plays a major role in determining the conformation of proteins and biological species in water (36). Hydrophobic solutes tend to minimize the contact of their hydrophobic regions with water either by aggregating or adjusting their conformation. The hydrophobic effect is important in a wide range of phenomena, such as adhesion, wetting, cavitation, and rapid coagulation of hydrophobic particles. Many industrial technologies take advantage of the destabilization of aqueous colloidal suspensions when macroscopic surfaces of the particles are rendered hydrophobic in nature. While hydrophobic interaction between nonpolar solutes in aqueous solution is considered to be "short ranged", the situation is surprisingly different for the interaction between hydrophobic macroscopic bodies (37,38). Long-range attraction, which is considerably larger than the van der Waals interaction, is found to exist between these macroscopic hydrophobic surfaces.

1.2.2 Direct measurement of hydrophobic forces

The first set of measurements of hydrophobic forces between macroscopic surfaces were carried out by Israelachvili and Pashley (37,39) in 1982 using a surface force apparatus (SFA) which was originally developed by Tabor's group in England. Initially, they used this apparatus to measure the van der Waals force between mica surfaces in air or vacuum (40). Following Tabor's work, Israelachvili and Adams in Australia in 1978 (32) designed an apparatus to measure forces between mica surfaces immersed in a liquid or vapor medium. They showed experimental force *vs.* distance profiles between two mica surfaces in the presence of dilute 1:1 and 2:1 electrolyte solutions and compared their results with the theoretical DLVO forces. The agreement is remarkably good at all separations, indicating that the DLVO theory is basically sound. Currently, the Israelachvili-type apparatuses are in wide use for studying various phenomena such as wetting, adhesion, friction and lubrication studies in a liquid medium.

Fig. 1.1 shows the schematic diagram of SFA. Two thin (1-4 μm) molecularly smooth mica sheets, each silvered on one side is glued silver side down onto curved silica disks. One of the disks is mounted on a weak spring while the other is attached to a cylindrical piezo crystal arrangement. The surfaces are then brought into contact, while a white light is directed onto one of the silvered faces. Only certain wavelengths are allowed to pass through. When the emerging light reaches a spectrometer, these

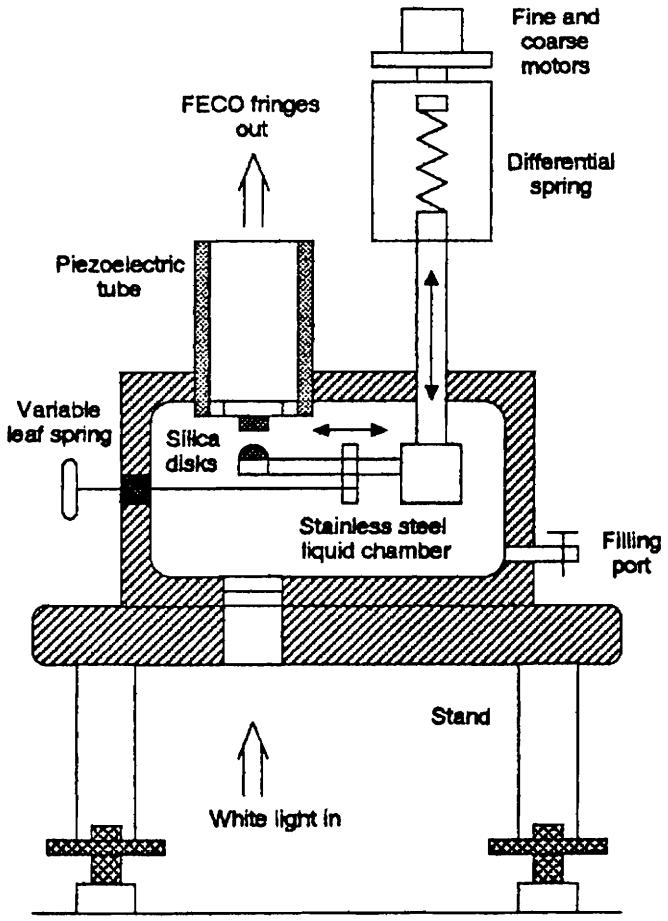

Figure 1.1 Schematic diagram of surface force apparatus Mark IV.

wavelengths split up and appear as an array of fringes in the spectrometer. These fringes are called "Fringes of Equal Chromatic Order" (FECO) which have been studied extensively by Tolansky (41). When a thin film is introduced in between the two mica sheets the fringes will shift towards longer wavelengths. By measuring the shift in these fringes, the distance between the surfaces, i.e., the thickness of the sandwiched thin layer, can be measured with a precision of 0.1-0.2 nm.

The force (F) is measured by monitoring the deflection of the spring relative to the calibrated value at large distances where no force is exerted between the surfaces. From Hooke's law, $F=kX$, where k is the spring constant and X is the deflection of the spring, the magnitude of the force (F) can be calculated. The surfaces "jump" into contact when the slope of the force (dF/dX) is greater than k. The k can be adjusted in the apparatus to enable the measurement of stronger attractive forces at closer distances. The most serious limitation of this technique is the restriction on the types of surfaces available for study. The SFA uses mostly transparent samples like mica, although silica (42) and alumina- coated mica (43,44) surfaces have been used successfully.

For this reason, a new type of surface force apparatus has been developed recently by Parker using piezoelectric-bimorph technology (45). In this apparatus, a piezo electric force sensor consisting of two slabs of piezo material fastened together with their polarization directions facing each other. Under applied force, a compressive strain is produced on one slab and an expansion is produced in the other. This results in a

development of charge which can be used to measure displacement and force. The main advantage with this apparatus is that it can use opaque surfaces for force measurements.

More recently, atomic force microscopes (AFM) (46-48) have been used for direct force measurements. AFM is designed originally to measure forces between a sample surface and a pyramidal tip (Silicon Nitride) as a function of displacement of the sample. Sample displacement is controlled by a piezoelectric crystal that moves towards the cantilever tip at a desired frequency. The force exerted by the micro-fabricated cantilever tip is known from the deflection. This is monitored by a laser beam reflected from the back of the cantilever to fall onto a sensitive split photo diode. In order to obtain force measurements comparable to other geometries, *e.g.* between two crossed cylinders and two spheres, a sphere is attached at the end of the pyramidal tip (see Fig. 1.2). This allows force measurements with a sphere-plate configuration, which can be converted to energy between two flat surfaces using Derjaguin's approximation (49). Ducker *et al.* (50) used modified AFM to measure the repulsive forces between a glass sphere and a silica surface while Rabinovich and Yoon used it for measuring attractive force between silanated glass and silica surfaces (51).

All of these techniques are widely used for force measurements; however, SFA is preferred over bimorph-SFA or AFM for studying of adhesion, lubrication and wetting phenomena. This is because of the precision optical method used in SFA for the distance

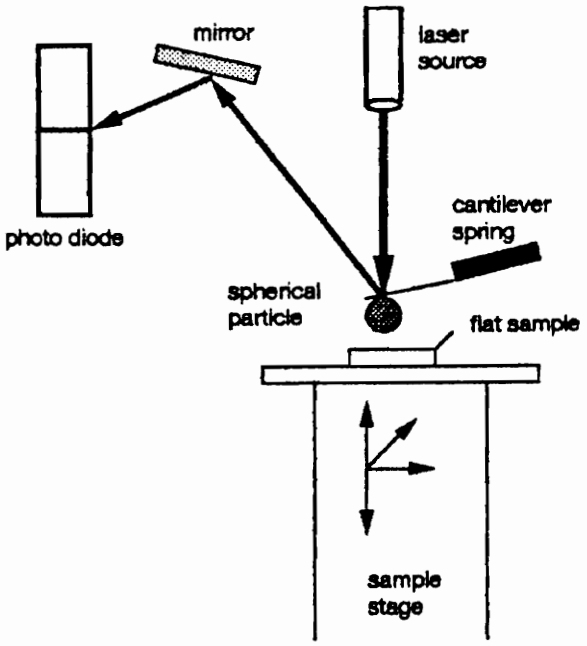

Figure 1.2 Schematic diagram of modified atomic force microscopy.

measurements. Bimorph-SFA (45) and Modified AFM (50,51), on the other hand, can be used to measure the forces between opaque samples.

1.2.3 Hydrophobic force

1.2.3.1 *Short- and long-range hydrophobic forces*

In the first set of measurements carried out by Israelachvili and Pashley (37,39), the surface forces were measured between mica surfaces immersed in cetyltrimethylammonium bromide (CTAB) solutions. CTAB molecules dissociate in water to form CTA^+ ions, which adsorb on the negative surface charge sites of the mica surface. As a result of adsorption, the surfaces become hydrophobic. The force-distance curves measured by Israelachvili and Pashley (37,39) indicated the presence of hydrophobic force in 0-10 nm range in addition to the electrical double-layer and van der Waals forces considered in the DLVO theory. The hydrophobic force (F) was stronger than the van der Waals force, and decayed exponentially with the separation distance (H) as follows:

$$\frac{F}{R} = C_O \exp\left(-\frac{H}{D_0}\right), \qquad \textbf{[1]}$$

in which R is the radius of curvature of the mica surfaces, C_0 is a constant (-140 mN/m) and D_0 is the decay length 1.0±0.1 nm.

Over the last decade, it has been shown that the hydrophobic forces are surprisingly long-ranged extending upto 100 nm. They are about 10-1000 times stronger than the van der Waals force (51,52-62). Such long-range attractive forces are observed between mica surfaces coated with double-chain amines, such as dioctadecyldimethylammonium bromide (DDOAB) (52,55,57,58) and fluorocarbons (53,61), using the Langmuir-Blodgett technique. More recently, long-range hydrophobic forces have been measured between silanated silica surfaces with trimethylchlorosilane (TMCS) (51,54), and octadecyltrichlorosilane (ODTCS) (51,60). Owing to the difficulty in describing the long-range hydrophobic forces using single exponential function, a double-exponential force law was used:

$$\frac{F}{R} = C_1 \exp\left(-\frac{H}{D_1}\right) + C_2 \exp\left(-\frac{H}{D_2}\right), \qquad \textbf{[2]}$$

in which C_1 and C_2 are the pre-exponential parameters. D_1 is referred as "short-range" decay lengths which are in the range of 1-2 nm and D_2 the "long-range" decay lengths which are in the range of 10-30 nm. Measured hydrophobic forces can also be described by a power law (63):

$$\frac{F}{R} = -\frac{K}{6H^2}, \qquad \textbf{[3]}$$

in which K is a fitting parameter. Equation [3] is of the same form as the van der Waals force; therefore the value of K can be directly compared with the Hamaker constants.

It should be noted that all these functional forms are empirical in nature. Although theoretical rationale has been given to the single exponential form (64-66) and the power law (67), there is a great deal of uncertainties regarding the origin of hydrophobic force and, therefore, the theoretical expression. As for the double exponential form (Eq. [2]) which fits the long-range hydrophobic force better, there have been no theoretical rationale given.

1.2.3.2. *Origin of hydrophobic force*

There are several theories proposed in the literature to describe the origin of hydrophobic forces. At first, it was thought that the hydrophobic forces are due to structural changes of the water molecules in the vicinity of the surfaces. This arises due to poor hydrogen-bonding characteristics of the hydrophobic surfaces (68-71). The structural and orientational changes rendered by the hydrophobic surfaces in the nearest layer of water are considered to propagate through the adjacent water layers in the solution. However, simulations studies (72,73) showed the perturbation of water structure extending only upto 5 to 6 layers of water molecules from the surface. Therefore, the structural effect may explain a short-range hydrophobic force at best (64). However, there are ample experimental evidence to show that the attractive hydrophobic

forces are long-range interactions, which extend upto a distance equivalent to 250-300 water molecule diameters (51-61).

Therefore, an alternate approach has been suggested on basis of classical continuum electrostatics. Attard (65) proposed that that the measured long-range hydrophobic force may be due to anomalous dielectric behavior of the solvent in the adjacent aqueous liquid layer. Podgornik (66) showed, however, that based on such an assumption one cannot exceed the limit dictated by the Lifshitz theory (74). He then suggested that the long-range hydrophobic forces are due to fluctuating electric field associated with the lateral mobility of the ions adsorbed at the solid/liquid interfaces (66).

Based on the arguments presented above, Tsao *et al.* (55,79,80) and Rabinovich *et al.* (51,60,81) suggested that long-range hydrophobic forces may originate from the correlation of the large in-plane dipoles associated with the domains of adsorbed hydrocarbons.

Recently, Miklavic *et al.* (82) modeled the interaction between two uniformly charged surfaces with patch-wise adsorption of surfactant (charged domains). They showed analytically that the non-DLVO attractive force can be explained by the electrostatic correlation between charges associated with the domains, which move laterally to maximize the attractive force. This model is qualitatively similar to the domain theory suggested by Tsao *et al.* (55,79,80) and Rabinovich *et al.* (51,60,81). In accordance with the electrostatic nature of the long-range hydrophobic forces, Tsao *et al.*

(79) and Rabinovich and Yoon (60) found that the range of attraction decreased with salt concentration. Also, the experimental observations indicated that the range of hydrophobic force decreases with temperature, suggesting that the hydrocarbon chain ordering is an important factor in forming large domains and hence long-range hydrophobic force (51,55).

Another theory for the origin of long-range hydrophobic forces is related to the metastability of the water films in the vicinity of hydrophobic surfaces. When the contact angle of the hydrophobic solid exceeds 90°, vapor cavities can be formed spontaneously at the metastable interlayer. Therefore, capillary forces related to the cavitation has been considered as the origin of the long-range hydrophobic forces. Yushchenko *et al.* (83) carried out a theoretical analysis for cavitation between two hydrophobic spheres. They showed that the macroscopic cavities can form between hydrophobic surfaces with contact angle (θ) greater than 90° and cause an attractive forces which can be greater than the molecular forces. However, the macroscopic cavitation requires a large activation energy. A simple free energy analysis of cavitation suggests that the work of formation of cavity, w_c, may be given as (83):

$$w_c = -\frac{\pi H^2 \gamma_{LV}}{2\cos\theta}, \qquad [4]$$

in which H is the distance, γ_{LV} is interfacial tension of water, and θ is the liquid contact angle on the solid. Eq. [4] shows that the w_c decreases with the increase in θ and decrease

in H and γ_{LV}. When H=0.3 nm, γ_{LV} =72 mN/m and θ=95°, w_c becomes 30 kT. When the H is increased to 0.5 nm, w_c becomes as large as 83 kT at room temperature, which is much higher than the activation energy (50 kT) needed for thermally nucleating the cavities. These calculations show that macroscopic cavities will nucleate only at very close separation distances, which is consistent with the findings of direct force measurements. The formation of cavities (or air bubbles) have been seen only when the surfaces retreat from each other and never during the approach cycle (84).

Thermodynamically, cavitation should be facilitated at elevated temperatures; however, the long-range hydrophobic forces have actually decreased with the increase in temperature (51,55). For this reason, Tsao *et al.* (79) ruled out the cavitation theory although it has been argued by Christenson *et al.* (86) that one can not support such conclusion in the absence of contact angle data and its temperature dependence. Related to metastability of the interlayer, Ruckenstein and Churaev (85) suggested that the fluctuations at the hydrophobic surface-water interface can correlate hydrodynamically and produce long-range attractive force (85).

Recently, Yaminsky and Ninham (67) suggested that cavitation can occur below the thermodynamic regime due to thermal fluctuation of intermolecular voids in a metastable liquid near hydrophobic surface. It has been suggested that the subcritical cavities can align themselves to form a gas bridge (like a cylindrical column) between two nonwetting parallel plates at sufficiently closer separation (H). Based on such

considerations, these authors derived an expression for the attractive pressure (*P*) as given below:

$$P = -2E\left(\frac{kT}{2\pi\gamma_{LV}}\right)^2 \frac{(1-\cos\theta)}{(v_m^{1/3}H^3)}, \qquad \textbf{[5]}$$

in which E the elasticity modules for the lateral expansion of the cylindrical gas bridge, k the Boltzmann constant, T the temperature, γ_{LV} the liquid-vapor interfacial tension, v_m the molecular volume, θ the contact angle, and H the distance between the surfaces. Eq. [5] may be rearranged to render the form of the non retarded van der Waals force as follows:

$$P = -\frac{K}{6\pi H^3}, \qquad \textbf{[6]}$$

in which K is a constant. For θ=90°, γ_{LV} =70 mJ/m^2, $v_m^{1/3}$ =0.3 nm, and E=2x10^9 N/m^2, eq. [5] gives a value of K as 2x10^{-20} J. This value is larger than the Hamaker constant for hydrocarbons (1x10^{-20} J) but is comparable to that of mica (A_{131}=2.2x10^{-20} J). However, the K value calculated as such is substantially lower than the values reported by Rabinovich and Yoon (60) for the hydrophobic forces between ODTCS-coated silica surfaces. The K values reported by Rabinovich and Yoon (60) are in the range of 2.8-3.5x10^{-16} J, which is nearly four orders of magnitudes larger than that predicted by the subcritical cavitation theory. Thus, the subcritical cavitation theory seem to underestimate the attractive forces.

It may be concluded that there are no satisfactory explanations for the hydrophobic forces between macroscopic bodies. One of the contributing factors for this

confusion is the discrepancies between different sets of experimental measurements. In the following sections, the experimental work reported in literature are summarized.

1.2.3.3 *Effect of electrolytes*

There have been several studies directed towards elucidating the origin of long-range hydrophobic force in aqueous solutions. According to those theories relating the hydrophobic forces to electrostatic correlations, one would expect a decrease in the hydrophobic force with the increase in electrolyte concentration due to screening effect. Christenson *et al.* (57) used tetrapentyl ammonium bromide, a 1:1 electrolyte, between fluorocarbon coated mica surfaces. It was shown that the long-range decay lengths and magnitudes decrease with the increase in electrolyte concentration, while short-range decay lengths and magnitudes remain unaffected. However, two problems were cited in interpreting the data. First, the surfaces prepared by L-B monolayers are metastable and very often degrade with time. This occurs due to the ion-exchange between the cations of the electrolyte and the cationic surfactant adsorbed on the surface. Second, there is a degree of uncertainties in the fitting procedure that is used to estimate the decay lengths. Although it is qualitatively well established that the observed attractive force decreases with the increase in electrolyte concentration, Christenson *et al.* (87) showed that the effect of the salt mainly reduces the preexponential factor (C_2 in Eq. [2]) rather than long-range decay length (D_2). Rabinovich and Yoon (60) suggested, however, that the long-

range decay length (D_2) should be determined by the Debye length ($1/\kappa$) and the average distance between the domains, which in turn varies with the number and size of the domains. They derived a simple formula relating the long-range decay length with the electrolyte concentration as shown below:

$$\frac{1}{D_2^2} = 10.5z^2 C_{el} + \left(\frac{\pi}{a}\right)^2, \qquad [7]$$

in which D_2 is the decay length, z the valance of the electrolyte, C_{el} the electrolyte concentration, and a the average distance between charges on each surface which may be referred as lattice parameter. Eq. [7] fits the published data of Tsao *et al.* (79) and Christenson *et al.* (83) at low electrolyte concentrations by assuming a as 76 and 44 nm, respectively. However, eq. [7] does not fit the D_2 values accurately at higher concentrations and some other data given in the literature (60). Also, it is difficult to explain the force measurements obtained by other workers where hydrophobic forces show no electrolyte dependence (54,57,79). Therefore, the long-range hydrophobic force can not be explained solely by electrostatic correlation forces.

1.2.3.4 *Effect of temperature*

Tsao *et al.* (55) reported that the long-range hydrophobic forces decrease with the increase of temperature from 25 to 50°. The change in force with increasing temperature was attributed to the change in hydrocarbon chain order of the surfactant monolayer.

With well ordered monolayers, the measured hydrophobic forces were long-ranged, whereas when the chains were melted and disordered the forces were less long-ranged. However, Christenson *et al.* (86) argued that the measurements made in this temperature range by Tsao *et al.* (55), particularly with the monolayers of dieicosyldimethyl ammonium (DEHA) ions, show no significant change in the forces at long-range (beyond 20 nm) within the experimental error. Nevertheless, Rabinovich *et al.* (81) reported that the chain-order parameter decreases with increasing temperature and, hence, the magnitude of both the long-range and the short-range forces.

1.2.3.5 *Effect of dissolved gases*

In view of the recent work of Craig *et al.* (88,89) and Rabinovich *et al.* (60) it appears that dissolved gases between hydrophobic surfaces do increase the long-range hydrophobic forces. Rabinovich *et al.* (60) showed that the hydrophobic forces measured between ODTCS-coated silica surfaces are considerably higher in the presence of argon-saturated water than in deareated water. However, these authors did not note any vapor phase cavitation on the approach of the surfaces. They suggested that invisible microbubbles or bridges of dissolved gas molecules could have caused this increased hydrophobic forces. Recently, more evidence for the dissolved gas effect have been reported. Meagher and Craig (62) showed that the net attractive forces between polypropylene (hydrophobic) surfaces decreased by degassing of water. Pashley and

Karaman (90) showed that dodecane-in-water emulsion is stabilized by degassing. The role of dissolved gas molecules in the creation of long-range hydrophobic forces was discussed by Ninham and coworkers (67,88,89)

1.2.3.6 *Effect of solvent*

Parker and Claesson (91) studied force measurements between fluorocarbon monolayers in water and ethylene glycol (EG) which have comparable bulk physical properties. Water and ethylene glycol gave contact angles of 110° and 96°, respectively. The force measurements conducted in ethylene glycol also showed cavitation while retreating the surfaces; however, the attractive force was reduced considerably. Although the presence of cavitation and the absence of long-range hydrophobic force may appear contradictory, one should consider the fact that the viscosity of EG is 20 times larger than that of water, which may influence the dynamics of cavitation and the behavior of the metastable film in-between the fluorocarbon-coated surfaces.

1.2.3.7 *Interaction between hydrophilic and hydrophobic surfaces*

There have been relatively few studies made on the interaction between hydrophilic and hydrophobic surface. The first measurement was made by Claesson *et al.* (92) between DDOA coated mica and bare mica surfaces. The results indicated a net attractive force over the range of 0-80 nm, which was stronger than those measured

between two hydrophobic surfaces. These authors suggested that the attractive forces in the longer separation distances (above 20 nm) may be due to electrical double layer interactions. They considered that the double-layer forces may be caused by positive charge due to excess $DDOA^+$ ions adsorbed and the negative charges of the bare mica surfaces. At smaller separation distances, the attractive forces may be due to the hydrophobic interactions or the ion-ion correlations not accounted for by the DLVO theory. Recently, Tsao *et al.* (79) measured long-range attractive forces in a similar system. They suggested that the attraction between the asymmetric surfaces was due to the correlation of dipoles. Other investigators (60,93) conducted force measurements between a hydrophobic and a hydrophilic silica surfaces (60,93) to observe only short-range attractive forces.

1.2.4 Extended DLVO theory

Despite the fact that the origin of hydrophobic force is still unclear, its existence between macroscopic bodies has been proved beyond a doubt. Therefore, it is necessary to extend the DLVO theory by including the contributions from hydrophobic forces to describe bubble-particle interaction, hydrophobic coagulation, dewatering processes, etc. According to extended DLVO theory the total energy of interaction (V_t) is given as follows (26,27):

$$V_t = V_e + V_d + V_h, \qquad \textbf{[8]}$$

in which V_e, V_d, and V_h are the electrical, van der Waals, and hydrophobic energy components, respectively. As previously mentioned, Yoon and coworkers (28,29) used eq. [8] to calculate a long-range hydrophobic force with a decay length of D_0=13.6 nm for quartz amine flotation system. This value compares well with those measured between methylated silica cylinders by Rabinovich and Derjaguin (54) and other long-range hydrophobic forces reported in the literature for double-chain amines. However, it is almost an order of magnitude longer than those measured with water soluble surfactants such as DAHCl and CTAB (37,39,94-97). DAHCl is commonly used for hydrophobizing the solid particles in flotation. It should be noted, however, that no one has yet reported long-range hydrophobic forces with water soluble surfactants.

1.2.5 Hydrophobic force measurements for amine surfactant systems

Many investigators have conducted direct force measurements between mica surfaces coated with water soluble cationic surfactants such as cetyltrimethylammonium bromide (CTAB) (37,96,97), dodecylamine hydrochloride (DAHCl) (94,95) and, octylammonium chloride between mica surfaces (94). With these surfactants, only short-range hydrophobic forces were obtained with D_0 values in the range of 1-2 nm (37,89).

The reason is probably that the hydrocarbon chains are sparsely packed and, hence, do not present ordered layer to the aqueous phase. In case of mica, the crystallographic area per negative charge is 0.48 nm^2 of the surface, which is twice as large as the cross-sectional area (0.25 nm^2) of ammonium head group. Even with silica whose area per charge is close to the head group size of ammonium ions, it may be difficult to form close packed layer, because not all the silanol groups would become negative charge sites, on which cationic surfactants can adsorb. In this case, the surfactant adsorption would result in sparsely-populated monolayers, which are not conducive to long-range hydrophobic forces. In deed, Parker *et al.* (97) observed only short-range hydrophobic forces between CTAB-coated glass surfaces.

At higher concentrations, additional surfactant ions may adsorb with their polar head groups pointing towards the solution phase forming a 'flip-flop' layers. The formation of a flip-flop layer is a means of minimizing the free energy of the system. Despite the increase in the packing density of hydrocarbon chains on the mica surface, the flip-flop orientation renders the surface hydrophilic because the polar groups of the additional surfactants point toward the solution phase. As a result, only short-range hydrophobic force are seen (94,95). Recently, direct force measurements were conducted by Rutland *et al.* (95) in the presence of 10^{-4} M DAHCl, which is above the point of charge reversal (p.c.r), as function of pH between mica sheets. These authors reported that at pH 8-9, the neutral amines (DA), formed as a result of hydrolysis, coadsorb in-

between the DAH^+ ions on the mica surface to render the surface more hydrophobic. Although these authors have mentioned that the hydrophobic forces increase under this condition, it is not unambiguously discernible from their measured force curves, and no increase in decay lengths have been observed.

Unlike soluble ammonium surfactants, the monolayers formed by the insoluble double-chain surfactants such as DDOAB are more closely packed. As a result, long-range hydrophobic forces with decay lengths (D_2) in the range of 9-25 nm are observed (38,57,58). Rabinovich *et al.*(81) showed that the higher the packing density of hydrocarbon chains the stronger the long-range hydrophobic force.

Both the short- and long-range decay lengths i.e., (D_0, D_1 and D_2) reported in the literature are plotted *vs.* advancing water contact angles (θ_a) in Fig. 1.3. The data can be divided into two groups. The first group include the long-range decay lengths (D_2) obtained with double chain amine surfactants (52,53,55,79,80), fluorocarbons (61,85), and ODTCS (51,60). The second groups of data include the short-range decay lengths (D_0) obtained with water soluble amines such as DAHCl and CTAB.

A striking feature of Figure 1.3 is that there seems to be a *missing link* between short- and long-range hydrophobic forces. Finding the condition under which the short- and long-range forces are linked together may be the key in understanding the origin of hydrophobic force.

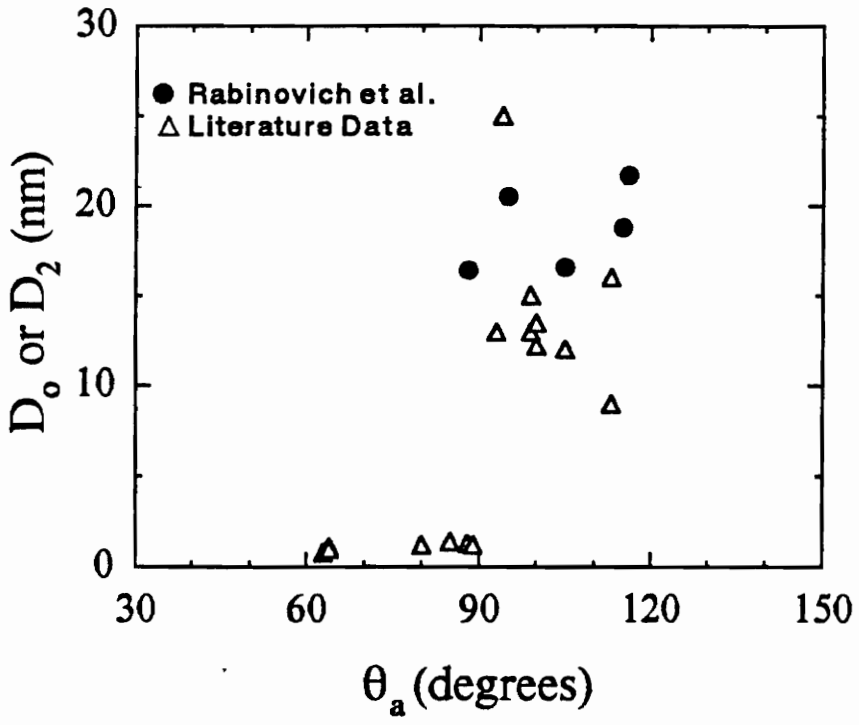

Figure 1.3 D_2 vs. advancing angle (θ_a) plot for mica surfaces coated with DAHCl, DDOAB (hollow triangles), and ODTCS (filled circles) at pH 5.7. Note that the medium range hydrophobic decay lengths $D_2 \approx$3-10 nm are missing.

1.2.6 Amine flotation

1.2.6.1 *Coadsorption*

In flotation, amines are the most widely used surfactant for hydrophobizing and floating oxides, silicates, and aluminosilicates. One of the most interesting aspects of amine flotation system is the strong dependence of flotation recovery on pH (98-100). Given in Fig. 1.4 is the work of Fuerstenau (98), which shows the relationships between the ζ-potential, contact angle, surface coverage, and flotation recovery when using DAHCl for the flotation of quartz. The maximum recovery is observed at pH 9.0-10.3 (98-100) for which various mechanisms were suggested. Gaudin and Fuerstenau (99) suggested that the coadsorption of neutral amine (DA) and the ammonium ions (DAH^+) is responsible for the maximum flotation. The concentration of the neutral amine reaches a maximum at the pH of maximum flotation. The coadsorption of DA and DAH^+ reduces the electrostatic repulsion between the polar groups of the neighboring DAH^+ ions, thereby increases the adsorption density. Furthermore, the adsorption mechanism allows formation of close-packed hydrocarbon chains on the surfaces. The increased adsorption density is evidenced by the increase in contact angle from 20° at pH 8 to about 90° at pH 10 in the presence of $4x10^{-5}$ M of dodecylammonium acetate. Correspondingly, the flotation recovery increased from 12 to 88%. The neutral surfactant species also play an important role with other surfactants such as oleate, and hydroxamate (98-101). Smith

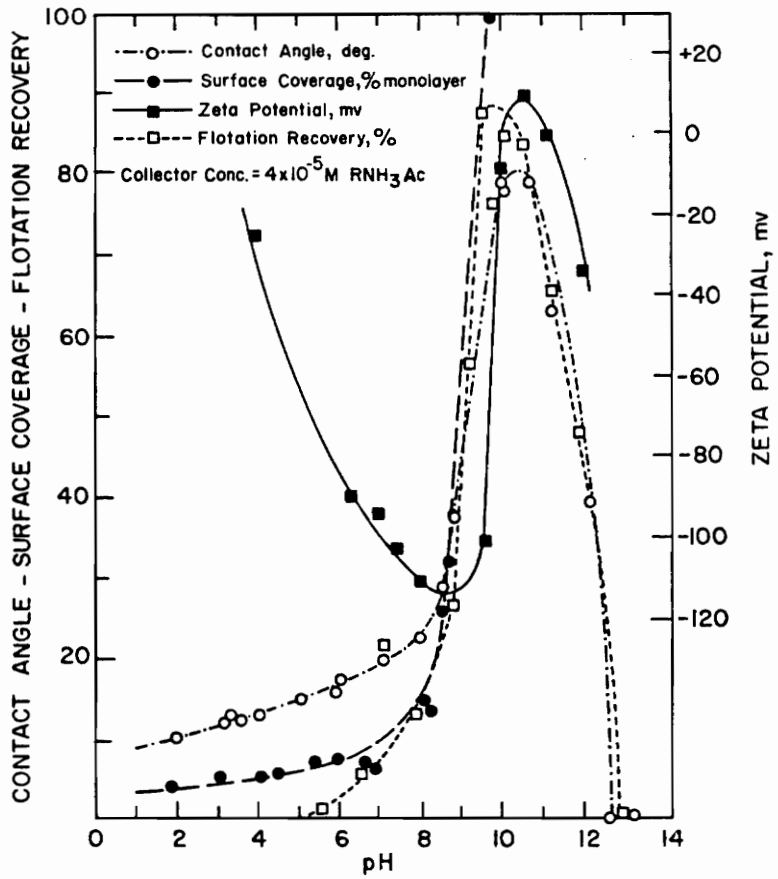

Figure 1.4 Correlation between conatct angle, adsorption density, zeta-potential and flotation recovery of quartz (98).

(103) measured water contact angles on quartz in DAHCl solutions in the absence and presence of dodecanol. He observed a significant increase in contact angle in the presence of neutral surfactant, which was attributed to the coadsorption mechanism. In this system, the alcohol has the same function as neutral amine.

Somasundaran and co-workers (100) suggested a different mechanism. According to these authors, a highly surface active ionomolecular complexes ($DAH^+.DA$) is formed in solution and subsequently adsorb at the solid surface. It should be noted, however, that both the coadsorption and ionomolecular mechanisms suggest an increase in the adsorption density at the solid surface at the pH of maximum flotation.

Recently, Laskowski and coworkers (104,105) suggested that the maximum flotation recovery in the pH range of 9-10.3 is a preprecipitation phenomenon. Using light scattering studies they showed that the bulk precipitation of dodecylamine species occur at pH 10 in 10^{-4} M DAHCl solution (105), and suggested that polyassociates may form at lower concentrations before the onset of bulk precipitation. They included ionomolecular complexes also as part of the preprecipitation phenomenon.

1.2.6.2 *Contact angle and flotation*

While the results of Fuerstenau (98) indicate a good correlation between the equilibrium contact angles and maximum flotation recovery, it has been shown by Iwasaki *et al.* (106) in hematite-amine system and Smith and Lai (107) in quartz-amine

system that good flotation occurs even when the equilibrium contact angles is low. This discrepancy is suggested to have been caused by the nonequilibrium (dynamic) condition at the three-phase contact. This is evidenced by the decrease in contact angle with time, which may be attributed to the changes in gas/liquid interfacial tension (107). Finch and Smith (108) later confirmed this phenomenon by dynamic surface tension measurements at gas/liquid interface in the presence of amine. These investigators suggested that the maximum flotation may be related to the dynamic surface tension behavior, which is pronounced at the pH of maximum flotation.

1.3 Research Objectives

The overall research objective of this investigation is to measure long-range hydrophobic forces with water soluble surfactants.

The specific goals of this research are the following:

a) conduct direct force measurements with mica surfaces in dodecylammonium chloride (DAHCl) solutions in the presence and absence of octanol and dodecanol,

b) determine the contributions from hydrophobic forces using the extended DLVO theory,

c) discuss the origin of hydrophobic forces on the basis of the data obtained in the present work,

d) measure the long-range hydrophobic forces with mica in DAHCl solutions at different pHs and study the mechanisms involved in the coadsorption of dodecylammonium (DAH^+) ions and dodecylamine (DA), and

e) investigate the role of hydrophobic force in flotation.

It is hoped that the results obtained in the present investigation is useful in estimating the hydrophobic force parameters that can be used for modeling bubble-particle interactions in flotation processes.

1.4 Report Organization

Studies conducted in the present work are reported in three separate chapters from 2-4. Each chapter comprises of an introduction, experimental, results, discussion, and conclusions sections.

In Chapter 2, the direct force measurements conducted between mica surfaces in DAHCl solutions are presented. The measurements were conducted in the presence and absence of octanol to study the coadsorption mechanism. Varying compositions of DAHCl and octanol were used to find the conditions for maximum hydrophobic force. Both advancing and receding contact angles were measured to establish a relationship

between the hydrophobic parameters and contact angle. The extended DLVO theory has been used to deconvolute the total interaction energies and estimate the hydrophobic interaction parameters. Flotation experiments were conducted using quartz to demonstrate the role of long-range hydrophobic forces in flotation.

In Chapter 3, a longer chain alcohol (dodecanol) was used as the coadsorbing neutral surfactant at the DAHCl-mica system at pH 5.7. The use of longer chain alcohol gave rise to longer-range hydrophobic forces. The extended DLVO theory was used to deconvolute the total force gradients and obtain the force parameters. The decay lengths obtained in Chapter 2 and 3 are plotted vs. advancing contact angles, along with those reported in the literature, to establish a relationship between the force parameters and the contact angle. The sharp transition in the decay length at the contact angle of 90° has been discussed with special relevance to origin of hydrophobic forces.

In Chapter 4, direct force measurements were conducted with mica surfaces in DAHCl solutions at different pHs. The role of neutral amine formed as a result of hydrolysis is discussed in view of the coadsorption mechanism. The results are correlated with the flotation and contact angle measurements of Fuerstenau (98) in order to study the role of hydrophobic force in flotation.

Summary and conclusions of this investigation are presented in Chapter 5 and Chapter 6 provides some future recommendations.

1.5 References

1. Leja, J., "*Surface Chemistry of Froth Flotation,*" Ch. 9, Plenum. New York (1982).
2. Hauberk, H., Proceedings, XVII Int. Min. Process. Congr. Sydney, May 23-28 (1993).
3. Yoon, R.-H., Proceedings, 2nd Int. Sym. on East Asian Resources Recycling Tech. Seoul, October, 14-16 (1993).
4. Maker, H. V., Proceedings, Int. Conf. on the Recycling of Metals, 319 (1992).
5. Fuerstnau, D. W., *Principles of Mineral Flotation* Ed. King, R. P., 1 (1982).
6. Sutherland, K. L., and Wark, J. W., *Principles of Flotation* AIMM, Melbourne 1955.
7. Klasson, V. I., and Mokrousov, V. A., *An introduction to the theory of flotation*, Butterworths, London 1963.
8. Joy, A. S., and Robinson, A. J., in Recent Progress in Surface Science (Eds. Danielli, J. F., Pankhurst, K. G. A., Riddiford, A.C.,) Vol. 2. Acad. Press, New York 1964.

9. Wills, B. A, *Mineral Processing Technology. (4th edition)* Pergamon Press, New York (1988).

10. Sutherland, K. L., *J. Phys. Chem.* **52,** 394 (1948).

11. Flint, L. R., and Howarth, W. J., *Chem. Engg. Sci.* **26,** 1155 (1971).

12. Trahar, W. J., and Warren, L. J., *Int. J. Mineral Process.* **3,** 103 (1976).

13. Yoon, R.-H, and Luttrell, G. H., "The Effect of Bubble Size on Fine Particle Flotation," in Frothing in Flotation: The Jan Leja Volume, Mineral Processing and Extractive Metallurgy Review, J.S. Laskowski, ed., Gordon and Breach Science Publishers, Ltd., New York, **5,** 101 (1989).

14. Luttrell, G. H., and Yoon, R.-H., "Column Flotation - A Review," Proceedings, Engineering Foundation Conference, "Beneficiation of Phosphate: Theory and Practice," Palm coast, FL. Dec. (1993); in press.

15. Yoon, R.-H., Adel, G. T., Luttrell, G. H., Mankosa, M. J., and Weber, A. T., Interfacial Phenomena in Biotechnology and Materials Processing, Eds. Attia, Y. A., Moudgil, B. M., and Chander, S., Elsevier, Amsterdam (1988).

16. Yoon, R.-H., and Luttrell, G. H., *Coal Preparation,* **2,** 179 (1986).

17. Collins, G. L., and Jameson, G. J., *Chemical Engineering Science,* **32,** 239 (1977).

18. Trahar, W. J., *Int. J. Mineral Process.* **3,** 151 (1976).

19. Reay, D., and Ratcliff, G. A., *Can. J. Chem. Eng.* **51,** 178 (1973).

20. Sutherland, K. L., *J. Phys. Colloid. Chem.* **52,** 394 (1948).

21. Schubert, H., Preprint, Workshop on the Flotation of Sulfide Minerals, Stockholm, Sweden, 1984.

22. Derjaguin, B. V., and Landau, L., *Acta Physicochim. URSS* **14,** 633 (1941).

23. Verwey, E. J. W., and Overbeek, J. Th. G., "Theory of the Stability of Lyophobic Colloids," Elsevier, Amsterdam, (1948).

24. Derjaguin, B. V., and Duhkin, S. S., *Trans. Inst. Min. Metall.*, **70,** 221 (1961).

25. Derjaguin, B. V., and Duhkin, S. S., Proc. *Int, Miner. Process. Congr.*, Warszawa **2,** 21 (1979).

26. Xu, Z., and Yoon, R.-H., *J. Colloid Interface Sci.* **132,** 532 (1989).

27. Xu, Z., and Yoon, R.-H., *J. Colloid Interface Sci.* **134,** 427 (1990).

28. Yoon, R.-H., Plenary paper presented at the XVII International Mineral Processing Congress, September 23-28, Dresden, Germany; *Aufbereitungs-technik.* **32,** 474 (1991).

29. Yordan, J., Ph.D Thesis, Dept. of Mining Eng. Virginia Polytechnic Institute and State University, (1989).

30. Schimmoller, B. K., Luttrell, G. H., and Yoon, R.-H., *Proceedings of the VXII International Mineral Processing Congress,* Sydney, Australia, May 23-28, **3,** 751 (1993).

31. Schimmoller, B. K., Luttrell, G. H., and Yoon, R.-H., *Proceedings of Engineering Foundation Conference on Dispersion and Aggregation.*, March 15-20, Palm Coast, Florida.

32. Israelachvili, J. N., and Adams, G. E., *J. Chem. Soc., Faraday Trans. 1* **74,** 975 (1978).

33. Tanford, C. The hydrophobic effect, 2nd ed.; Wiley: New York, (1973).

34. Franks, F., Water: a comprehensive treatise; Franks, F., Ed.; Plenum: New York,; Vol.4, pp 1 (1975).

35. Israelachvili, J. N., Mitchell, D. J., and Ninham, B. W., *J. Chem. Soc. Faraday Trans. I* **72,** 1525 (1976).

36. Kauzmann, W., *Adv. Protein Chem.* **14,** 1 (1959).

37. Israelachvili, J. N., and Pashley, R. M., *Nature.* **300,** 341 (1982).

38. Pashley, R. M., McGuiggan, P. M., Ninham, B. W., and Evans, D. F., *Science* **229,** 1088 (1985).

39. Israelachvili, J. N., and Pashley, R. M., *J. Colloid Interface Sci.* **98,** 500 (1984).

40. Tabor, D., and Winterton, R. H. S., *Proc. R. Soc. London,* A **312,** 435 (1969).

41. Tolansky, S., *An Introduction to Interferometry*. London: Longmans 1973.

42. Horn, R. G., Smith, D. T., and Haller, W., *Chem. Phys. Lett.* **162,** 404 (1989).

43. Horn, R. G., Clarke, D. R., and Clarkson, M. T., *J Mater. Res.* **3(3),** 413 (1988).

44. Steinberg, S., Ducker, G. V., Hyukjin, C. F., Tseng, M. Z., Clarke, D. R., and Israelachvili, J. N., *Science* **260,** 656 (1993).

45. Parker, J. L., *Langmuir* **8,** 551 (1992).

46. Binnig, G., Quate, C., and Gerber, G., *Phys. Acta. Lett.* **56,** 930 (1986).

47. Hansma, P. K., Elings, V. B., Marti, O., and Bracker, C. E., *Science* **242,** 209 (1988).

48. Rugar, D., and Hansma, P. K., *Physics Today*, October 23 (1990).

49. Derjaguin, B. V., *Kolloid. Zh.* **69,** 155 1934.

50. Ducker, W. A., Senden, T. J., and Pashley, R. M., *Nature (London),* **353,** 239 (1991).

51. Rabinovich, Y. I., and Yoon, R.-H., *Langmuir*, **10,** 1903 (1994).

52. Christenson, H. K., Fang, J., Ninham, B. W., and Parker, J. L., *J. Phys. Chem.* **94,** 8004 (1990).

53. Claesson, P. M., and Christenson, H. K., *J. Phys. Chem.* **92,** 1650 (1988).

54. Rabinovich, Y. I., and Derjaguin, B. V., *Colloids Surf.* **30,** 243 (1988).

55. Tsao, Y., Yang, S. X., Evans, D. F., and Wennerstrom, H., *Langmuir* **7,** 3154 (1991).

56. Kurihara, K., Kato, S., and Kunitake, T., *Chemistry Letters* 1555 (1990).

57. Christenson, H. K., Claesson, P. M., Berg, J., and Herder, P. M., *J. Phys. Chem.* **93,** 1472 (1989).

58. Claesson, P. M., Blom, C. E., Herder, P. C., and Ninham, B. W., *J. Colloid Interface Sci.* **114,** 234 (1986).

59. Parker, J. L., and Claesson, P. M., *Langmuir* **10,** 635 (1994).

60. Rabinovich, Y. I., and Yoon, R.-H., *Colloids and Surfaces* **93,** 263 (1994).

61. Christenson, H. K., Claesson, P. M., *Science* **239,** 390 (1987).

62. Meagher, L., and Craig, S. J., *Langmuir* **10,** 2736 (1994).

63. Rabinovich, Y. I., and Derjaguin, B. V. : Proc. 5th Hungarian Conference on Colloid Chem. Hungary, Budapest, Lorand Eothos Univ. (1988).

64. Eriksson, J. C., Ljunggren, S., and Claesson, P. M., *J. Chem. Soc. Faraday. Trans. 2.* **85,** 163 (1989).

65. Attard, P., *J. Phys. Chem.* **93,** 6441 (1989).

66. Podgornik, V., Rau, D. M., and Parsegian, V. A., *J. Chem. Phys.* **91(9),** 5840 (1989).

67. Yaminsky, V. V., and Ninham, B. W., *Langmuir* **9,** 3618 (1993).

68. Marcelja, S., Mitchell, D. J., Ninham, B. W., and Sculley, M., *J. Chem. Soc. Faraday. Trans. 2.* **73,** 630 (1977).

69. Luzar, A., Svetina, S., and Zeks, B., *Chem. Phys. Lett.* **96,** 485 (1983).

70. Pratt, L. R., and Chandler, D. J., *J. Chem. Phys.* **92** 3683 (1977).

71. Pangali, C., Rao, M., and Berne, B. J., *J. Chem. Phys.* **71,** 2975 (1979).

72. Marchesi, M., *Chemical Physics Letters* **97,** 224 (1983).

73. Lee, C. Y., McCommon, J. A., and Rossky, J., *J. Phys. Chem.* **80,** 4448 (1984).

74. Lifshitz, E. M., *Sov. Phys.,* JETP(Engl transl), **2,** 73 (1956).

75. Delamarche, E., Michael, B., Gerber, Ch., Anselmetti, D., Guntherodt, H.-J., Wolf, H., and Ringsdorf, H., *Langmuir* **10,** 2869 (1994).

76. Kjaer, K, Als-Nielsen, J., Helm, C. A., Tipperman-Krayer, P., and Möhwald, H., *J. Phys. Chem.* **93,** 3200 (1989).

77. Bain, C. D., and Whitesides, G. M., *Angew. Chem. Int. Ed. Engl.* **28,** 506 (1989).

78. Scott, H. L., *Chem. Phys. Lett.* **109,** 570 (1984).

79. Tsao, Y., Evans, D. F., and Wennerstrom, H., *Langmuir* **9,** 779 (1993).

80. Tsao, Y., Evans, D. F., and Wennerstrom, H., *Science* **262,** 547 (1993).

81. Rabinovich, Y. I., Guzonas, D. A., and Yoon, R.-H., *Langmuir* **9,** 1168 (1993).

82. Miklavic, S. J., Chan, D. Y. C., White, L. R., and Healy, T. W., *J. Phys. Chem.* **98,** 9022 (1994).

83. Yushchenko, V. S., Yaminsky, V. V., and Shchukin, E. D., *J. Colloid Interface Sci.* **96,** 307 (1983).

84. Christenson, H. K., Claesson, P. M., and Pashley, R. M., *Proc. Indian Acad. Sci.*, **78,** 379 (1987).

85. Ruckenstein, E., and Churaev, N. V., *J. Colloid Interface Sci.* **147,** 535 (1991).

86. Christenson, H. K., Parker, J. L., and Yaminsky, V. V., *Langmuir* **8,** 2080 (1992).

87. Christensson, H. K., Claesson, P. M., and Parker, J. L., *J. Phys. Chem.* **96,** 6725 (1992).

88. Craig, S. J. V., Ninham, B. W., and Pashley, R. M., *J. Phys. Chem.* **97,** 39 10192 (1993).

89. Craig, S. J. V., Ninham, B. W., and Pashley, R. M., *Nature* **364,** 317 (1993).

90. Pashley, R. M., and Karaman, M. E., To be published (1994).

91. Parker, J. L., Claesson, P. M., *Langmuir* **8,** 757 (1992).

92. Claesson, P. M., Herder, P. C., Blom, C. E., and Ninham, B. W., *J. Colloid Interface Sci.* **118,** 68 (1987).

93. Ducker, W. A., Xu, Z., and Israelachvili, J. N., *Langmuir* **10,** 3279 (1994).

94. Herder, P. C., *J. Colloid Interface Sci.* **134,** 346 (1990).

95. Rutland, M., Waltermo, A., and Claesson , P. M., *Langmuir* **8,** 176 (1992).

96. Kekicheff, P., Christenson, H. K., and Ninham, B. W., *Colloids and Surfaces* **40,** 31 (1989).

97. Parker, J. L., Yaminsky, V. V., and Claesson, P. M., *J. Phys. Chem.* **97,** 29 7706 (1993).

98. Fuerstenau, D. W., *Trans AIME.* **208** 1365 (1957).

99. Gaudin, A. M., and Fuerstenau, D. W., *Trans AIME.* **202** 958 (1955).

100. Somasundaran, P., and Ananthapadmanabhan, K.P. : (Ed) Mittal, K.L., Solution Chemistry of Surfactants. New York : Plenum Press 777-800 (1979).

101. Natarajan, R., and Fuerstenau, D. W., *Int. J. Min. Process.* **11,** 139 (1983).

102. Somasundaran, P., Healy, T. W., and Fuerstenau, D. W., *J. Phys. Chem.* **68,** 3562 (1964).

103. Smith, R. W., *Trans AIME.* **226,** 427 (1963).

104. Laskowski, J. S., "Challenges in Mineral Processing" Ch.2, 15 (1989).

105. Castro, S. H., Vurdela, R. M., and Laskowski, J. S., *Colloids and Surfaces* **21,** 87 (1986).

106. Iwasaki, I., Cooke, S. R. B., and Kim, Y. S., *Trans AIME*, **223,** 113 (1962).

107. Smith, R. W., and Lai, R. W. M., *Trans AIME*, **235,** 413 (1966).

108. Finch, J. A., and Smith, R. W., *Trans IMM.* **81,** C213 (1972).

CHAPTER 2 EFFECT OF OCTANOL ON THE LONG-RANGE HYDROPHOBIC FORCES BETWEEN DODECYLAMINE-COATED MICA SURFACES

2.1 Introduction

The classical DLVO theory predicts the stability of lyophobic colloidal suspensions based on the balance between electrical repulsion and dispersion attraction. It is now well documented, however, that the theory fails with very hydrophobic and very hydrophilic colloidal suspensions, and that the theory needs to be extended by incorporating a structural force term (1-6). The first two papers of this series dealt with the cases of primary and secondary hydration forces stabilizing silica and rutile suspensions (5,6). On the other hand, hydrophobic coal particles are unstable even when the ζ-potential is high, because of the hydrophobic forces not considered in the classical DLVO theory (3,4). It has also been shown that adhesion between air bubbles and hydrophobic mineral particles suspended in water is induced by the hydrophobic force, and methods of estimating its contributions to the adhesion force have been described (7,8).

Hydrophobic forces were first measured by Israelachvili and Pashley (9) with mica surfaces in equilibrium with cetyltrimethylammonium bromide (CTAB) solution.

They were relatively short-ranged and decayed exponentially in the 0-10 nm range:

$$\frac{F}{R} = C_0 exp(-\frac{H}{D_o}) \qquad [1]$$

in which R is the curvature of cylindrical mica surfaces, D_o the decay length and C the pre-exponential parameter, which is negative for hydrophobic interaction. Later investigations showed the existence of long-range hydrophobic forces which are best described by a double-exponential function:

$$\frac{F}{R} = C_1 \exp(-\frac{H}{D_1}) + C_2 \exp(-\frac{H}{D_2}) \qquad [2]$$

in which the first term represents the `short-range' hydrophobic force and the second term the long-range hydrophobic force. In some cases, the hydrophobic force can also be described by a power law (10):

$$\frac{F}{R} = \frac{K}{6H^2} \qquad [3]$$

in which K is the only fitting parameter. Eq. [2] is of the same form as the dispersion force. Although, Eriksson *et al.* (11) derived a theoretical expression in single exponential form, it does not provide a rationale for the long-range hydrophobic force; therefore, Eq. [2] and [3] are still considered empirical in nature.

Many theories have been proposed regarding the origin of the hydrophobic force. These include entropic force due to configurational rearrangement of water

molecules when two hydrophobic surfaces approach each other (12-16), capillary force due to cavitation in the vicinity of hydrophobic surfaces (17), hydrodynamic correlation between fluctuating interfaces (18), charge correlation (19), and correlation of dipoles on hydrophobic domains (20,21).

The hydrophobic forces measured between mica surfaces coated by the Langmuir-Blodgett (L-B) technique with insoluble double-chain amines, such as dimethyldioctadecyl-ammonium bromide (DDOAB) (12,22-25) and fluorocarbons (17,26), show D_1 values typically in the range of 1-2 nm at $H<10$ nm and D_2 in the range of 10-26 nm at longer distances. The D_2 values are substantially larger than D_o's measured with soluble amines such as dodecylamine hydrochloride (DAHCl) (27,28) and CTAB (9) on mica, which may be attributed to the higher degree of hydrocarbon chain ordering on the mica surface. It has been shown recently by Rabinovich *et al.* (21,29) that both the C and D parameters change linearly with hydrocarbon chain order parameter.

In modeling hydrophobic interactions using the extended DLVO theory, there remains an uncertainty regarding the decay lengths of the hydrophobic forces involved. Based on stability measurements, Xu and Yoon (3,4) modeled the hydrophobic coagulation of coal particles to obtain $D_o=10.3$ nm. This value was close to those ($D_o=12.2$ and 13.6 nm) reported by Rabinovich and Derjaguin (30) from their direct

force measurements conducted with methylated glass fibers. For bubble-particle interactions, the value of D_o was calculated to be 13.6 nm (7,8). However, these values are much larger than those obtained with mica surfaces coated with soluble single-chain surfactants, but shorter than some of those with insoluble double-chain surfactants.

Herder (27) measured short-range hydrophobic forces (D_o=1-2 nm) with mica surfaces coated by DAH^+ molecules at pH 5.7. He suggested that the short decay length is due to the fact that hydrocarbon chains adsorbed on mica are only sparsely-packed (27). In alkaline solutions (=pH 9.5-10.1) of 10^{-4} M DAHCl, where it hydrolyses, Rutland *et al.* (28) reported to have observed long-range hydrophobic forces but no changes in decay length were reported. Nevertheless, these authors attributed the appearance of the long-range hydrophobic force to the coadsorption of neutral amines (DA) with ammonium (DAH^+) ions, which results in the formation of a more compact monolayer. This suggestion is consistent with the work of Gaudin and Fuerstenau (31), who showed that maximum flotation recovery of quartz occurs at the pH where DAHCl hydrolyses to form DA. Later work by Smith (32) showed that the presence of nonionic surfactants such as dodecanol increases the water contact angle of DAH^+ coated quartz surface.

The purpose of the present investigation was to study the effect of octanol on

the hydrophobic forces between mica surfaces coated with DAHCl. If the neutral surfactant coadsorbs with DAH^+ ions, it may be possible to detect long-range hydrophobic forces with longer decay lengths than observed previously with amine alone. It is hoped that the results of the present investigation will be helpful in providing appropriate decay lengths for modeling hydrophobic interactions in mineral and coal processing.

2.2 Experimental

2.2.1 Materials

Dodecylamine hydrochloride (DAHCl) obtained from Eastman Kodak was recrystallized from ethanol before use. Reagent grade octanol from Fisher Scientific was used as received. Conductivity water was obtained from a Nanopure II water treatment unit and deaerated under a vacuum for three hours before use. A silica sample (-100+200 mesh) was obtained from Wako Chemicals, Japan. It was cleaned with 1 M HCl and then washed thoroughly with water before use for flotation. The mica specimen used for direct force measurements was obtained from Unimica Corp., N.Y.

2.2.2 Surface forces measurements

The direct force measurements were carried out using a Mark IV surface force apparatus (from Anutech, Pty.) designed similar to Tabor and Winterton (33) and Israelachvili and Adams (34). Two molecularly smooth mica surfaces were silvered on one side and then glued silver-side down onto silica disks using Epon 1004 from Shell Chemical Co. The separation distance between the two mica surfaces was measured using multiple beam interferometry based on the method of fringes of equal chromatic order (FECO). The separation was measured with an accuracy of ± 0.2 nm. The surface force apparatus was controlled using the SF-Scribe CV-78 software on a Macintosh computer.

The zero separation point for each experiment was measured in air, after which water was added to the apparatus. The force-distance curve obtained in Nanopure water was compared with those in literature (27,34) to ensure that the mica surfaces were clean. A 10^{-3} M DAHCl stock solution was prepared in Nanopure water, while a 10^{-3} M octanol stock solution was prepared in 1% (by volume) ethanol-in-water solution. Requisite amounts of the DAHCl and octanol stock solutions were injected to a known volume of Nanopure water in the chamber to obtain desired concentrations. The pH of the DAHCl-octanol solution was about 5.7. Initial measurements were made with amine alone; the stock solution was injected with the mica surfaces

separated by about 1 mm, and the measurements initiated after three hours of equilibration.

After the completion of the force measurements with amine alone, the mica surfaces were separated, an aliquot of the octanol stock solution was injected, and the system equilibrated for three hours before initiating the force measurements. In each series of measurements, the adhesion force ($F(0)/R$) and the jump distance were recorded.

The stronger attractive forces at closer distances were measured using the gradient method, in which the distance at which two mica surfaces jump into contact with each other is recorded by successively varying the stiffness of the spring. The spring constant was taken as the gradient (dF/dH) at the jump distance. This technique is also referred to as jump method (9).

2.2.3 Contact angle measurements

Both the advancing and receding contact angles were measured using a Rame-Hart goniometer. Freshly cleaved mica surfaces were immersed in DAHCl and octanol solutions at pH 5.7. After 30 minutes of equilibration, they were taken out of the solution and dried under a stream of nitrogen gas. Contact angles were then measured using the sessile drop technique with Nanopure water. These measurements were

reproducible within ± 2°.

2.2.4 Flotation experiments

Flotation tests were conducted using a standard microflotation cell. The silica sample was conditioned in DAHCl solutions for 30 minutes before flotation. When studying the effect of octanol, the silica sample was conditioned initially in a DAHCl solution for 30 minutes and, then, conditioned for another 30 minutes after the addition of the octanol stock solution. Each flotation test was conducted for five minutes using nitrogen bubbles.

2.3 Results

2.3.1 Direct force measurements

Figure 2.1 shows the force-distance curves obtained with mica surfaces in Nanopure water and in DAHCl solutions of varying concentrations. The results are similar to those reported in literature (27). The DLVO force curves, obtained using the algorithms developed by Chan *et al.* (35), are superimposed on the experimental data. The upper boundary of the theoretical force curves is based on the constant charge model, while the lower limit represents the constant potential model. The

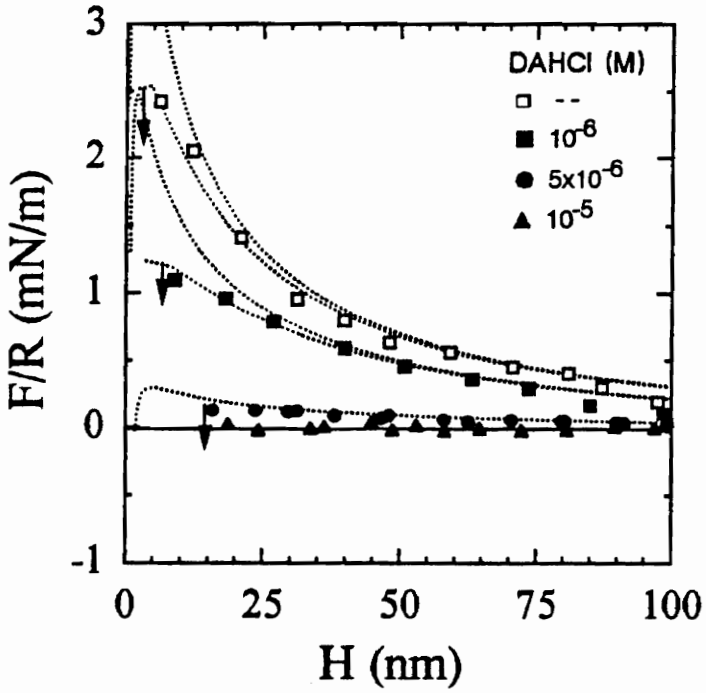

Figure 2.1 *F/R* vs. *H* between mica surfaces in various DAHCl solutions at pH 5.7. The upper and lower dotted curves represent the constant charge and constant potential models, respectively, of the DLVO theory obtained using $A_{131}=2.2\text{x}10^{-20}$ J, $\Psi_o=-170$ mV and $\kappa^{-1}=96.0$ nm. for Nanopure water; -125 mV and 76.1 nm at 10^{-6} M DAHCl; and -35 mV and 68.0 nm at $5\text{x}10^{-6}$ M DAHCl. The arrows represent the distance at which the two surfaces jump into contact due to attractive forces.

dispersion force has been calculated using the Hamaker constant (A_{131}) of 2.2×10^{-20} J. The surface potential (ψ_o) given for each curve represents the value used to best-fit the experimental data using the DLVO theory.

The experimental data obtained in Nanopure water can be best-fit with ψ_o=-170 mV and κ^{-1}=96 nm. It is shown that the repulsive force decreases with increasing DAHCl concentration. Two reasons may be given. The first is the charge neutralization due to the adsorption of DAH^+ ions on the negatively-charged mica surfaces. Table 2.1 shows the changes in ψ_o and charge density (given as the area per unit surface charge) at different DAHCl concentrations. The second is that the adsorption renders the mica surface hydrophobic; however, the attractive hydrophobic force is discernable only at shorter separation distances ($H < 15$ nm). The evidence for the hydrophobic force is also given by the fact that jump distances are significantly larger than predicted by the classical DLVO theory. As shown in Table 2.1, the jump distance increases with increasing amine concentration, indicating that the surface becomes more hydrophobic. Also shown in this table are the adhesion forces ($F(0)/R$), which are the maximum forces measured when the two surfaces are pulled apart after the contact. It has been shown that $F(0)/R = \alpha\gamma_{sl}$, α being in the range of 3π and 4π (36) and γ_{sl} the interfacial tension.

TABLE 2.1

Results of surface force measurements with dodecylamine hydrochloride at pH 5.7.

Conc. of Amine (M)	Area per Charge (nm^2)	Surface Potential (Ψ_o) (mV)	Jump Distance (nm)	Adhesion Force (mN/m) ±25
- -	30.5	-170	3.0	125
$1x10^{-6}$	65.0	-125	7.0	150
$5x10^{-6}$	410.0	- 35	14.0	250
$1x10^{-5}$	- -	0	14.0	250

Figure 2.2 compares the force curve obtained in 10^{-6} M DAHCl solution with that obtained in 10^{-6} M DAHCl and 0.05% ethanol solution. It shows that the short-chain alcohol does not affect the DAHCl adsorption.

Figure 2.3 shows the force curves obtained in Nanopure water and in 10^{-6} M octanol solution (prepared in 1% ethanol-in-water solution). The two curves show no difference from each other, indicating that octanol alone does not adsorb on mica.

Figure 2.4 shows the effect of octanol addition on the force curves obtained in 10^{-6} M DAHCl solution. As shown, the repulsive force is further reduced by octanol addition, indicating that the neutral surfactant brings additional DAH^+ ions onto the mica surface. As a result of this *coadsorption*, ψ_o is increased from -125 to -70 mV, and the area per charge increased from 65 to 184 nm^2 (Tables I & II). The decrease in repulsive force at shorter distances can be accounted for by both charge neutralization and increased hydrophobic attraction. The increase in jump distance from 7 to 10 nm also indicates the increase in hydrophobic attraction due to the coadsorption of octanol. Raising the octanol addition from 10^{-7} to 10^{-6} M does not appreciably increase the coadsorption.

Figure 2.5 shows the force curves obtained at higher concentrations of octanol and DAHCl. At $5x10^{-7}$ M octanol, the repulsive force almost completely disappears at

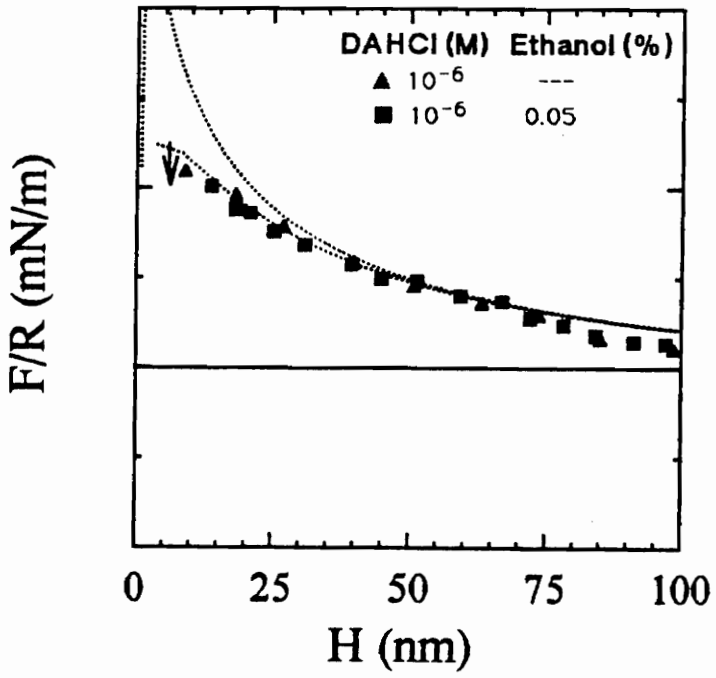

Figure 2.2. *F/R* vs. *H* between mica surfaces in 10^{-6} M DAHCl with and without ethanol at pH 5.7. The upper and lower curves represent the constant charge and constant potential models, respectively, of the DLVO theory obtained using $A_{131}=2.2\text{x}10^{-20}$ J, $\Psi_o=-125$ mV and $\kappa^{-1}=76.1$ nm. The arrow shows the jump distance.

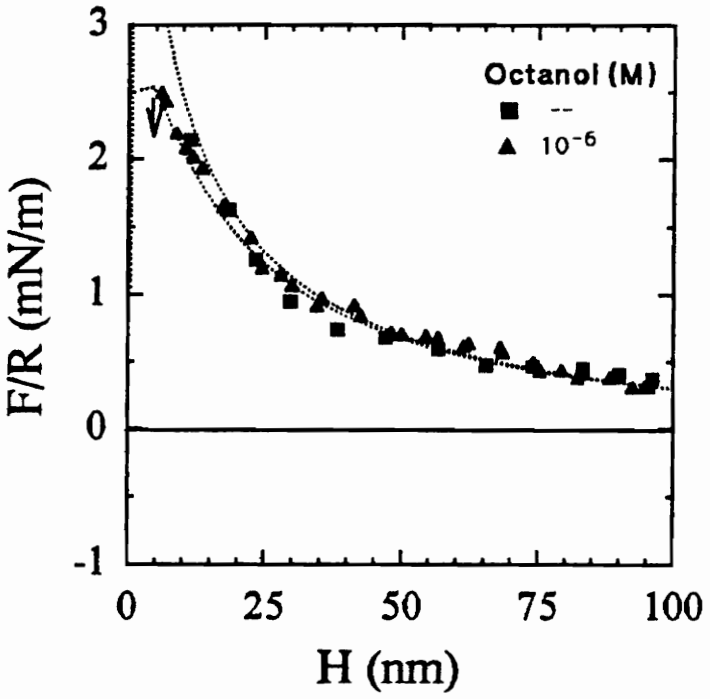

Figure 2.3. Effect of octanol on the *F/R* vs. *H* curves obtained with mica surfaces at pH 5.7. The upper and lower curves represent the constant charge and constant potential models, respectively, of the DLVO theory obtained using $A_{131}=2.2\text{x}10^{-20}$ J, $\Psi_o=-170$ mV and $\kappa^{-1}=96.0$ nm. The arrow shows the jump distance.

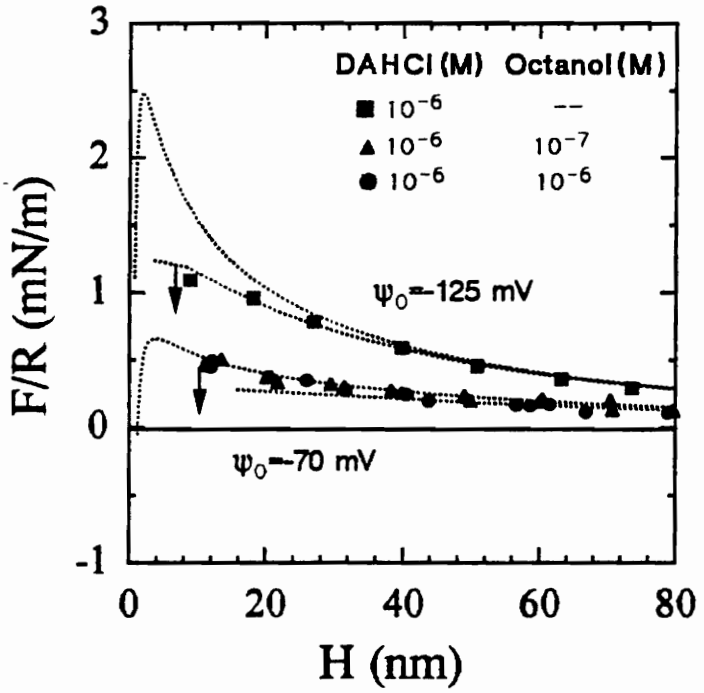

Figure 2.4. *F/R* vs. *H* between mica surfaces in 10^{-6} M DAHCl solutions with varying amounts of octanol at pH 5.7. The upper and lower curves represent the constant charge and constant potential models, respectively, of the DLVO theory obtained using $A_{131}=2.2\text{x}10^{-20}$ J, $\Psi_o=-125$ mV and $\kappa^{-1}=76.1$ nm without octanol; $\Psi_o=-70$ mV and $\kappa^{-1}=76.1$ nm with 10^{-7} M octanol; and -70 mV and 76.1 nm at 10^{-6} M octanol. The arrows show the jump distance.

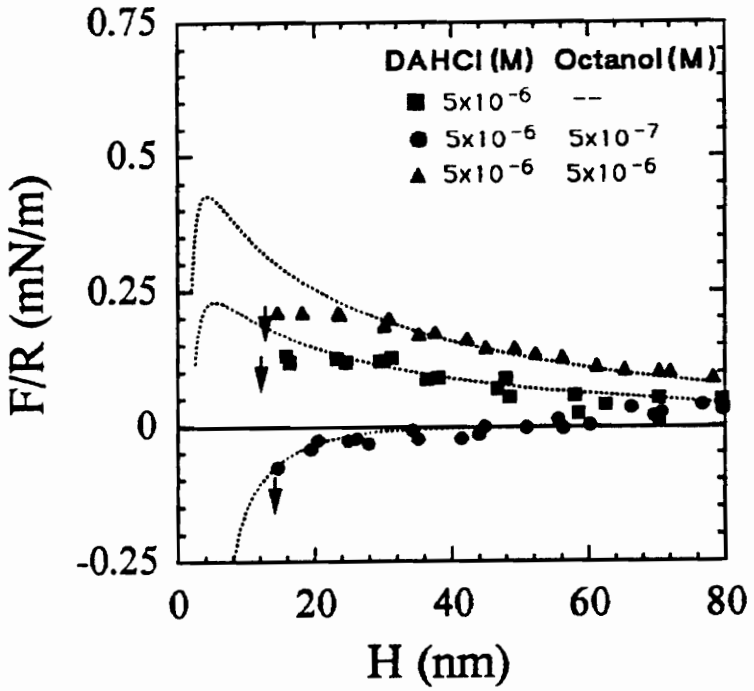

Figure 2.5. *F/R* vs. *H* between mica surfaces in $5x10^{-6}$ M DAHCl solutions with varying amounts of octanol at pH 5.7. The upper and lower curves represent the constant charge and constant potential models, respectively, of the DLVO theory obtained using $A_{131}=2.2x10^{-20}$ J, $\Psi_o=-35$ mV and $\kappa^{-1}=68.0$ nm without octanol; $\Psi_o=0$ mV at $5x10^{-7}$ M octanol; and $\Psi_o=+45$ and $\kappa^{-1}=68$ nm at $5x10^{-6}$ M octanol. The arrows show the jump distance.

TABLE 2.2

Results of surface force and contact angle measurements with dodecylamine hydrochloride and octanol at pH 5.7

Concentration (M)		Area pre Charge	Surface Potential (mV)	Jump Distance	Adhesion. Force
Amine	Octanol	(nm^2)	(Ψ_o)	(nm)	(mN/m) ±25
$1x10^{-6}$	$1x10^{-7}$	184.0	-70.0	10.0	200
$1x10^{-6}$	$1x10^{-6}$	184.0	-70.0	10.0	225
$5x10^{-6}$	$5x10^{-7}$		0.0	16.0	375
$5x10^{-6}$	$5x10^{-6}$	303.0	45.0	16.0	350
$1x10^{-5}$	$1x10^{-6}$	0.4	350.0	--	--

longer distances, with a weak attractive force appearing in the 0-45 nm range. The jump occurs at about 16 nm and the adhesion force increases to 375 mN/m. It is interesting that at $5x10^{-6}$ M octanol the repulsive force is actually increased, indicating that the DAH^+ ions coadsorbing with octanol gives rise to a bilayer (or a `flip-flop' layer (37)) formation. The DLVO fit gives $\psi_o = +45$ mV and 303.0 nm^2 of surface area per charge.

At 10^{-5} M DAHCl and no octanol, the mica surface becomes completely neutralized as shown in Figure 2.6, which is in close agreement with the results of Herder (27). In the presence of 10^{-6} M octanol, however, the repulsive force becomes even greater than in Nanopure water, which may be attributed to charge reversal due to the flip-flop layer formation. The DLVO fit gives $\psi_o = +350$ mV and 0.4 nm^2 of surface area per charge. When the octanol concentration is further increased to $5x10^{-5}$ M, very large repulsive forces are observed as shown in Figure 2.7. At the same time, the closest contact distance moves from 0 to 35 nm. At 10^{-5} M DAHCl and octanol, even larger repulsive forces are observed and the contact distance shifts further outward to 47.5 nm. Also, the force measurements conducted under this condition exhibit hysteresis; the measurements made while increasing the separation distance are significantly lower than those made while decreasing it. A similar observation was made by Rutland *et al.* (28) with amine-coated mica surfaces at a pH above 10.3.

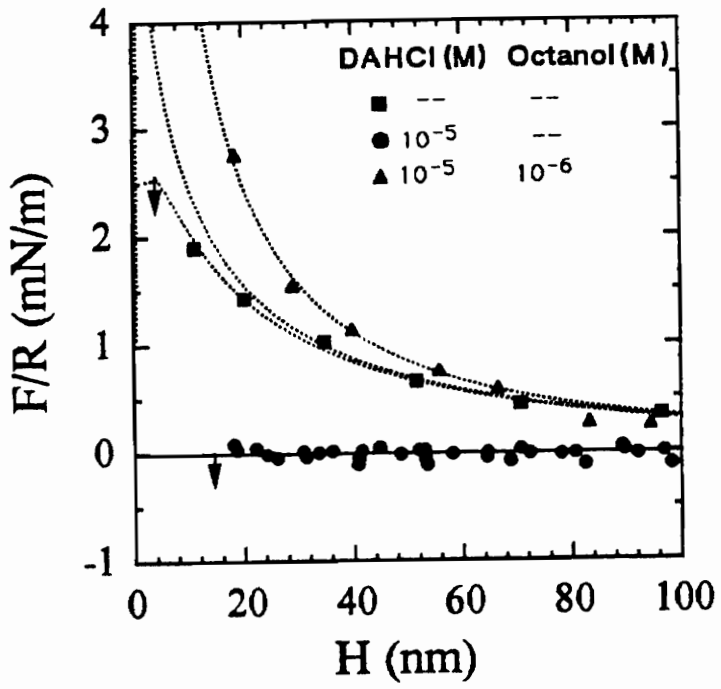

Figure 2.6. *F/R* vs. *H* between mica surfaces at 10^{-5} M DAHCl and pH 5.7 with and without octanol. In the absence of octanol, Ψ_o becomes zero, but at 10^{-6} M octanol large repulsive force is observed, indicating a charge reversal; the force curve can be fitted with Ψ_o= +350 mV and κ^{-1}=43 nm. This repulsive force is larger than in Nanopure water, which can be fitted with Ψ_o=-170 mV and κ^{-1}=96 m. The arrows shows the jump distance.

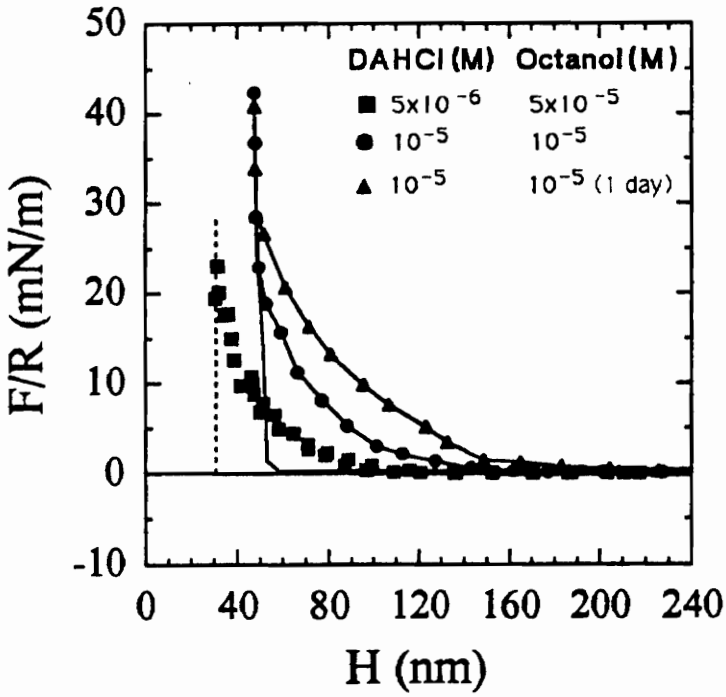

Figure 2.7. *F/R* vs. *H* curves between mica surfaces in solutions containing both DAHCl and octanol at pH 5.7. At $5x10^{-6}$ M DAHCl and $5x10^{-5}$ M octanol, large repulsive forces which cannot be explained by the Poisson-Boltzmann equation are observed; but the force measurement shows no hysteresis. At higher DAHCl and octanol concentrations, larger steric forces are observed and the measurements exhibit hysterisis; the hysteresis becomes more significant 24 hours after octanol addition.

These authors attributed the hysteresis to the steric repulsion due to the presence of phase-separated hydrated dodecylamine droplets, which is consistent with the findings of Castro *et al.* (38). Although it is uncertain whether amine precipitates at pH 5.7 in the presence of octanol, a similar explanation might be afforded to the observation made in the present work. An alternative explanation may be the formation of mixed micelles on the surface, which could form at relatively low concentrations because of the high surface activity of the amine-octanol complexes. Apparently, the micellization (or precipitation) is a slow process as the surface forces become further increased when the system is equilibrated for one day after the addition of octanol.

2.3.2 Contact Angle Measurements

Table 2.3 gives advancing and receding contact angles measured on mica with water droplets containing known amounts of DAHCl and octanol. The contact angles obtained in the present work are slightly lower than those reported by Herder (27), which may be attributed to the shorter equilibration time (3 hours) compared to those of Herder (24 hours). Indeed, the contact angles measured after 24 hours of equilibration gave contact angles 3 to 4 degrees higher than those measured after 3 hours of equilibration. Note that octanol addition increases both the advancing and receding angles, indicating an increase in hydrophobicity. However, the receding

TABLE 2.3

Results of advancing and receding angles

Concentration (M)		Contact Angle (deg)		
DAHCl	Octanol	θ_a	θ_r	$\theta_a - \theta_r$
1×10^{-6}	-	60	35	25
5×10^{-6}	-	80	60	20
1×10^{-5}	-	85	65	20
1×10^{-6}	1×10^{-7}	63	45	18
1×10^{-6}	1×10^{-6}	64	45	19
5×10^{-6}	5×10^{-7}	84	72	12
5×10^{-6}	5×10^{-6}	84	65	19
1×10^{-5}	1×10^{-6}	81	48	33

angles increase more than the advancing angles, resulting in a significantly reduced hysteresis. This finding suggests that in the presence of octanol the surface coating becomes more homogeneous. Note further that the contact angle hysteresis is minimum at $5x10^{-6}$ M DAHCl and $5x10^{-7}$ M octanol, at which hydrophobic force becomes most significant (see Figure 2.5). Therefore, the increased hydrophobic force in the presence of octanol can be related to the increased homogeneity of the surface, which in turn may reflect a higher degree of hydrocarbon chain ordering on the mica surface. Earlier work has also shown a direct correlation between the chain order and hydrophobic force (21).

2.3.3 Flotation results

Figure 2.8 shows the flotation test results obtained with silica using DAHCl and a mixture (1:1) of DAHCl and octanol as collector at pH 5.7. With amine alone, the floatability begins to increase above 10^{-5} M and reaches a maximum of 78% at $4x10^{-5}$ M. According to Gaudin and Fuerstenau (31), the floatability of quartz increases sharply at the critical hemi-micelle concentration (c.h.c.) of amine, which is usually 100 times lower than the critical micelle concentration (c.m.c.). In the presence of dodecylammonium ions and octanol, the floatability begins to increase sharply at $5x10^{-6}$ M, indicating that octanol significantly reduces c.h.c. This finding suggests that

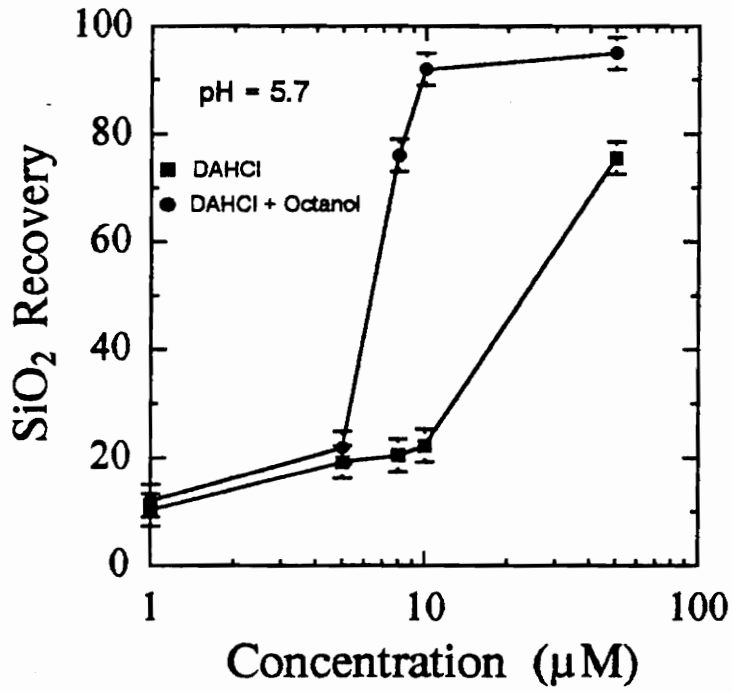

Figure 2.8. Floatability of silica in DAHCl and octanol solutions at pH 5.7.

octanol helps produce close-packed monolayer and renders the surface more hydrophobic. According to Smith (32), the contact angle of quartz in $4x10^{-4}$ M DAHCl is only 30° at pH 5.7 but increases to 50° at $4x10^{-4}$ M DAHCl and $1.4x10^{-4}$ M dodecanol. Thus, the flotation results support the findings of the surface force measurements conducted with mica that coadsorption of amine and octanol results in increased hydrophobicity.

2.4 Discussion

The surface force measurements were conducted at pH 5.7, where dodecylamine is completely ionized to DAH^+ ions. Under this condition, the adsorption mechanism should be controlled mainly by columbic attraction. According to the adsorption kinetic studies conducted by Chen *et al.* (37), the DAH^+ ions adsorb as dipoles on the mica surface, i.e., carrying their negatively charged counter ions (Cl^-) with them, which also partially retain their counter ions (K^+). Thus, the initial adsorption mechanism is controlled by a dipole-dipole interaction. The oppositely charged counter ions subsequently unite to form an ion pair, which slowly diffuses out of the head group region, leaving behind the head groups that are now bound to the surface much more strongly *via* columbic attraction. It should be noted, however, that the adsorption mechanism may be different on silica substrate as has recently been

shown by Parker *et al.* (39).

The surface force, contact angle and flotation experiments conducted in the present work showed that mica and silica surfaces contacted with DAHCl solutions become more hydrophobic when a small amount of octanol is added. Similarly, Smith (32) showed that quartz immersed in DAHCL solutions exhibit substantially larger contact angles in the presence of dodecanol. Also, the work of Gaudin and Fuerstenau (31) showed that neutral amine (DA) coadsorbs with DAH^+ ions on quartz, rendering the surface more hydrophobic.

More recently, Rutland *et al.* (28) suggested that mica surfaces immersed in 10^{-4} M DAHCl undergo charge reversal at low pH, and that at pH 8-9 the adsorption of neutral amines renders the monolayer more compact and hydrophobic. It should be noted, however, that the force curves obtained by Rutland *et al.* do not actually support this claim. For one thing, there were no significant reduction in the force curves as the pH was raised to 8-9. For another, the adhesion force did not change with pH. Moreover, the jump distance did not change significantly. The most significant change in their force measurements was that the distance at which two mica surfaces contact each other was substantially increased at pH 8-9 and 10^{-4} M DAHCl concentration. This seems to support the work of Laskowski and his colleagues (38,40) that DAHCl precipitates under the conditions employed by Rutland *et al.* (28).

The force measurements conducted in the present work is below the region of precipitation. Therefore, the increased hydrophobicity of mica in the presence of octanol may also be attributed to the coadsorption. The strongest evidence for the increased hydrophobicity is the fact that the measured force becomes net negative (attractive) when an appropriate amount of octanol ($5x10^{-7}$ M) is added to $5x10^{-6}$ M of DAHCl solution. Without adding a neutral surfactant such as octanol, no one has yet observed net negative forces between mica surfaces coated with soluble surfactants. The attractive forces become even stronger when dodecanol rather than octanol is added to DAHCl solution, as will be reported later (41). Other evidence for the increased hydrophobicity due to coadsorption includes increases in jump distance, adhesion force (see Table 2.2) and contact angle (Table 2.3).

It may be envisioned that octanol molecules coadsorb in-between the DAH^+ ions adsorbed on mica, thereby increasing the packing density and, hence, the ordering of adsorbed hydrocarbon chains. This is possible because DAH^+ ions do not form a close-packed monolayer on mica. Theoretically, each DAH^+ ion occupies the center of the oxygen hexagon vacated by the K^+ ion, occupying 0.48 nm^2 of the surface (27). This area is almost twice as large as the cross-sectional area (0.25 nm^2) of DAH^+ ion.

When DAH^+ ions occupy all the sites vacated by K^+ ions, the surface charge must be neutralized. This occurs at 10^{-5} M DAHCl, as evidenced by the disappearance

of the repulsive force (Figure 2.1). This concentration may be referred to as point of charge reversal (p.c.r.), because mica surface acquires positive charge when DAHCl concentration is further increased. Figure 2.9a schematically represents the mica surface at p.c.r. Herder (27) showed that at $4x10^{-5}$ M DAHCl, ψ_o increases to +60 mV at pH 5.7. Thermodynamically, a flip-flop orientation, shown in Figure 2.9b, should be favored under this condition, because it minimizes the electrostatic repulsion between the head groups. A mica surface with flip-flop orientation of DAH^+ ions should render the surface hydrophilic, because the head groups point toward the aqueous phase.

A neutral surfactant such as octanol can more readily place its polar head closer to the polar heads of the adsorbed DAH^+ ions, as shown in Figure 2.9c. An important consequence of such an orientation is that the mica surface becomes hydrophobic rather than hydrophilic. As compared to the case at p.c.r. (Figure 2.9a), the hydrophobicity should increase because the hydrocarbon chains are more closely-packed, allowing water molecules to be excluded more completely from the surface. The coadsorption should also increase the hydrocarbon chain ordering, which has been shown to directly affect the hydrophobic force parameters (21). At p.c.r., the thickness of the adsorption layer is 0.5-0.7 nm. Coadsorption of octanol does not appreciably increase the thickness of the adsorption layer, probably because of the shorter chain length of

octanol as compared to that of dodecylamine. It has been found, however, that coadsorption of dodecanol increases the thickness significantly, as will be reported in a future communication (41). Herder (27) reported the thickness of the flip-flop adsorption layer formed at $4x10^{-5}$ M DAH^+ to be 0.7-0.8 nm at pH 5.7.

An interesting observation made in the present work is that the coadsorption of octanol not only increases hydrophobic force, but also significantly reduces the double-layer repulsion force. For example, ψ_o increases from -125 to -70 mV by the addition of 10^{-7}-10^{-6} M octanol at 10^{-6} M DAHCl (Figure 2.4, Table 2.2). This finding suggests that coadsorption of octanol brings down additional DAH^+ ions from solution. It is possible that octanol-DAH^+ complexes form in solution and, then, subsequently adsorb on the mica surface. This explanation is akin to the theory put forth by Somasundaran and his co-workers (42) that the adsorption of DAHCl on quartz is maximum at a pH closer to its pK_b (=10.2), where the concentration of the DA·DAH^+ complexes is maximum. Because of the high affinity of the octanol·DAH^+ complexes for mica surfaces, the charge is reversed at a substantially lower DAHCl concentration than without octanol. Recall that p.c.r. occurs at 10^{-5} M in the absence of octanol (Figures 2.1 and 2.6). In the presence of $5x10^{-6}$ M octanol, the charge has already been reversed at $5x10^{-6}$ M DAHCl; the data obtained from the surface force measurements can be fitted by the DLVO theory with ψ_o=+45 mV (Figure 2.5). When a smaller

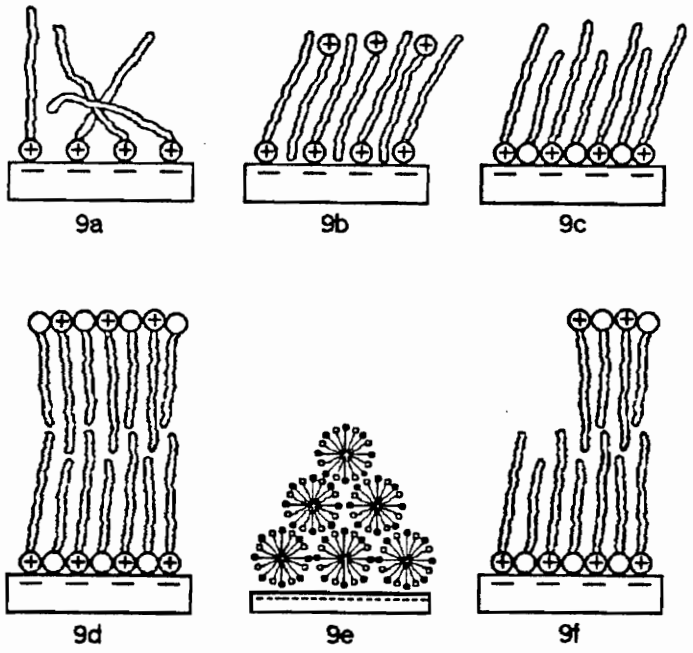

Figure 2.9. Schematic representation for the adsorption of DA^+ ions and octanol molecules on mica.

amount (10^{-6} M) of octanol is added at p.c.r., ψ_o increases further to +350 mV as shown in Figure 2.6. Under these conditions, formation of mixed bilayers such as shown in Figure 2.9d may be possible.

Two reasons may be given for the lowering of p.c.r. in the presence of octanol. One is that the repulsive electrostatic force between the charged heads is reduced, and the other is that hydrocarbon chains are more closely packed, both leading to increased negative free energy change. The lowering of p.c.r. may be similar to the lowering of c.m.c. in mixed surfactant systems; Herzfeld *et al.* (43), showed that the c.m.c. of DAHCl decreases in the presence of various alcohols. It is also consistent with earlier findings that c.h.c of DAHCL on quartz decreases in the presence of dodecanol (32). Similar conclusion can be drawn from the flotation experiment conducted in the present work.

When octanol concentration is increased beyond 10^{-5} M, very large repulsive forces, which cannot be described by the Poisson-Boltzmann equation, are observed as shown in Figure 2.7. At the same time, the contact point moves outward by 35 to 47 nm. These findings suggest that the large repulsive forces are due to a steric repulsion, which may be ascribed to multilayers of micellar adsorption as shown in Figure 2.9e. Assuming that the micellar radius is 1.8 nm, there may be 6 to 8 layers of micelles on each side of mica plates. If the micelles are of the same size and form a well-ordered

structure, the surface force measurements would have shown an oscillation (44). Since no oscillation has been observed in the present work, the micelles may be considered polydispersed and the adsorption layer disordered. It is not likely that the steric force is due to precipitation because the mixed solutions of DAHCl and octanol were clear.

Many investigators (27,28) showed that soluble surfactants (such as dodecylamine) can form self-assembled monolayers on mica surfaces, but the long-range hydrophobic force is not as large as the case for the monolayers formed by insoluble, double-chain surfactants such as dimethyldioctadecylammonium bromide (DDOAB) or acetate (DDOAA). Tsao *et al.* (24) and Rabinovich *et al.* (45) measured long-range hydrophobic forces with decay lengths in the range of 9-26 nm, while self-assembled monolayers have decay lengths in the range of 1-2 nm (9,27,28). The surface force measurements conducted in the present work with amine alone also show short decay lengths. In the presence of octanol, however, the hydrophobic forces observed with DAH^+-coated mica surfaces increase substantially, suggesting that the decay length should be higher. At $5x10^{-6}$ M DAHCl and $5x10^{-7}$ M octanol (see Figure 2.5), repulsive forces disappear completely at separation distances below 50 nm, jump distance increases to 16 nm, the adhesion force increases to 375 mN/m and the contact angle hysteresis reduces to a minimum, all of which pointing to increased hydrophobic force due to coadsorption.

The changes in decay length with octanol addition may be determined using the extended DLVO theory (3,4):

$$V_t = V_e + V_d + V_s \qquad \textbf{[4]}$$

where V_e, V_d, V_s are the electrical, dispersion, structural components of total interaction energy (V_t) between two flat surfaces. At relatively low surface potentials ($\psi_o < 50$ mV), V_e can be approximated by (46):

$$V_e = 2\varepsilon\,\varepsilon_o\kappa\,\psi_o^2 \exp(-\kappa H) \qquad \textbf{[5]}$$

in which ε_o is the permittivity of free space, ε the dielectric constant, κ the Debye reciprocal length, and ψ_o is the surface potential. The dispersion interaction energy can be obtained by (47):

$$V_d = -\frac{A_{131}}{12\pi H^2} \qquad \textbf{[6]}$$

in which A_{131} (=2.2x10^{-20} J) is the Hamaker constant for mica. Using Derjaguin's approximation (48), one can also derive an expression for V_s from Eq. [2]:

$$V_s = \frac{C_1}{2\pi}\exp(-\frac{H}{D_1}) + \frac{C_2}{2\pi}\exp(-\frac{H}{D_2}) \qquad [7]$$

The force curves obtained at $5x10^{-6}$ M DAHCl and 0 to $5x10^{-6}$ M octanol (Figure 2.5) are fitted using the extended DLVO theory (Eq. [4]), and replotted in Figure 2.10. The same data are also fitted with the classical DLVO theory (dotted lines) for comparison. As shown, the extended DLVO theory gives significantly better fit in all three cases. When no octanol is used, the data can be fitted with only a short-range hydrophobic force with D_1=1.4 nm. As the octanol concentration is increased to$5x10^{-7}$ M, it becomes necessary to use the double-exponential function with D_1=1.2 nm and D_2=6.8 nm. This is the largest decay length that has ever been observed with soluble surfactants adsorbed on mica. When the octanol concentration is increased to $5x10^{-6}$ M, V_t becomes repulsive due to the reverse orientation of the DAH^+ ions in the second layer, which gives rise to ψ_o= +45 mV. The extended DLVO fit requires V_s with D_1=1.2 nm and D_2=4.0 nm. The decrease in D_2 from 6.8 to 4.0 nm may be ascribed to the reduction of hydrophobic area by the inverse orientation of DAH^+ and octanol in the second layer (see Figure 2.9f).

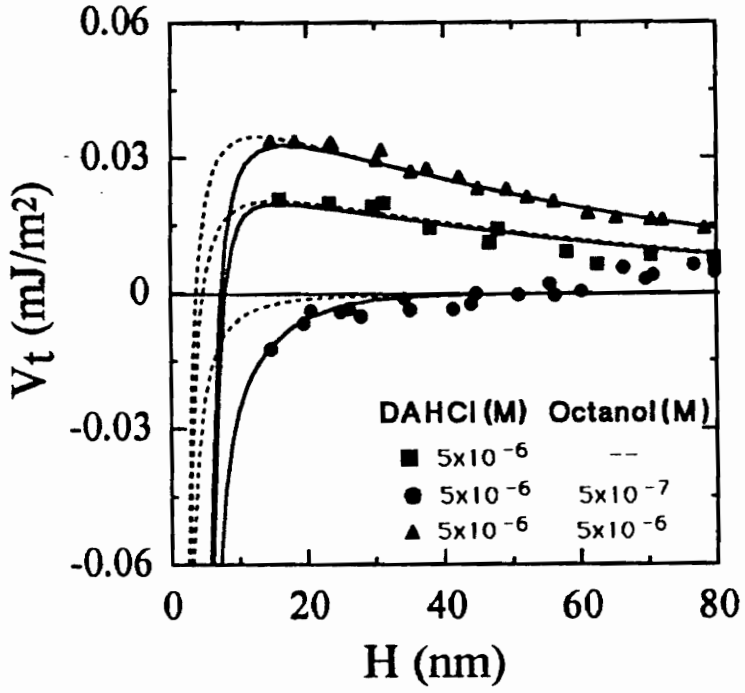

Figure 2.10. V_t vs. H between mica surfaces in $5x10^{-6}$ M of DAHCl and varying concentration of octanol at pH 5.7. The dotted and solid lines represent the classical and extended DLVO fits, respectively. The hydrophobic force parameters are as follows: C_1=-50 mN/m and D_1=1.4 nm at $5x10^{-6}$ M DAHCl; C_1=-50 mN/m, C_2=-0.5 mN/m, D_1=1.2 nm and D_2=6.8 nm at $5x10^{-6}$ M DAHCl and $5x10^{-7}$ M octanol; C_1=-50 mN/m, C_2=-0.5 mN/m, D_1=1.2 nm and D_2=4.0 nm at $5x10^{-6}$ M DAHCl and $5x10^{-6}$ M octanol.

The force measurements discussed heretofore have been conducted using the so-called `equilibrium' method. This method cannot be used for measuring strong attractive forces at closer distances, because the two surfaces jump into contact when the force gradient (*dF/dH*) exceeds the spring constant. However, by successively using stiffer springs as the distance is reduced, one can obtain a *dF/dH* (normalized by curvature *R*) vs. *H* curve as shown in Figure 2.11. The filled squares represent the data points obtained using the gradient method at 5×10^{-6} M DAHCl, 5×10^{-7} M octanol and pH 5.7. The data can be fitted by the extended DLVO theory:

$$\frac{d(F/R)}{dH} = \frac{A_{131}}{3H^3} - \frac{C_1}{D_1}\exp\left(-\frac{H}{D_1}\right) - \frac{C_2}{D_2}\exp\left(-\frac{H}{D_2}\right) \qquad \textbf{[8]}$$

which is obtained by differentiating Eq. [4], after substituting Eqs. [5]-[7] to it, assuming that $V_e=0$. The solid line going through the data points represents Eq. [8] with $A_{131}=2.2\times10^{-20}$ J, $C_1=-40$ mN/m, $C_2=-0.5$ mN/m, $D_1=1.2$ nm and $D_2=6.8$ nm. The empty circles shown in Figure 2.11 represent the data points obtained using the equilibrium method. The data, *F/R*, obtained using the equilibrium method have been converted to *d(F/R)/dH* as follows. For each *F/R* value obtained at a given *H*, a set of C_1 and C_2 values that can satisfy the following equation:

$$\frac{F}{R} = -\frac{A_{131}}{6H^2} + C_1 \exp(-\frac{H}{D_1}) + C_2 \exp(-\frac{H}{D_2}) \quad \textbf{[9]}$$

is found using the values of D_1=1.2 nm and D_2=6.8 nm. These parameters are then used to calculate the value of *d(F/R)/dH* using Eq. [8]. It is interesting that the two sets of data points obtained using the gradient and equilibrium methods are contiguous with each other.

In Figure 2.11, the dashed curve going through the points represents the force curve obtained by substituting the double-exponential function of Eq. [8] with a power law (Eq.[3]). The value of the fitting parameter used for obtaining this curve is 1.0×10^{-19} J, which is 4.5 times larger than the Hamaker constant.

Also shown in Figure 2.11 for comparison are the normalized force gradient for the van der Waals force and for the mica surfaces coated with soluble (DAHCl (27), CTAB (9)) and insoluble (DDOAA (20,24)) amines. It can be seen that in the presence of octanol the long-range hydrophobic force is observed as manifested by the large value of D_2 (=6.8 nm). Although this may be attributed to the higher degree of hydrocarbon chain ordering brought about by the coadsorption of octanol, the monolayer is still not as highly ordered as that of double-chain amines. Further work is in progress to determine the order parameters of the amine- and octanol-coated mica

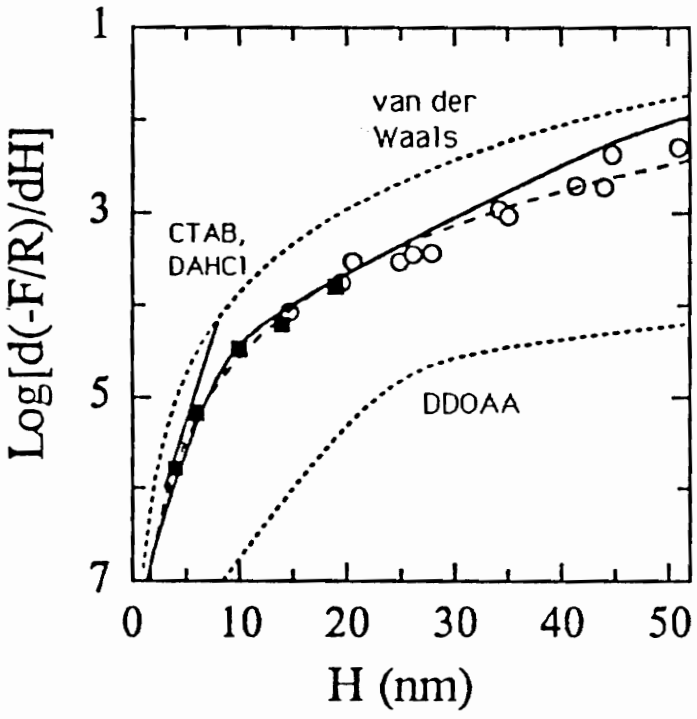

Figure 2.11. Normalized force gradient vs. H between mica surfaces in $5x10^{-6}$ M DAHCl and $5x10^{-7}$ M octanol at pH 5.7. The squares represent the data obtained using the gradient method, while the circles represent the data obtained using the equilibrium method. The solid line represents an extended DLVO fit incorporating a double exponential function for the hydrophobic force (Eq. [8]): $A_{131}=2.2x10^{-20}$ J, $C_1=-40$ mN/m, $C_2=-0.5$ mN/m, $D_1=1.2$ nm, and $D_2=6.8$ nm. The dashed line represents an extended DLVO fit with power law representing the hydrophobic force: $K=-1.0x10^{-19}$ J. Also shown for comparison are the normalized force gradients for the nonretarded van der Waals force and for the mica surfaces coated with soluble (DAHCl and CTAB) and insoluble (DDOAB) surfactants. The soluble surfactants without octanol show only the short-range hydrophobic force.

surfaces using the ATR-FTIR technique described by Rabinovich *et al.* (29).

The flotation results obtained with silica support the findings of the surface force measurements. That the floatability is increased substantially in the presence of octanol can be explained in light of the coadsorption mechanism, which is responsible for the appearance of the long-range hydrophobic force.

2.5 Conclusions

Effect of octanol addition on the surface force measurements conducted with dodecylamine-coated mica surfaces has been studied at pH 5.7. It has been found that octanol coadsorbs on mica, resulting in increased packing density and probably a higher degree of hydrocarbon chain ordering on the mica surface. The consequence of this structural change in the adsorption layer is an increased hydrophobic force. The force measurements conducted at an optimal combination of dodecylamine and octanol show net attractive forces at separation distances below approximately 50 nm. The force curve can be described by an extended DLVO theory incorporating a hydrophobic force term represented by a double exponential function with decay lengths of 1.2 and 6.8 nm. Thus, a major consequence of the octanol addition is the appearance of a long-range hydrophobic force with considerable decay length. However, the hydrophobic force is

not as strong and long-ranged as has been observed with insoluble double-chain surfactants adsorbed on mica.

The octanol addition reduces the point of charge reversal (p.c.r.), suggesting an increased adsorbability of dodecylammonium ions in the presence of a neutral surfactant. When octanol or dodecylammonium ions are added after p.c.r. has been reached, large repulsive forces are observed possibly due to the formation of mixed dodecylamine-octanol bilayers or micelles.

2.6 References

1. Churaev, N. V., and Derjaguin, B. V., *J. Colloid Interface Sci.* **103,** 542 (1985).
2. Dai, Q., Sasaki, H., Usui, S., and Kaisheva, M., *J. Colloid Interface Sci.* **139,** 30 (1990).
3. Xu, Z., and Yoon, R.-H., *J. Colloid Interface Sci.* **132,** 532 (1989).
4. Xu, Z., and Yoon, R.-H., *J. Colloid Interface Sci.* **134,** 427 (1990).
5. Yotsumoto, H., and Yoon, R.-H., *J. Colloid Interface Sci.* **157,** 426 (1993).
6. Yotsumoto, H., and Yoon, R.-H., *J. Colloid Interface Sci.* **157,** 434 (1993).
7. Yoon, R.-H., Plenary paper presented at the XVII International Mineral Processing Congress. September 23-28, Dresden, Germany; *Aufbereitungs-technik.* **32,** 474 (1991).
8. Yordan, J., Ph.D Thesis, Dept. of Mining Eng. Virginia Polytechnic Institute and State University, (1989)
9. Israelachvili, J. N., and Pashley, R. M., *J. Colloid Interface Sci.* **98,** 500 (1984).
10. Rabinovich, Y. I., and Derjaguin, B. V., " Proc. 5th Hungarian Conference on Colloid Chem. Hungary, Budapest, Lorand Eothos Univ. (1988).
11. Eriksson, J. C., Ljunggren, S., and Claesson, P. M., *J. Chem. Soc.,*

Faraday Trans. 2 **85,** 163 (1989).

12. Claesson, P. M., Blom, C. E., Herder, P. C., and Ninham, B. W., *J. Colloid Interface Sci.* **114,** 234 (1986).

13. Marcelja, S., Mitchell, D. J., Ninham, B. W., and Sculley, M. J., *J. Chem. Soc. Faraday Trans. 2* **73,** 630 (1977).

14. Luzar, A., Svetina, S., and Zeks, B., *Chem. Phys. Lett.* **96,** 485 (1983).

15. Pratt, L. R., and Chandler, D. J., *J. Chem. Phys.* **67,** 3683 (1977).

16. Rao, M., Pangali, C., and Berne, B. J., *J. Chem. Phys.* **71,** 2975 (1979).

17. Claesson, P. M., and Christenson, H. K., *J. Phys. Chem.* **92,** 1650 (1988).

18. Ruckenstein, E., and Churaev, N. V., *J. Colloid Interface Sci.* **147,** 535 (1991).

19. Podgornik, R., *J. Chem. Phys.* **91,** 5840 (1989).

20. Tsao, Y, Evans, D. F., and Wennerstrom, H., *Langmuir* **9,** 779 (1993).

21. Rabinovich, Y. I., Guzonas, D. A., and Yoon, R.-H., *Langmuir* **9,** 1168 (1993).

22. Pashley, R. M., McGuiggan, P. M., Ninham, B. W. and Evans, D. F., *Science* **229,** 1088 (1985).

23. Parker, J. L., Cho, D. L., and Claesson , P. M., *J. Phys. Chem.* **93,** 6121 (1989).

24. Tsao, Y, Yang, S. X., Evans, D. F.,and Wennerstrom, H., *Langmuir* **7,** 3154 (1991).

25. Christenson, H. K., Fang, J., Ninham, B. W., Parker, J. L., *J. Phys. Chem.* **94,** 8004 (1990).

26. Christenson, H. K., Claesson, P. M., Berg, J., Herder, P. M., *J. Phys. Chem.* **93,** 1472 (1989).

27. Herder, P. C., *J. Colloid Interface Sci.* **134,** 346 (1990).

28. Rutland, M., Waltermo, A., and Claesson, P. M., 1992, *Langmuir* **8,** 176 (1992).

29. Rabinovich, Y. I., Guzonas, D. A., and Yoon, R.-H., *J. Colloid Interface Sci.* **155,** 221 (1993).

30. Rabinovich, Y. I., and Derjaguin, B. V., *Colloids Surf.* **30,** 243 (1988).

31. Gaudin, A. M., and Fuerstenau, D. W., *Trans AIME.* **202,** 958 (1955).

32. Smith, R. W., *Trans AIME.* **226,** 427 (1963).

33. Tabor, D., and Winterton, R. H. S., *Proc. R. Soc. London,* A **312,** 435, (1969)

34. Israelachvili, J. N., and Adams, G. E., *J. Chem. Soc., Faraday Trans. 1* **74,** 975 (1978).

35. Chan, D. Y. C., Pashley, R. M., and White, L. R., *J. Colloid Interface Sci.*

77, 283 (1980).

36. Israelachvili, J. N., *Surface Science Reports,* **14,** 109 (1992).

37. Chen, Y. L., Chen, S., Frank, C., and Israelachvili, J. N., *J. Colloid Interface Sci.* **153,** 244 (1992).

38. Castro, S. H., Vurdela, R. M., and Laskowski, J. S., *Colloids Surf.* **21,** 87 (1986).

39. Parker, J. L., Yaminsky, V. V., and Claesson, P. M., *J. Phys. Chem.* **97,** 7706 (1993).

40. Laskowski, J. S., " Challenges in Mineral Processing," Eds. K.V.S. Sastry and M. C. Fuerstenau, AIME, pp 15-34, (1988).

41. Ravishankar, S. A., and Yoon, R.-H., manuscript in preparation

42. Somasundaran, P., and Ananthapadmanabhan, K. P.," Solution Chemistry of Surfactants," Ed. Mittal, K. L., **2,** p. 777. Plenum Press. New York. 1979.

43. Herzfeld, S. H., Corrin, M. L., and Harkins, W. D., *J. Physical and Colloid Chemistry,* **54,** 271 (1950).

44. Bergeron, V., and Radke, C. J., *Langmuir* **8,** 3021 (1992).

45. Rabinovich, Y. I., Guzonas, D. A., and Yoon, R.-H., to be published.

46. Derjaguin, B. V., Churaev, N. V., and Muller., *Surface Forces* Consultants Bureau, New York, (1987).

47. Israelachvili, J. N., Intermolecular and Surface Forces, Academic Press 1990.

48. Derjaguin, B. V., *Kolloid. Zh.* **69,** 155 (1934).

CHAPTER 3 LONG-RANGE HYDROPHOBIC FORCES WITH DODECYLAMINE COATED MICA SURFACES IN THE PRESENCE OF DODECANOL

3.1 Introduction

Direct force measurements conducted with mica (1-4) and silica (5) in the presence of water soluble amines such as dodecylamine hydrogenchloride (DAHCl) and cetyltrimethylammonium bromide (CTAB) showed the presence of attractive forces that are stronger than the London-van der Waals dispersion forces originating from fluctuating electromagnetic dipole moments. The attractive forces are referred to as hydrophobic forces, whose origin is a subject of considerable debate. The hydrophobic forces measured with water-soluble surfactants are relatively short-ranged, being discernible at separation distances in the 0-15 nm range. The measured hydrophobic forces (F) are usually described using an exponential function:

$$\frac{F_h}{R} = C_O \exp\left\{-\frac{H}{D_O}\right\}, \qquad [1]$$

in which H is the closest separation distance between two curved surfaces with curvature R, and C_0 and D_0 are constants. With soluble surfactants, the decay length (D_0) are usually in the range of 1-2 nm.

When the force measurement were conducted with insoluble double-chain surfactants deposited on mica surfaces using the Langmuir-Bloggett technique, the attractive hydrophobic forces were measurable up to 100 nm separation distances (6-11). The measured forces are usually described by a double exponential function:

$$\frac{F}{R} = C_1 \exp\left\{-\frac{H}{D_1}\right\} + C_2 \exp\left\{-\frac{H}{D_2}\right\}, \qquad \textbf{[2]}$$

in which the first term represents the "short-range" hydrophobic forces, the second term representing the "long-range" hydrophobic forces. The results obtained with dioctadecyldimethylammonium (DDOA) bromide (6-9) and fluorocarbon surfactants (10,11) on mica and octadecylchlorosilane (ODTCS) on silica (12) show D_1 in the range of 1-2 nm and D_2 in the range of 10-26 nm.

It is also possible to describe the long-range hydrophobic forces using a power law (13):

$$\frac{F}{R} = -\frac{K}{6H^2}, \qquad \textbf{[3]}$$

where K is a constant. Eq. [3] is of the same form as the non-retarded van der Waals force; therefore, one can directly compare the values of K with the Hamaker constants. The values of K obtained with ODTCS-coated silica surfaces are in the range of 2.8-3.5x10^{-16} J (12), which are more than three-orders of magnitudes larger than the Hamaker constants of silica in water (10^{-20} J). Eq. [3] was also used for describing the forces measured with mica surfaces coated with a mixed monolayer of dodecylamine and octanol (14); the K values is 3.3x10^{-19} K, which is an order of magnitude larger than the Hamaker constant of mica in water (2.2x10^{-20} J).

The reason that water-soluble, single-chain surfactants give only short-range hydrophobic forces with D_2 less than 2 nm can be attributed to the geometric constraints associated with the adsorption mechanism. Single-chain cationic surfactants adsorb on mica at the centers of oxygen hexagons vacated by K^+ or Na^+ ions. Each adsorption site represents 0.49 nm^2 of the surface, while each hydrocarbon chain in a close-packed monolayer occupies only 0.20 nm^2. Therefore, single-chain surfactants cannot form close-packed monolayers on mica. Double-chain cationic surfactants such as DDOA, on the other hand, can be deposited on mica by the L-B technique to form a close-packed monolayer. Thus, it may be necessary to have close-packed monolayers to create long-range hydrophobic forces. A close-packed monolayer presents a layer of well-ordered hydrocarbon chains to the aqueous phase, which may affect the ordering of water molecule in the vicinity and contribute to creating long-range hydrophobic forces.

Furthermore, a vertical orientation of hydrocarbon chains presents CH_3 groups which are more hydrophobic than CH_2 groups (15). It has been shown that an increase in hydrocarbon chain ordering increases the hydrophobic force. (8,9,13). It has also been shown that long-range hydrophobic forces can be observed with soluble, single chain surfactants such as DAHCl in the presence of neutral surfactant such as octanol (14). It is believed that the neutral surfactant coadsorb in-between the dodecylammonium (DAH^+) ions adsorbed on mica, so that close-packed monolayers can be formed.

It is now well established that surfactant adsorption occurs in patches. Fuerstenau and his co-workers (16,17) recognized changes in slope in their adsorption isotherms, which was ascribed to hemimicelle formation on the surface. When hydrocarbon chains associate with each other, the water molecules forming the "ice-berg" structures around neighboring chains are squeezed out into solution, resulting in an increase in the entropy of the system and, hence, the free energy of adsorption. The hydrocarbon chain association is distinguished from the hydrophobic interaction between macroscopic bodies in that it is controlled by the short-range forces (shorter than D_0, D_1 and D_2) related to the ice-berg structure.

Some investigators consider that hydrophobic forces originate from the correlation of large dipole moments (12,13,17) or charges (18,19) associated with domains (patches or hemimicelles). In addition to being able to explain the long-range hydrophobic forces observed in experiments, the proposed models provide an explanation

for the screening effects due to electrolytes (8,9). Other investigators consider cavitation as the origin of hydrophobic force (20.21). Thermodynamically, macroscopic cavitation should occur only on or near hydrophobic surfaces whose contact angles are greater than 90°; however, hydrophobic forces are observed with less hydrophobic surface (1-4). Furthermore, the macroscopic cavitation has not been observed during the approach cycles of direct force measurements, possibly due to the large activation energies involved in cavitation (21,22). For these reasons, Yaminsky and Ninham (23) considered density fluctuations due to subcritical cavitation as the origin of hydrophobic forces.

In the proposed work, surface force measurements have been conducted with mica surfaces in the presence of DAHCl and dodecanol. The neutral surfactant may overcome the geometric constraints in forming close-packed monolayers on mica, and thereby give rise to long-range hydrophobic forces. The hydrophobic forces may be stronger than the case of using octanol as the coadsorbing neutral surfactant due to the longer hydrocarbon chain. The results are compared with those reported in literature to discuss the origin of hydrophobic forces.

3.2 Experimental

3.2.1 Materials

Dodecylamine hydrochloride (DAHCl) and dodecanol were obtained from Eastman Kodak Co. The dodecylammonium salt was recrystallized from ethanol before use, while dodecanol was used as received. Reagent grade potassium chloride was obtained from Fischer Scientific Co, and roasted at 600 °C before use to remove possible organic impurities. Conductivity water was prepared by passing double-distilled water through a Nanopure II water treatment unit and deaerating it under vacuum for three hours.

3.2.2 Surface forces measurements

Direct force measurements were carried out using a Mark IV surface force apparatus (from Anutech Pty.), which is similar to that of Tabor (24) and Israelachvili (25). Two molecularly smooth mica surfaces were silvered on one side and then glued silver-side down onto silica disks using Epon 1004 (Epoxy resin) from Shell Chemical Co. The separation distance between the two mica surfaces was measured using the multiple beam interferometry technique based on the method of fringes of equal chromatic order (FECO) (26). The separation was measured with an accuracy of ±0.2

nm. The surface force apparatus was controlled using the SF-Scribe CV-78 software on a Macintosh computer.

In each experiment, the zero separation distance was determined in air before filling the stainless steel chamber of the SFA with solution. The force-distance curve obtained in Nanopure water at pH 5.7 was compared with those in literature (3,14,) to ensure that the mica surfaces were clean. A stock solution of DAHCl (10^{-3} M) was prepared in Nanopure water, while a stock solution of dodecanol (10^{-3} M) was prepared in absolute alcohol because of its low solubility in water. Requisite amounts of these stock solutions were injected to the Nanopure water in the chamber to obtain a solution containing desired amounts of DAHCl and octanol. The amine stock solution was injected with the mica surfaces separated by 1 mm. The measurements were initiated after three hours of equilibration. After completion of the force measurements with amine alone, the mica surfaces were separated by 1 mm from each other and then an aliquot of the dodecanol stock solution was injected. The force measurements were initiated three hours after the injection of dodecanol solution to ensure equilibration. In each force measurement, the adhesion force (F(0)/R) and the jump distance were also measured.

In force measurements, two surfaces jump into contact when the slope of the force curve becomes equal to or greater than the spring constant (k). By successively increasing k, one can measure stronger forces (or pressures) at closer distances. This

method is referred as "jump" method. In these measurements, the values of k, which is equal to the force derivative normalized by the radius of curvature (d(F/R)/dH), is plotted as a function of the distance (H) at which the jump occurs.

3.2.3 Contact angle measurements

Freshly cleaved mica surfaces were immersed in solutions of different DAHCl and dodecanol compositions at pH 5.7. After three hours of equilibration, the mica sheets were pulled out of the solution and blow-dried in a stream of nitrogen. The water contact angles (both advancing and receding) were measured using the sessile drop technique using a Rame-Hart goniometer. Approximately ten measurements were made at various spots on a mica sheet and averaged.

3.3 Results

3.3.1 Direct force measurements

Figure 3.1 shows the force *vs.* distance curves obtained in Nanopure water and in a $5x10^{-5}$ M dodecanol solution at pH 5.7. The theoretical DLVO curves, obtained by using the algorithm developed by Chan *et al.* (27), are also shown for comparison. The upper curve is based on the constant charge model, while the lower one represents the

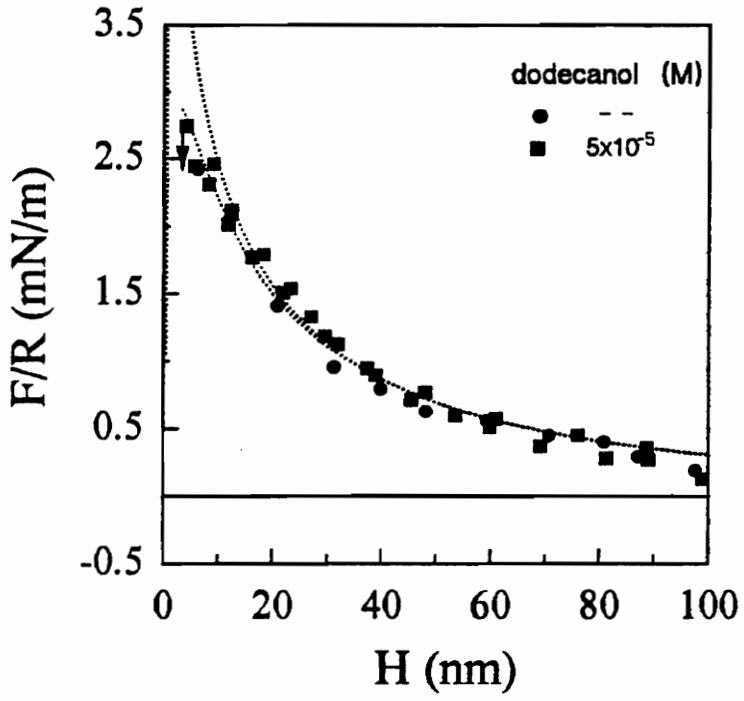

Figure 3.1. *F/R vs. H* between mica surfaces with and without dodecanol solutions at pH 5.7. The upper and lower curves (dotted lines) represent the constant charge and constant potential models of the DLVO theory, respectively. The DLVO theoretical curves were obtained using A_{131}=2.2x10^{-20} J, Ψ_o=-170 mV and κ^{-1}=96.0 nm for Nanopure water and 5x10^{-5} M dodecanol. The arrows represent the distance at which the two surfaces jump into contact due to attractive forces.

constant potential model. Both have been obtained using: Hamaker constant (A_{131}) of $2.2x10^{-20}$ J, Debye length (κ^{-1}) of 96 nm, and surface potential (ψ_o) of -170 mV.

As is shown in Figure 3.1, the force *vs.* distance curves obtained with or without dodecanol are practically the same, indicating that there is no detectable adsorption of dodecanol on mica in Nanopure water. A similar observation was made with octanol as described in Chapter 2 and in Reference 14.

Since the dodecanol stock solution was prepared in ethanol, the force measurements were also conducted in 0.05% and 1% ethanol solutions in the presence of 10^{-6} M DAHCl. As shown in Fig. 3.2, the force curves obtained with and without ethanol (up to 1%) are practically the same, indicating that the short chain alcohol does not influence the adsorption of DAH^+ ions on the mica surface.

Figure 3.3 shows the force measurements conducted in a 10^{-6} M of DAHCl solution with and without dodecanol. With DAHCl alone, the measured force curve is repulsive; however, the repulsive force is weaker than that measured in Nanopure water (see Fig. 3.1). The data can be fitted to the constant charge and constant potential models of the DLVO theory using the parameters of ψ_o=-125 mV and κ^{-1} =76.1 nm. The decrease in the repulsive force may be attributed largely to the charge neutralization of mica surfaces due to the adsorption of DAH^+ ions. The attractive hydrophobic force created by the adsorption of DAH^+ ions may also contribute to the reduced repulsive force; however, the attractive forces are discernible only at shorter separation distances

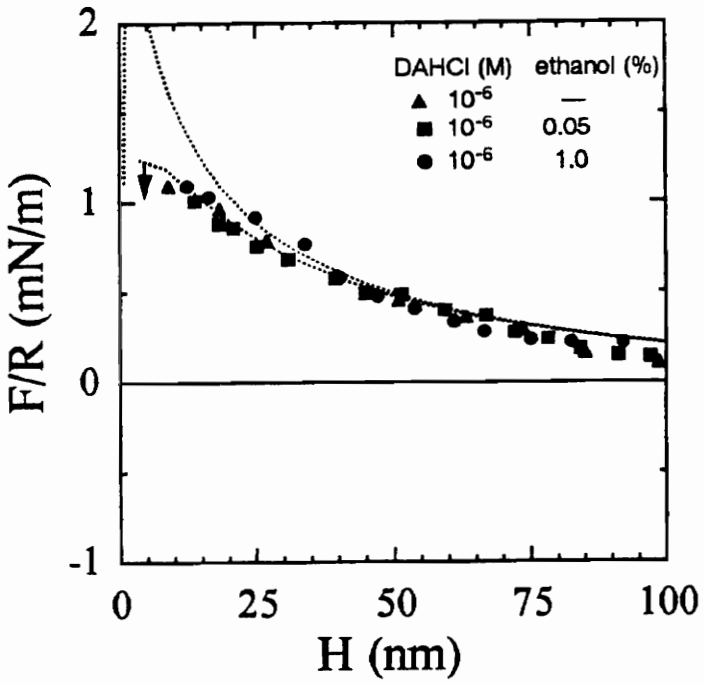

Figure 3.2. *F/R vs. H* between mica surfaces in 10^{-6} M DAHCl with and without ethanol at pH 5.7. The upper and lower curves (dotted lines) represent the constant charge and constant potential models, respectively, of the DLVO theory obtained using A_{131}=2.2x10^{-20} J, Ψ_o=-125 mV and κ^{-1}=76.1 nm. The arrow shows the jump distance.

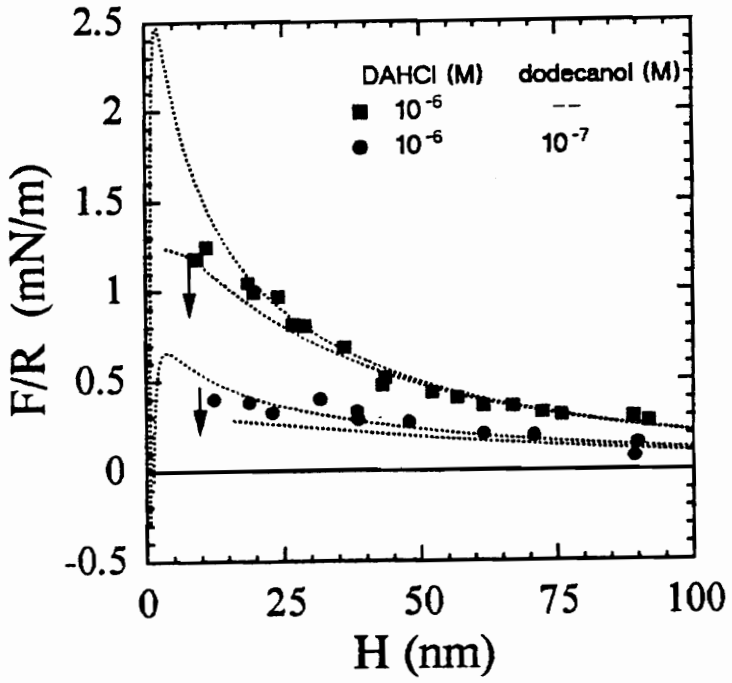

Figure 3.3. *F/R vs. H* between mica surfaces in 10^{-6} M DAHCl solutions with varying amounts of dodecanol at pH 5.7. The upper and lower curves (dotted lines) represent the constant charge and constant potential models, respectively, of the DLVO theory obtained using A_{131}=2.2x10^{-20} J, Ψ_o=-125 mV and κ^{-1}=76.1 nm without dodecanol; Ψ_o=-70 mV and κ^{-1}=76.1 nm with 10^{-7} M dodecanol; and -70 mV and 76.1 nm at 10^{-6} M dodecanol. The arrows show the jump distance.

(H<10 nm). As a result of this short-range hydrophobic force, the two mica surfaces jump into contact at 7 nm (Table 3.1). This distance is 4-5 nm larger than those predicted by the DLVO theory, in which van der Waals force is the only attractive force considered.

In the presence of dodecanol (10^{-7} M) and DAHCl (10^{-6} M), the repulsive force is further reduced beyond what can be obtained with DAHCl alone. One might consider that the decrease in the repulsive force may be due to the increase in the hydrophobic force caused by the adsorption of dodecanol; however, the decrease is too large to be accounted for by the hydrophobic force alone particularly at larger separation distances. Therefore, the decrease in repulsive force is largely due to the additional adsorption of DAH^+ ions caused by dodecanol. The force curve obtained in the presence of dodecanol can be fitted by the DLVO theory with ψ_o=-70 mV, which is substantially less negative than that (ψ_o=-125 mV) obtained without dodecanol. The additional adsorption of DAH^+ ions increases the area per charge from 65 to 184 nm^2 as shown in Table 3.1. Note here that the jump distance increases from 7 to 11 nm in the presence of dodecanol, which suggests that the dodecanol addition also increases the attractive hydrophobic force. Thus, the increased hydrophobicity may be attributed to an increased adsorption of both DAH^+ ions and dodecanol. This observation is consistent with the coadsorption mechanism proposed by Fuerstenau (17) and Smith (28) to explain increased water contact angle on quartz when DAH^+ ions are co-present with neutral surfactants such as DAHCl and normal alcohol.

TABLE 3.1

Results of surface force and contact angle measurements with dodecylamine hydrochloride in the presence of octanol and dodecanol at pH 5.7

Concentration (M)			Area per Charge	Surface Potential	Jump Distance	Adhesion Force	Contact Angle (deg)			Force Parameters (mN/m)		(nm)		(10^{-19} J)
DAHCl	Dodecanol	Octanol	(nm^2)	ψ_0 (mV)	(nm)	(mN/m)	θ_a	θ_r	(θ_a-θ_r)	C_1	C_2	D_1	D_2	K
$1x10^{-6}$	--	--	65.0	-125.0	7.0	150	83	45	18	--	--	--	--	--
$1x10^{-6}$	$1x10^{-7}$	--	184.0	-70.0	11.0	200	64	45	20	-40	--	1.0	--	--
$5x10^{-6}$	--	--	410.0	-35.0	14.0	250	80	60	20	-40	--	1.1	--	--
$5x10^{-6}$	--	$5x10^{-7}$	--	--	18.0	350	84	72	12	-40	-0.5	1.2	6.8	1.0
$5x10^{-6}$	--	$5x10^{-6}$	303.0	+45	16.0	350	84	65	19	-40	-0.5	1.2	4.0	0.7
$5x10^{-6}$	$1x10^{-7}$	--	--	--	18.0	375	88	80	8	-45	-1.2	1.2	6.8	1.5
$5x10^{-6}$	$5x10^{-7}$	--	--	--	24.0	400	88	86	4	-45	-1.2	1.3	9,0	3.3
$5x10^{-6}$ *	$5x10^{-7}$	--	688.8	+10.0	9.0	300	86	68	20	-10	-0.35	1.2	4.5	--
$5x10^{-6}$	$5x10^{-6}$	--	151.0	+90.0	14.0	350	88	78	10	-40	-1.0	1.2	4.5	0.8
10^{-5}	--	--	--	0.0	14.0	250	85	65	20	-45	--	1.3	--	--

* contains $1\ 0^{-4}$ M KCl

The force measurements obtained at a higher concentration of DAHCl ($5x10^{-6}$ M) are shown in Figure 3.4. In the absence of dodecanol, the data can be fitted by the DLVO theory with ψ_o=-35 mV, with the 'jump' occurring at H=14.0 nm. When 10^{-7} M of dodecanol is added, the repulsive force becomes almost zero at longer separation distances, but in the 0-40 nm range the force becomes net attractive. The attractive force is significantly stronger than the non-retarded van der Waals force (or DLVO forces at ψ_o=0). Furthermore, the jump distance becomes as large as 18.0 nm in the presence of dodecanol, while at the same time a large adhesion force (350 mN/m) is observed as shown in Table 3.1. The thickness of the adsorbed layer is about 0.8 nm. These results demonstrate that in the presence of dodecanol, the hydrophobicity of DAH^+-coated mica surface is greatly increased. It may be noted that the attractive forces obtained at $5x10^{-7}$ M octanol are comparable to those obtained at $1x10^{-7}$ M dodecanol in the presence of $5x10^{-6}$ M of DAHCl (Chapter 2; Reference 14). That dodecanol requires five times lower concentration as compared to octanol may be attributed to its longer hydrocarbon chain. It appears that the longer chain alcohol can more readily coadsorb with DAH^+ ions forming a more close-packed monolayer. Rabinovich and Yoon (12) showed that an increased ordering of hydrocarbon chains, which is caused by increased packing density, gives rise to a stronger hydrophobic force.

When dodecanol concentration is increased to $5x10^{-7}$ M at $5x10^{-6}$ M DAHCl, the surface force becomes attractive at separation distances as far as 75 nm. This represents

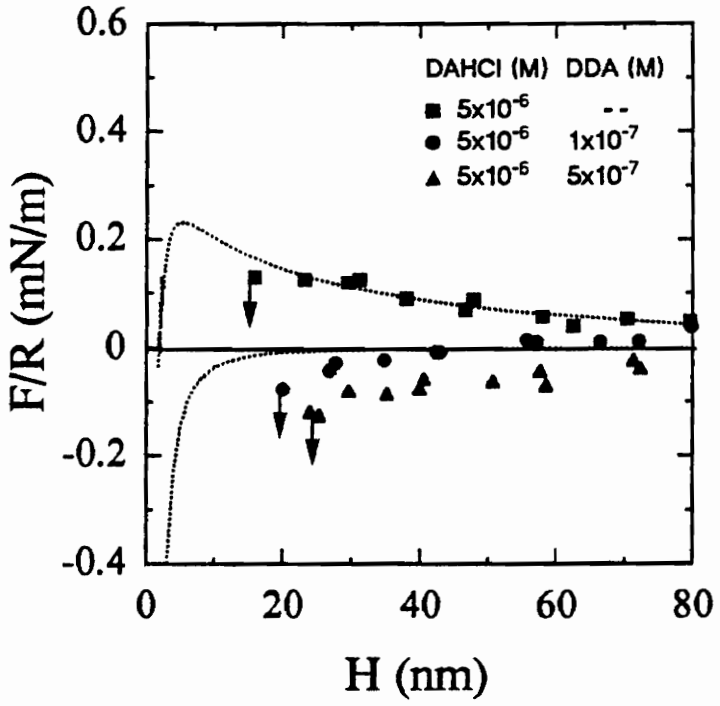

Figure 3.4. *F/R vs. H* between mica surfaces in $5x10^{-6}$ M DAHCl solutions with varying amounts of dodecanol at pH 5.7. The upper dotted line (dotted line) represents the constant charge model of the DLVO theory obtained using A_{131}=$2.2x10^{-20}$ J, Ψ_o=-35 mV and κ^{-1}=68.0 nm without dodecanol and the lower dotted line indicate the van der Waals force with Ψ_o=0 mV and A_{131}=$2.2x10^{-20}$ J at $1x10^{-7}$ M and $5x10^{-7}$ M dodecanol. Note that the attractive forces measured in the presence of dodecanol is much stronger than the van der Waals forces, suggesting that there is long-range hydrophobic force. The arrows show the jump distance.

the longest net attractive force reported in the literature with water-soluble surfactants adsorbed on mica. The strong attractive force causes a jump to occur at 24 nm, and gives rise to a large adhesion force (400 mN/m) as shown in Table 3.1. Also, the thickness of the adsorbed layer increases from 0.8 to 1.1 nm as the dodecanol concentration increases from 10^{-7} to $5x10^{-7}$ M, suggesting that the hydrocarbon chains stand up more vertically due to increased packing density.

The long-range attractive forces measured in the presence of dodecanol with $5x10^{-6}$ M DAHCl can be deconvoluted using the extended DLVO theory (14), according to which the total interaction energy (V_t) can be given as (14):

$$V_t = V_e + V_d + V_s \qquad \textbf{[4]}$$

where V_e, V_d,, and V_s are the electrical, dispersion and structural components of the total interaction energy (V_t) between two flat surfaces. The expressions for V_e and V_d are the same as those detailed in the procedure given in reference 14 (chapter 2). Using Derjaguin's approximation (29), an expression for V_s can be derived from Eq. [2] as:

$$V_s = \frac{C_1}{2\pi}\exp\left\{-\frac{H}{D_1}\right\} + \frac{C_2}{2\pi}\exp\left\{-\frac{H}{D_2}\right\}, \qquad \textbf{[5]}$$

and from Eq. [3] as:

$$V_s = \frac{-K}{12\pi H^2}. \qquad \textbf{[6]}$$

Eq. [6] has advantages over Eq. [5] in that it has only one parameter (K), and that it is of the same form as that of dispersion force; therefore, the value of K may be directly compared with the Hamaker constant. Shown in Figure 3.5 are the V_t vs. H profiles obtained from the data shown in Figure 3.4 using Derjaguin's approximation (29). The DLVO curves are represented by the solid lines while Eq. [4] with the exponential force law (Eq. [5]) and with power law (Eq. [6]) are shown by dashed and dotted lines, respectively. Clearly, the extended DLVO theory including the hydrophobic energy gives a better fit in all the cases.

The most significant finding from these results is the appearance long-range net attractive force. In the absence of dodecanol, the data can be fitted by the extended DLVO theory with a short-range (D_0 =1.4 nm) hydrophobic energy term. There is no need to consider contributions from a long-range hydrophobic force term to fit the data, i.e., D_2=0. In the presence of 10^{-7} M dodecanol, however, it is necessary to use Eq. [5] (dashed line) with C_1=-45 mN/m, D_1=1.2 nm, C_2=-1.2 mN/m and D_2=6.8 nm. At 5×10^{-6} M DAHCl and 10^{-7} M dodecanol, the power law fitting coefficient (K) is about 1.5×10^{-19} J, which is 7 times larger than the Hamaker constant. Note that the hydrophobic force parameters (D_2=6.8 nm and K=1.5×10^{-19} J) obtained with 5×10^{-6} M DAHCl and 10^{-7} M dodecanol are comparable to those obtained with 5 times higher concentration of octanol at the same DAHCl concentration (14). The results suggest that the longer hydrocarbon chain alcohol is more effective in creating long-range hydrophobic force.

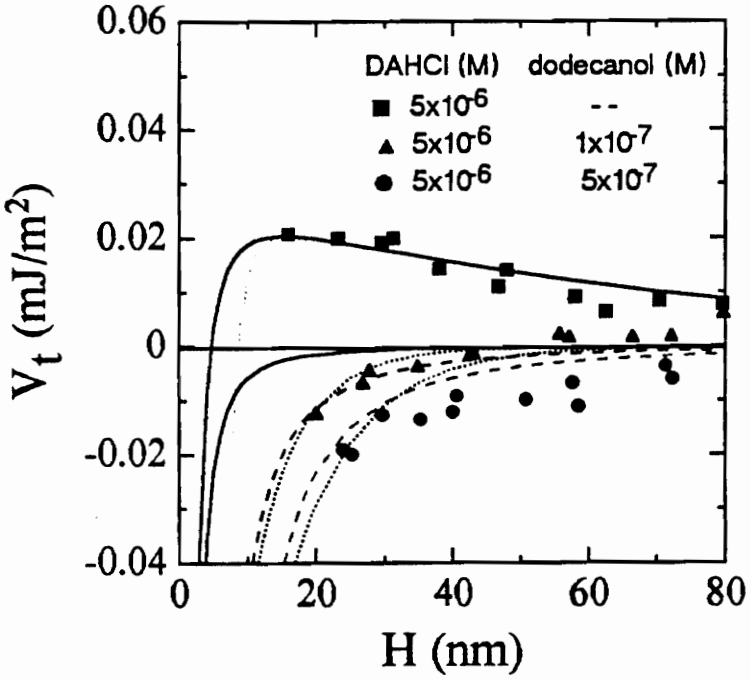

Figure 3.5. V_t *vs.* H between mica surfaces in 5x10^{-6} M of DAHCl and varying concentration of dodecanol at pH 5.7. The energy vs distance profiles are fitted using classical (solid lines) and extended DLVO theory including hydrophobic force described by double-exponential form (Eq. [2]; dotted lines) and power law function (Eq. [3]; dashed lines). The hydrophobic force parameters for the double exponential form are as follows: C_1=-50 mN/m and D_1=1.4 nm at 5x10^{-6} M DAHCl; C_1=-50 mN/m, C_2=-1.2 mN/m, D_1=1.2 nm and D_2=6.9 nm at 5x10^{-6} M DAHCl and 1x10^{-7} M dodecanol; C_1=-50 mN/m, C_2=-1.2 mN/m, D_1=1.2 nm and D_2=9.0 nm at 5x10^{-7} M DAHCl and 5x10^{-7} M dodecanol. The power law fitting coefficients are found to be 1.5x10^{-19} and 3.3x10^{-19} J when the dodecanol concentrations are, respectively, 1x10^{-7} and 5x10^{-7} M.

When the dodecanol concentration is increased from 10^{-7} to $5x10^{-7}$ M in $5x10^{-6}$ M DAHCl solution, even stronger attractive energies are shown (see Figure 3.5). At $5x10^{-7}$ M dodecanol, D_2 increased from 6.8 to 9.0 nm with other hydrophobic force parameters remaining about the same as those obtained with 10^{-7} M dodecanol (see Table 3.1). This is the largest long-range decay length reported in the literature with water soluble surfactants. Also, with the increase in dodecanol concentration from 10^{-7} to $5x10^{-7}$ M, the power law fitting coefficient (K) increased from $1.5x10^{-19}$ to $3.3x10^{-19}$. Note also that the value of K obtained with $5x10^{-7}$ M dodecanol was three-times larger than that with octanol, suggesting that the hydrocarbon chain length plays an important role in determining the magnitudes of the long-range hydrophobic forces.

Figure 3.6 shows the d(-F/R)dH *vs.*H plot obtained using the jump method in a solution containing $5x10^{-6}$ M DAHCl and $5x10^{-7}$ M dodecanol. By dividing the values given in the ordinate with 2π, one can convert the data to disjoining pressure. An important advantage of the jump method is that force measurements can be made at closer separation distances than using the equilibrium method. The data obtained in the present work are compared with the values of d(-F/R)/dH calculated for the van der Waals attraction (upper dashed line) and the force measurements conducted using mica surfaces coated with CTAB (1,2), DAHCl (3,4) and DDOA monolayers (6-9). Also shown for comparison are the d(-F/R)/dH values obtained in a $5x10^{-6}$ M DAHCl solution containing $5x10^{-7}$ M of octanol (14) (solid squares). Clearly, the attractive force

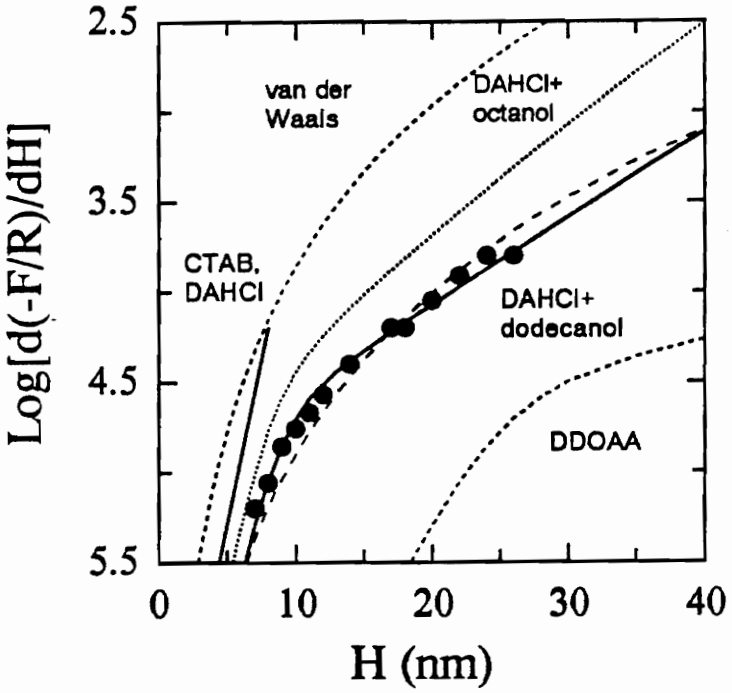

Figure 3.6. Normalized force gradient vs. H between mica surfaces in $5x10^{-6}$ M DAHCl and $5x10^{-7}$ M dodecanol at pH 5.7. The solid line represents an extended DLVO fit incorporating a double-exponential function for the hydrophobic force (Eq. [9] and [12]): A_{131}=2.2x10^{-20} J, C_1=-45 mN/m, C_2=-1.2 mN/m, D_1=1.3 nm, and D_2=9.0 nm. The broken line represents an extended DLVO fit with power law representing the hydrophobic force (Eq. {9] and [13]): K=3.3x10^{-19} J. Shown for comparison are the normalized force gradients for the nonretarded van der Waals force (upper dashed line). Also indicated are the force gradients obtained with the mica surfaces coated with soluble DAHCl and CTAB (solid straight line) and the double exponential fit obtained for the force gradients data using insoluble (DDOAB) surfactants (lower dashed line) and DAHCl/octanol mixed monolayer (dotted line) (14). The DAHCl and dodecanol mixed monolayers show stronger hydrophobic forces compared to pure DAHCl/octanol mixed monolayers.

measurements (solid circles) made in the presence $5x10^{-6}$ M DAHCl and $5x10^{-7}$ M dodecanol are stronger than the van der Waals force and the short-range hydrophobic forces measured with DAHCl or CTAB (solid straight line) alone. On the other hand, they are substantially weaker than those measured using mica surfaces coated with insoluble double-chain surfactants such as DDOAA (8) (lower dashed line). An important observation to be made with Figure 3.6 is that the forces measured in the presence of $5x10^{-7}$ M dodecanol and $5x10^{-6}$ M DAHCl are considerably stronger than those obtained with $5x10^{-7}$ M octanol and $5x10^{-6}$ M DAHCl, indicating that the effect of chain length of coadsorbing long-chain alcohols on the long-range hydrophobic forces.

The attractive forces measured by the 'jump' method can be also used to determine the decay lengths (D_2) with help of the extended DLVO theory. According to the extended DLVO theory, the total disjoining pressure (Π) may be given as:

$$\Pi = \Pi_e + \Pi_d + \Pi_h \qquad [7]$$

where Π_e, Π_d, and Π_h are the electrical, dispersion and hydrophobic components of disjoining pressure. The disjoining pressure (Π) can be related to force gradient between curved surfaces as:

$$\Pi = -\frac{1}{2\pi}\frac{d(F/R)}{dH}. \qquad [8]$$

From Eqs. [7] and [8], one can obtain:

$$\frac{d(F/R)}{dH} = \frac{d(F_e/R)}{dH} + \frac{d(F_d/R)}{dH} + \frac{d(F_h/R)}{dH} \qquad [9]$$

where the subscripts *e*, *d*, and *h* refer to the electrical, dispersion, and hydrophobic component of the force gradients.

At low surface potentials ($|\psi_o|<25$ mV), the electrical component of Eq. [9] becomes:

$$\frac{d(F_e/R)}{dH} \cong -\frac{\varepsilon\varepsilon_o}{\pi}\kappa^2\psi_o^2 e^{-\kappa H}, \qquad [10]$$

in which ε_o is the permittivity of free space, ε the dielectric constant of the medium (water), κ^{-1} the Debye length, and ψ_o the surface potential. Also, the dispersion component of Eq. [9] becomes:

$$\frac{d(F_d/R)}{dH} = \frac{A_{131}}{3H^3}, \qquad [11]$$

in which A_{131} (=2.2x10^{-20} J) is the Hamaker constant for mica.

On the other hand, the hydrophobic force component of Eq. [9] can be given in two different functional forms as described previously. One is in double-exponential form:

$$\frac{d(F_h / R)}{dH} = -\frac{C_1}{D_1}\exp\left\{-\frac{H}{D_1}\right\} - \frac{C_2}{D_2}\exp\left\{-\frac{H}{D_2}\right\}, \qquad \textbf{[12]}$$

in which all the parameters have the same meanings as in Eq. [2], and the other is a power law (13,14):

$$\frac{d(F_h / R)}{dH} = \frac{K}{3H^3} \qquad \textbf{[13]}$$

in which K is a constant.

Figure 3.6 shows the extended DLVO fits for the data obtained in a solution containing 5×10^{-7} M dodecanol and 5×10^{-6} M DAHCl: the solid line represents Eq. [9] with Eq. [12] for the hydrophobic force term, while the dotted line represents Eq. [9] with Eq. [13] for the hydrophobic force term. Also shown in this figure for comparison is the double-exponential fit (dotted line) for the data obtained with 5×10^{-7} M octanol 5×10^{-6} M DAHCl. Only the unretarded van der Waals and hydrophobic forces have been considered, while the double-layer force is assumed to be zero. As shown, the double-

exponential form appears to fit the data better than the power law for the DAHCl/dodecanol system. It has been shown, however, that reverse is true for the DAHCl/octanol system (14). Table 3.1 shows the hydrophobic force parameters used to fit the experimental data using the extended DLVO theory. Note that use of dodecanol in place of octanol affects mainly the long-range component of the hydrophobic force: at $5x10^{-6}$ M DAHCl and $5x10^{-7}$ M octanol or dodecanol, C_2 decreases from -0.5 to -1.2 mN/m and D_2 increases from 6.8 to 9.0 nm, while the changes in C_1 and D_1 are minimal.

Figure 3.7 shows the effect of 10^{-4} M KCl on the surface forces measured in the presence of $5x10^{-6}$ M DAHCl and $5x10^{-7}$ M dodecanol. The KCl addition causes the net attractive force to disappear. In fact, the force curve can be fitted by the DLVO theory with ψ_o=10 mV and κ^{-1}=30.4 nm. Also, there is a marked decrease in the jump distance from 24 to 9 nm. Inspite of the disappearance of the net attractive force and the decrease in jump distance, the force data can not be fitted without considering contributions from hydrophobic force. The solid line in Figure 3.7 represents an extended DLVO fit with C_1= -10 mN/m, D_1=1.2 nm,, C_2=-0.35 mN/m, and D_2=4.5 nm. The decrease in hydrophobic force, which may be best represented by the decrease in D_2 from 9.0 to 4.5 nm, suggests that hydrophobic force decreases in the presence of electrolyte. Other investigators (8,9) showed also that hydrophobic force is screened by electrolyte as will be further discussed later. The appearance of the weak double-layer force in the presence of KCl may be attributed to bilayer formation. The presence of KCl may increase the

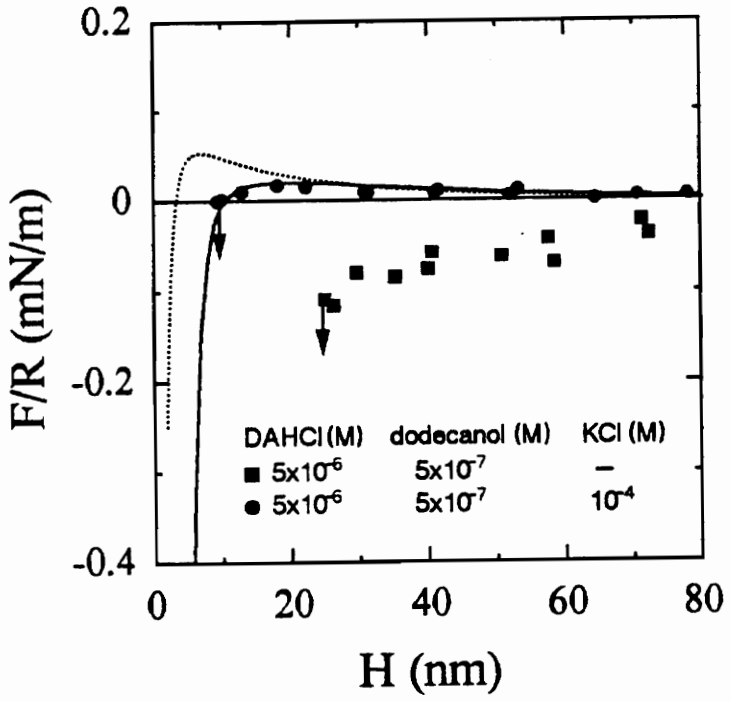

Figure 3.7. *F/R vs. H* between mica surfaces at $5x10^{-6}$ M DAHCl and $5x10^{-7}$ M dodecanol with and without 10^{-4} M Kcl at pH 5.7. In the absence of KCl, the forces are net attractive with Ψ_o = 0 mV. In the presence of $1x10^{-4}$ M KCl, however, the attractive forces are reduced considerably and a weak repulsive force is observed. The dotted line represents the constant charge model of the DLVO fit with Ψ_o = 10 mV, κ^{-1}=33.3 nm and A_{131}=$2.2x10^{-20}$ J. The solid line represent the extended DLVO fit to the force curve in the presence of $1x10^{-4}$ M KCl using C_1=-10 mN/m, C_2=-0.35 mN/m, D_1=1.2 nm, and D_2=4.5 nm. The arrows shows the jump distance. Note that the jump distance in the presence of electrolyte is reduced considerably.

attributed to bilayer formation. The presence of KCl may increase the surface activity of the DAH^+ ions, allowing bilayer formation. However, the thickness of the adsorbed layer measured using the SFA in the presence and absence of KCl remains the same (≅1.1 nm). Therefore, the DAH^+ ions adsorbed on top of the monolayer of mixed DAH^+/dodecanol (or hemimicelle) may have a flat orientation.

Figure 3.8 shows the d(-F/R)/dH *vs.* H plots obtained using the jump method at $5x10^{-6}$ M DAHCl and $5x10^{-7}$ M dodecanol with and without 10^{-4} M KCl. The force gradients (or attractive pressure) obtained in the presence of KCl are substantially smaller than those obtained in the absence of 10^{-4} M KCl, which is consistent with the data obtained using the equilibrium method at larger separation distances (Figure 3.7). The force gradients obtained with KCl are only marginally larger than those for the van der Waals pressure. The data points can be fitted to the extended DLVO theory (Eq. [9]) as shown by the solid line. At H≥9 nm, the force gradients calculated from the extended DLVO theory become larger than those due to the van der Waals force. This is because the calculation includes a small repulsive force, which can be fitted with ψ_o=10 mV, due to the bilayer formation. On the other hand, the force gradients obtained in the absence of KCl can be fitted to the extended DLVO theory with ψ_o=0 mV. An important finding from Figure 3.8 is that the data obtained in the presence of KCl can be fitted with a considerably weaker hydrophobic force than observed without KCl. As shown in Table 3.1, the long-range hydrophobic force constants (C_2=-0.35 mN/m and D_2=4.5 nm) obtained in the

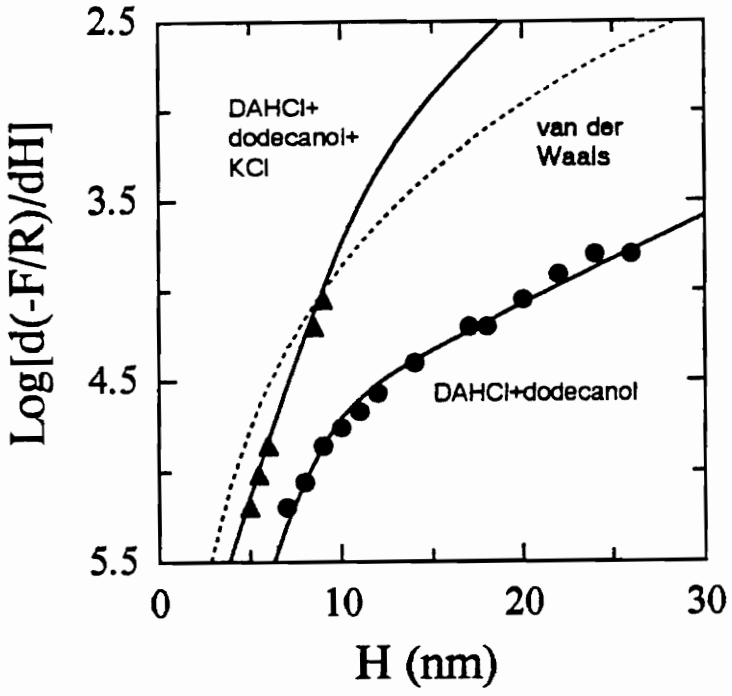

Figure 3.8. Normalized force gradient vs. H between mica surfaces in $5x10^{-6}$ M DAHCl, $5x10^{-7}$ M dodecanol, and $1x10^{-4}$ M KCl at pH 5.7 (triangles). The solid line represents an extended DLVO fit incorporating a double exponential function for the hydrophobic force (Eq. [9] and [13]): A_{131}=$2.2x10^{-20}$ J, C_1=-10 mN/m, C_2=-0.5 mN/m, D_1=1.1 nm, and D_2=4.5 nm. Also shown for comparison are the normalized force gradients for the nonretarded van der Waals force (dashed line) and for the DAHCl/dodecanol mixture with double exponential fit (solid lines). The presence of electrolyte reduces the hydrophobic force.

presence of 10^{-4} M KCl are considerably smaller than those (C_2=-1.2 mN/m and D_2=9.0 nm) obtained without KCl. These results are consistent with the findings with other hydrophobic systems (8,9,11), and support the view that hydrophobic force may be electrostatic in origin.

Figure 3.9 shows the force-distance profiles at higher concentrations of dodecanol. At $5x10^{-6}$ M dodecanol, the force curve becomes repulsive as shown in the inset. The data can be fitted to the DLVO theory with ψ_o =90 mV, which is substantially larger than the value (ψ_o=0 mV) obtained at $5x10^{-7}$ M dodecanol and $5x10^{-6}$ M DAHCl (Figure 3.7 and 3.8). Since the repulsive force is larger than the case without DAHCl (ψ_o=0 mV, Figure 3.1), the DAH^+ ions may be considered to adsorb on top of the first monolayer, forming a bilayer. Interestingly, the two mica surfaces coated with bilayers of mixed surfactants jump into contact at 14 nm, which indicates the presence of hydrophobic force. An extended DLVO fit shows that the hydrophobic force can be represented with both short- (D_1=1.2) and long- (D_2=1.5-2 nm) range decay lengths (see Table 3.1). It is possible that the surfactant adsorption in the second layer is still incomplete, or the molecules have more or less flat orientation. With a further increase in dodecanol concentration to 10^{-5} M at $5x10^{-6}$ M DAHCl, much larger repulsive forces are observed and the thickness of the adsorbed layer increased from 1.1 to 25 nm (Figure 3.9). Also, the force measurements showed hysteresis: the force measurements made while separating the two mica surfaces from each other are lower than those measured while approaching the surfaces. These findings are

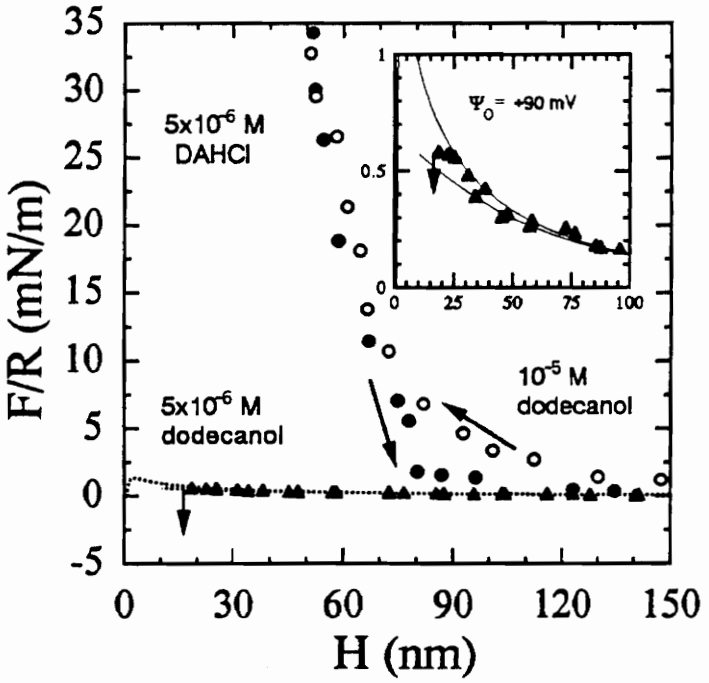

Figure 3.9. *F/R vs. H* between mica surfaces in the presence of $5x10^{-6}$ M DAHCl and varying concentrations of dodecanol at pH 5.7. At $5x10^{-6}$ M DAHCl and $5x10^{-6}$ M dodecanol, electrical repulsive forces reappeared, indicating a charge reversal. The force curve can be fitted with Ψ_o=+90 mV and κ^{-1}=43 nm, C_1=-40 mN/m, C_2=-1.0 mN/m, D_1=1.2 nm, and D_2=2.5 nm.. With further increase in dodecanol to 10^{-5} M, large repulsive force which cannot be explained by the Poisson-Boltzman equation are observed. The force measurements showed hysteresis. The arrows shows the jump distance.

higher concentrations of octanol and DAHCl (Chapter 2; Reference 14). Rutland *et al.* (30) reported similar results with mica surfaces in a 10^{-4} M DAHCl solution at pH 10.3. These investigators attributed the observation to the precipitation of phase-separated hydrated dodecylamine droplets. They actually observed the solution turning milky at pH 10.3, indicating phase-separation. In the present investigation, however, the $5x10^{-6}$ M DAHCl solution containing 10^{-5} M of dodecanol was clear at pH 5.7, indicating no phase separation. Therefore, the results observed at 10^{-5} M dodecanol may be explained by the adsorption of mixed micelles. Because the micelles are charged, the surface forces are highly repulsive. The hysterisis of the force measurement suggest that the adsorbed layer can be compressible irreversibly.

3.3.2 Advancing and receding angles

Table 3.1 shows the advancing and receding water contact angles measured on mica surfaces that have been equilibrated with solutions containing various amounts of DAHCl and dodecanol. Both advancing and receding angles increase with DAHCl and dodecanol concentrations, suggesting an increase in hydrophobicity. Advancing angle is maximum at $5x10^{-6}$ M DAHCl in the presence of 10^{-7} and $5x10^{-7}$ M dodecanol. However, the difference between advancing and receding angles becomes minimum at $5x10^{-7}$ M dodecanol, suggesting that the mica surface becomes most homogenous in a solution containing $5x10^{-6}$ M DAHCl and $5x10^{-7}$ M dodecanol. It is interesting that the

strongest hydrophobic force is also observed under this condition, D_2 becoming as large as 9 nm. This finding suggests that the hydrophobic force may be related to the ordering of hydrocarbons in the monolayer. The same can be said with the data obtained in DAHCl/octanol solutions as shown in reference 14 and partially in Table 3.1. However, the contact angle hysteresis is larger with octanol than with dodecanol, which may be attributed to the corrugation in the mixed monolayer of DAH^+ and octanol. A mixed monolayer of DAH^+ and dodecanol, on the other hand, should present a smoother surface toward the aqueous phase, which may be more conducive to creating a stronger hydrophobic force.

3.4 Discussion

The results obtained in the present work show that the hydrophobic forces measured with mica in DAHCl solutions increase sharply by the addition of small amounts of dodecanol. In the absence of dodecanol, only short-range hydrophobic forces have been measured with D_0 values in the range of 1.2-1.3 nm. These are consistent with those (1-2 nm) reported in the literature (1-5). In the presence of dodecanol, however, the hydrophobic forces become significantly stronger, as evidenced by the increase in 'jump' distance and the net attractive forces measured in $5x10^{-6}$ M DAHCl solutions containing 1 to $5x10^{-7}$ M dodecanol (Figure 3.4). The measured hydrophobic forces are so strong that it is necessary to use a double-exponential function (Eq. [2]), with the long-range

attributed to the coadsorption mechanism, in which dodecanol molecules adsorb in-between the DAH^+ ions adsorbed on mica surfaces. Since the crystallographic area per negative charge on mica is 0.48 nm^2 while the cross-sectional area of each hydrocarbon chain is 0.25 nm^2, there are sufficient rooms to accommodate the neutral surfactant molecules such as dodecanol. The results obtained in the present work are similar to those obtained with octanol as the neutral surfactant (14; Chapter 2); however, the values of D_2 are significantly larger than those measured with octanol because of the longer chain length.

The coadsorption mechanism was proposed originally by Gaudin and Fuerstenau (16), who observed that in the presence DAHCl the flotation of quartz increases sharply in the narrow pH range of 9.0-10.5. These authors suggested that the neutral dodecylamine (DA) molecules formed in solution as a result of hydrolysis (at pH close to its pK_a) coadsorb in-between the DAH^+ ions adsorbed on the quartz surface. This will reduce the electrostatic repulsion between the polar heads of the adsorbed DAH^+ ions, thereby increasing the adsorbability of the DAH^+ ions (16). A different mechanism was proposed by Somasundaran and his co-workers (31), who suggested that at pH close to the pK_a , ionomolecular complexes ($DAH^+ \cdot DA$) are formed in solution and then adsorb onto the surface. Since the $DAH^+ \cdot DA$ species represents effectively a longer chain surfactant, its adsorbability would be greater than that of DAH^+ ions. Despite the obvious difference between the two mechanisms, both suggest additional adsorption of DAH^+

ions on quartz in the presence of neutral surfactant such as dodecylamine. The direct force measurements conducted with mica in the present work support these mechanisms. The significant decrease in the surface potential (ψ_0) in the presence of dodecanol strongly indicates that the neutral surfactant causes additional adsorption of DAH^+ ions. In the present work, most of the surface force measurements have been conducted at $5x10^{-6}$ M DAHCl, which is below the point of charge reversal (p.c.r.=10^{-5} M); therefore, there must be sufficient vacant negative charge sites on which additional DAH^+ ions can adsorb.

When using DAHCl as a collector for quartz, the optimum flotation occurs in the narrow range of pH 9.0-10.5, and significant water contact angles are observed only at this pH range (17). Smith *et al.* (28) showed, however, that the lower pH limit at which significant contact angles are observed can be extended considerably in the presence of long-chain alcohols. This observation was explained by the authors in view of the coadsorption mechanism of Gaudin and Fuerstenau (16); however, the coadsorbing molecules are long-chain alcohols added artificially rather than the DA molecules that are naturally present in the system at pH close to the pK_a of DAHCl. As a result, Smith *et al.* (28) observed the pH ranges for significant water contact angles extends to well below the pK_a . This pH range becomes wider as the chain length of the long-chain alcohols becomes longer. These results are consistent with the direct force measurements obtained in the present work. Long-range hydrophobic forces have been observed at pH 5.7,

which is significantly lower than the pK_a. Also, the hydrophobic forces observed with dodecanol is stronger than those observed with octanol.

Subscribing to the iono-molecular complex theory, DAH^+ ions may form complexes with dodecanol and then adsorb on mica. The complex formation represents an increase in the effective hydrocarbon chain length of the cationic surfactants and, hence, an increase in the negative free energy of adsorption ($-\Delta G_{ad}$). Note here that the dodecanol concentration used in the present work is 10-50 times less than that of the DAHCl concentration ($5x10^{-6}$ M). It may be speculated, therefore, that DAH^+ ions may form clusters around each dodecanol molecule before adsorption takes place. For the case of the ionomolecular complexes formed between DAH^+ ion and DA, however, Somasundaran, *et al.* (31) suggested that multimers containing more than one DAH^+ ions are unlikely because of the electrostatic repulsion between the polar groups of the cationic surfactants. In this regard, the DAH^+·dodecanol complex that may form in solution may also be considered to be 1:1. Although the concentration of this complex may be only 2-10% of the DAHCl concentration, its adsorbability may be significantly larger than that of the DAH^+ ions owing to its longer chain. Therefore, the adsorption density of dodecanol on mica may be comparable to that of DAH^+ ions. It is possible that at the monolayer coverage, the DAH^+ to dodecanol ratio may be close to 1:1. It is well known that even at p.c.r. not all the K^+ ions are displaced by the DAH^+ ions. In the presence of dodecanol, however, more of the K^+ ions may be displaced by the DAH^+·dodecanol

dodecanol, however, more of the K^+ ions may be displaced by the DAH^+·dodecanol complexes due to its high adsorbability. The consequence of this would be the formation of a more compact monolayer.

The formation of monolayer of mixed surfactants between DAH^+ ions and dodecanol should increase the packing density of hydrocarbons on mica. The DAH^+ ions will adsorb on the negative charge sites at the center of oxygen hexagons, while the neutral surfactants coadsorb in-between the adsorbed DAH^+ ions possibly on the sites represented by siloxane groups. When sufficient number of dodecanol molecules coadsorb on the mica surface along with additional DAH^+ ions, the packing density of the hydrocarbon chains will increase, which should increase the hydrocarbon chain order. Rabinovich and Yoon (12) showed that stronger hydrophobic forces are observed when the hydrocarbon chain order is increased. The appearance of the long-range hydrophobic force with D_2 as large as 9.0 nm provides an evidence that hydrocarbon chain order is indeed important in determining the magnitudes of hydrophobic forces.

Figure 3.10 shows the decay lengths (D_0's and D_2's) of hydrophobic forces plotted against the advancing water contact angles (θ_a) of the surfaces with which the force measurements have been conducted. The data can be divided into three groups. The first group includes the data obtained with mica surfaces coated with self-assembled monolayers of DAHCl and CTAB, which give D_0's in the range of 1-2 nm (1-4). The second group includes the data obtained with the L-B deposited monolayers of DDOAB

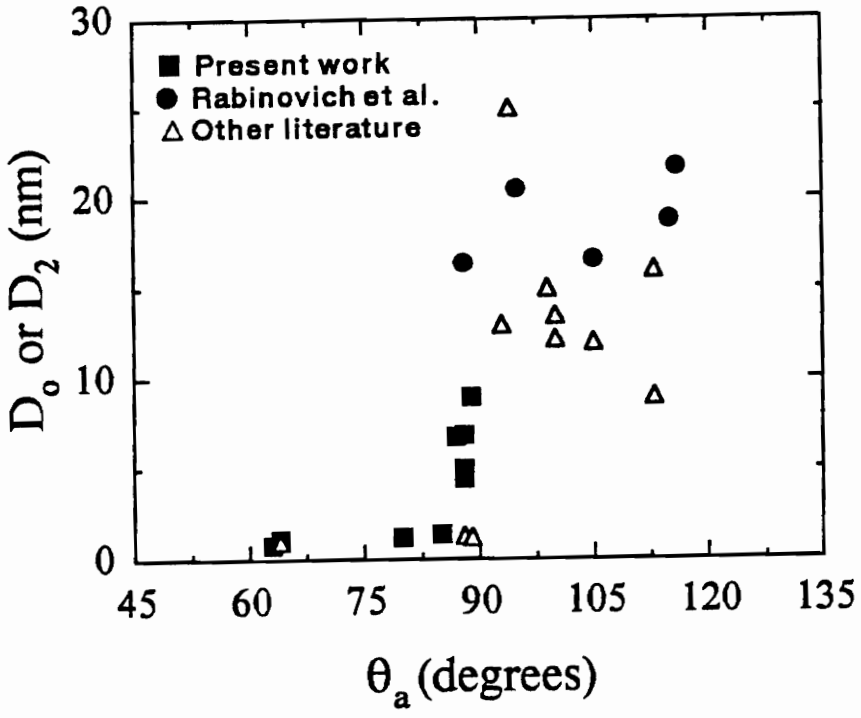

Figure 3.10. Long-range decay lengths D_2 *vs.* advancing angle (θ_a) plot obtained for DAHCl, DAHCl/octanol, DAHCl/dodecanol mixtures (squares) in the presence mica surfaces (14), DDOAB coated mica surfaces (triangles) (6-11), and ODTCS coated silica (circles) (12) at pH 5.7. Note that there is a sharp increase in the decay lengths D_2 from short- to long-range hydrophobic force when θ_a= 90°.

and fluorocarbons (6-11) on mica and octadecyltrichlorosilane (ODTCS)-deposited silica surface (12). This group of data are widely scattered, with D_2 values ranging from 10 to 26 nm. The third group include the data obtained with the self-assembled mixed monolayers of DAHCl and dodecanol, as obtained in the present work, and of DAHCl and octanol (14; Chapter 2). The decay lengths change little until θ_a reaches 90° and then increases sharply above this value. The sharp increase above θ_a=90° may indicate that the packing density of the hydrocarbons and, hence, the degree of ordering also increases sharply at this critical angle. Flinn *et al.* (32) showed that the surface coverage of ODTCS on silica, as measured by the intensities of CH_2 and CH_3 vibrations, increases sharply from 0.17 to 1.0 as θ_a increases from 84° to 101°.

The self-assembled monolayers of DAH^+ ions on mica are not closely-packed for the geometric reasons discussed previously. Nevertheless, it is possible that hydrocarbons associate with each other, forming domains (or patches). This phenomenon, which is also known as hemimicelle formation in the flotation literature, occurs at substantially (≈50-100 times) lower concentrations than the critical micelle concentration (c.m.c.) (33). The domain formation through the hydrocarbon chain association is a means of maximizing the free energy minimization of the system. In the absence of neutral molecules such as dodecanol, the size of the domains would be small because the distance between two adjacent polar heads of the DAH^+ ions adsorbed on mica are larger than that required to form closely-packed monolayers. Under this

expected as will be further discussed. When dodecanol coadsorbs with DAH^+ ions, however, the hydrocarbons in each domain should be more closely-packed and the size of the domains become larger. The hydrocarbon chains in a close-packed domain should present an ordered structure to the aqueous phase, which may be conducive to long-range hydrophobic forces. As will be discussed further, hydrophobic force may increase with increasing domain size. The D_2 values measured in the present work vary in the range of 4.0-9.0 nm, which may be a reflection of the size and number of domains, and the density of hydrocarbon chains in each domain. When 18 carbon long-chain surfactants are deposited on mica or on silica, the packing density and the domain size may be further increased, so that θ_a becomes larger than 90° and stronger hydrophobic forces are observed with D_2 in the range of 10-26 nm (6-13).

Formation of a close-packed monolayers of hydrocarbon chains of surfactant molecules have two important consequences. First, the water molecules will be squeezed out of the monolayer, breaking all the possible H-bond linkages between the surface and the bulk water. In 1969, Laskowski and Kitchener (34) measured ζ-potentials of methylated silica, which were essentially the same as those for pure silica. Since the Hamaker constant did not change with methylation, these authored speculated the presence of a non-DLVO force associated with the methylated silica. They considered that the methylation reduces the H-bonding component of the work of adhesion of water on silica. Blake and Kitchener (35) suggested further that minimizing the contributions

from the H-bonding is the most important aspect of hydrophobizing a surface. Second, a well-ordered hydrocarbon layer with vertical orientation presents CH_3 groups toward the aqueous phase. According to Zisman (15), the surface tensions (γ_{SV}) for the CH_3 and CH_2 groups are 23 and 31 mNm^{-1}, respectively; therefore, ordering of hydrocarbons should increase the hydrophobicity.

The CH_3 groups at the ends of a well-ordered hydrocarbon monolayer present dipole moments toward the aqueous phase, which in turn may induce orientation of water dipoles. Simulation of water structure in the vicinity of hydrophobic surfaces showed that water dipoles are oriented parallel with unipolar (or unidirectional) orientation (36-42). Such orientation occurs due to the lack of hydrogen-bonding between the water dipoles and the hydrophobic surfaces. Some investigators considered that the structural changes of the water layers in the vicinity of the hydrophobic surfaces is responsible for the hydrophobic force (43-46). However, the ordering of water molecules diminishes within a few layers from the surface, which makes it difficult to explain the long-range hydrophobic forces observed over a distances of 100 nm (47).

It is possible that the in-plane water dipoles are in patches (or domains). The unipolar orientation of in-plane dipoles should create larger dipole moments, which in turn correlate with the dipoles on the opposing surface to give rise to long-range hydrophobic forces. The magnitude of the dipole moment associated with each domain should vary depending on its size, and so should the hydrophobic force. As has already

been discussed, the domain size should increase with increasing adsorption density. Ideally, a close-packed monolayer should present a gigantic dipole moments. However, Monte Carlo simulation and STM studies showed that close-packed monolayers are imperfect and consists of a number of smaller domains (48,49). Tsao *et al.* (8,9) and Rabinovich and Yoon (12) also attributed hydrophobic forces to the correlation of large dipoles; however, these investigators considered dipole moments associated with the hydrocarbon chains rather than the dipole moments associated with the unipolar orientation of water dipoles. On the other hand, Miklavic *et al.* (50) showed that long-range attractive forces can originate from the correlation of charges associated with patches of adsorbed surfactants.

It is now well understood that close-packed monolayers of hydrocarbon chains are inclined with tilt angles of up to 33° normal to the surface (49,51,52). Tilting of the hydrocarbon chains may increase the dipole moment, because the horizontal component of the dipole moments associated with the CH_3 groups should increase with tilt angle.

The utility of the theories based on domain formation is that they can explain long-range attractive forces that exhibit screening effects of electrolytes (8,9,11). It has been shown that small additions of electrolytes (~10^{-5}-10^{-4} M) greatly diminishes long-range attractive forces, with 2:2 electrolytes, such as $MgSO_4$, showing more pronounced effects than 1:1 electrolytes (9,53). In the present study, it has been shown that D_2 is reduced from 9 to 4.5 by the addition of 10^{-4} M KCl (see Figures 3.7 and 3.8). In the

absence of electrolyte, the measured force curve was fitted with the Debye length (κ^{-1}) of 68.0 nm. In the presence of 10^{-4} M KCl, κ^{-1} is calculated to be 30.4 nm. That both D_2 and κ^{-1} decreased by a factor of approximately two may suggest that hydrophobic force is electrostatic in nature.

The results obtained in the present work in the presence of 10^{-4} M KCl cannot be explained solely by the screening effect (Figures 3.7 and 3.8). The appearance of repulsive force (ψ_0=+10 mV) in the presence of KCl suggests that additional DAH^+ ions (or DAH^+·dodecanol complexes) adsorb on the mica surface possibly with inverse orientation. It is well known that surface activity of ionic surfactants increase in the presence of electrolytes. For the reasons that have already been discussed, the mica surface is probably coated with a close-packed monolayer of mixed surfactants at $5x10^{-6}$ M DAHCl and $5x10^{-7}$ M dodecanol. Therefore, any additional adsorption of surfactants should result in a bilayer formation. However, the adsorbed species in the second layer may have a flat orientation, since ψ_0 is small and the thickness of the adsorption layer does not change in the presence of electrolyte.

The longest value of D_2 observed with octanol as a coadsorbing neutral surfactant is 6.8 nm, while the same with dodecanol is 9.0 nm. That the dodecanol gives longer range hydrophobic force may be attributed to its longer chain length, which should give more negative free energy of adsorption and, hence, larger domain size. Furthermore, the mixed monolayer of DAH^+ and dodecanol should present a smoother surface (because of

mixed monolayer of DAH^+ and dodecanol should present a smoother surface (because of equal chain lengths) than that of DAH^+ and octanol. The lower contact angle hysteresis observed with the mica surfaces coated with DAH^+ and dodecanol may be a manifestation of the surface smoothness. The smoother surface would be more conducive to the formation of larger domains of unipolar in-plane water dipoles and, hence, the longer-range hydrophobic forces.

One of the most striking features of Figure 3.10 is that the hydrophobic force is shown to increase sharply at θ_a=90°. The attractive forces measured above this value can no longer be described using Eq. [1]. It is necessary to use Eq. [2] incorporating the long-range component of the hydrophobic force with decay length D_2. The data obtained in the present work show that the long-range hydrophobic force begins to appear as θ_a approaches 90°, and D_2 increases sharply as the contact angle is further increased. The appearance of the long-range hydrophobic force has been attributed to the formation of close-packed monolayer, which may occur in the form of patches. The appearance of the long-range hydrophobic force at $\theta_a \approx 90°$ may not be coincidental. Flint et al (32) showed that the hydrocarbon tails of ODTCS molecules begin to stand-up vertically on silica at $\theta_a \approx 90°$, exposing CH_3 groups toward the aqueous phase.

Contact angle of 90° has another significance. Thermodynamically, the wetting tension becomes less than zero at θ>90°, i.e.,

$$\gamma_{SV} - \gamma_{SL} < 0 \qquad \textbf{[14]}$$

where γ_{SV} is the interfacial tension at the solid/vapor interface and γ_{SL} is the same at the solid/liquid interface. Equation [14] suggests that the free energy of a system decreases when a solid/liquid interface is replaced by a solid/vapor interface, i.e., the wetting film under consideration should recede spontaneously or cavitation should occur spontaneously at $\theta>90°$. This would be the case, of course, when the increase in free energy due to the vaporization of liquid and the creation of a vapor/water interface do not exceed the free energy decrease (21).

The Girifalco-Good-Fowkes equation modified by Tamai *et al.* (54) allows calculation of interfacial energy (γ_{12}) as follows:

$$\gamma_{12} = \gamma_1 + \gamma_2 - 2\sqrt{\gamma_1^d \gamma_2^d} - 2\sqrt{\gamma_1^p \gamma_2^p} \qquad \textbf{[15]}$$

in which γ_1 and γ_2 are the surface tensions of *1* and *2*, while the superscript *d* and *p* refer to the dispersion and polar components of the surface tension, respectively. Applying Eq. [15] to γ_{SV} and γ_{SL} of Eq. [14], the following relationship is obtained:

$$\gamma_L > 2\left(\sqrt{\gamma_S^d \gamma_L^d} + \sqrt{\gamma_S^p \gamma_L^p}\right). \qquad \textbf{[16]}$$

which is the necessary condition for $\theta>90°$. One can calculate the value of γ_S^d to be 23.8 mJ/m^2 for mica from its Hamaker constant ($A_{11}=10^{-19}$ J) using the following relationship (55):

$$A_{11} = 6\pi r_{11}^2 \gamma_S^d \qquad [17]$$

in which r_{11} is the inter-atomic distance in mica and $6\pi r_{11}^2$ is usually $1.44x10^{-18}$ m^2 (55). By substituting the values of $\gamma_L^d=22$ mJ/m^2 and $\gamma_L^p=50$ mJ/m^2 for water and the value of γ_S^d into Eq. [16], on can find the condition for $\theta>90°$ to be $\gamma_S^p<0.069$ mJ/m^2, or $I_{SL}^p(=2\sqrt{\gamma_S^p\gamma_L^p})<3.72$ mJ/m^2. The values of I_{SL}^p and water contact angles (θ) reported by Dann (56) and Hamilton (57) for various polymeric substrates show that θ is greater 90° when I_{SL}^p becomes less than 3.72 mJ/m^2. A similar observation has been made by Flinn *et al.*(32) for ODTCS-coated silica surfaces. Since the major contribution to I_{SL}^p is from the H-bonding of water molecules, these findings are consistent with Blake and Kitchener's that minimizing the contributions from H-bonded water is the most important aspect of hydrophobizing a surface (35).

Thus, several things occur at $\theta\approx90°$. First, hydrocarbon tails begin to stand-up to form a close-packed monolayer within a domain as shown by Flinn *et al.* (32). Second, presentation of the CH_3 groups, rather than the less hydrophobic CH_2 groups, toward the aqueous phase reduces the value of I_{SL}^p to below 3.72 mJ/m^2, and make the surface

become sufficiently hydrophobic to form cavitation. Third, the long-range hydrophobic force begins to appear at θ_a=90°. It is possible, therefore, that the long-range hydrophobic forces observed at θ_a above 90° may be attributed to cavitation. Yushchenko *et al.* (21) carried out a theoretical analysis for cavitation between two hydrophobic spheres and showed that in the presence of macroscopic cavities the attractive forces can be greater than molecular forces. For 1 μm spheres, the attractive force is extended up to 20 nm, while it reaches as far as 22 μm for 1 mm spheres. However, the cavitation requires a large activation energy; at θ=105° the energy barrier becomes as large as 100 kT at the separation distance (H) of 1 nm. Yaminsky *et al* (20) actually measured the attractive forces due to cavitation between glass spheres and plate in mercury as non-wetting liquid.

In direct force measurements, however, cavitation can be seen only when two hydrophobic surfaces retreat from each other after initial contact. No one is yet to see cavitation during the approach cycle. This may be due to the high activation energy associated with the cavitation. For this reason, Yaminsky and Ninham (23) suggested that subcritical cavitation caused by density fluctuation can give rise to long-range attractive forces. The subcritical cavitation occurs due to thermal fluctuation of intermolecular voids in a meta-stable liquid near hydrophobic surface. It is not a cavitation in ordinary sense in that the local expansions are below the level of elastic instabilities that result in the local rupture of the condensed phase. By considering

cylindrical subcritical cavities bridging two hydrophobic surfaces, these authors derived an expression for the attractive pressure (P):

$$P = -2E\left(\frac{kT}{2\pi\gamma_{lv}}\right)^2 \frac{(1-\cos\theta)}{(v_m^{1/3}D^3)}, \qquad \textbf{[18]}$$

where E is the elasticity modules for the lateral expansion of the cylindrical gas bridge, k the Boltzmann constant, T the temperature, γ_{LV} the liquid-vapor interfacial tension, v_m is the molecular volume, θ the contact angle, and D is the distance between the surfaces. Eq. [18] may be rearranged in the form of the non retarded van der Waals force:

$$P = -\frac{K}{6\pi D^3}, \qquad \textbf{[19]}$$

where K is a constant. For θ=90°, γ_{LV} =70 mJ/m^2, $v_m^{1/3}$ =0.3 nm, and E=2x10^9 N/m^2, Eq. [18] gives K=2x10^{-20} J, which is comparable to the Hamaker constant of mica (A_{131}=2.2x10^{-20} J). Even at θ=180°, K is only 4x10^{-20} J. Rabinovich and Yoon (12) also used a power law which is in the same form as the non-retarded van der Waals force to describe the attractive forces measured with ODTCS-coated silica surfaces. The K values reported by them are in the range of 2.8-3.5x10^{-16} J, which are nearly four orders of magnitudes larger than predicted by the subcritical cavitation theory. Thus, the subcritical cavitation theory underestimates the attractive force. However, there is a

degree of uncertainty in using the value of 70 mJ/m^2 for γ_{LV}. For very small cavities, the surface tension could be substantially smaller (58). Assuming a value of 20 mJ/m^2 for the γ_{LV}, K becomes $2.4x10^{-19}$ J, which may be more realistic.

One limitation associated with the subcritical cavitation theory is that it cannot explain the sudden appearance of the long-range hydrophobic forces at $\theta>90°$ as shown in Figure 3.10. Eqs. [18-19] suggests monotonic changes in the attractive pressure with respect to the contact angle. The critical cavitation theory is probably a better vehicle for explaining this experimental observation despite its own problems concerning the lack of evidence for macroscopic cavitation at longer separation distances. However, there is a possibility that microscopic, invisible cavities (or microbubbles) may nucleate on the hydrophobic domains, (whose microscopic contact angles can satisfy the thermodynamic requirement for cavitation,) and give rise to long-range hydrophobic forces. The domain theory discussed earlier is also useful for explaining the sharp transition at $\theta\approx90°$. As a result of the increased packing density, hydrocarbon tails begin to take-up vertical orientation, presenting the CH_3 groups toward the aqueous phase and making the domains more hydrophobic. Furthermore, the higher packing density should increase the degree of hydrocarbon chain ordering and the domain size, and, hence, create a stronger hydrophobic force.

3.5 Summary and Conclusions

Direct force measurements were conducted with mica surfaces in equilibrium with DAHCl and dodecanol. With the cationic surfactants alone, only short-range hydrophobic forces with decay lengths less than 2 nm were observed, as have been reported in the literature by other investigators. In the presence of the neutral surfactant, however, long-range hydrophobic forces were measured. At $5x10^{-6}$ M DAHCl and $5x10^{-7}$ M dodecanol, the decay length becomes as large as 9.0 nm, which represents the longest ever recorded hydrophobic force with soluble surfactants. Appearance of the long-range hydrophobic forces may be attributed to the coadsorption of dodecanol in-between the DAH^+ ions adsorbed on mica, which results in an increase in the packing density of hydrocarbon chains on the surface.

A plot of the decay lengths of the hydrophobic forces reported in the literature and obtained in the present work shows that the long-range hydrophobic forces begin to appear at advancing contact angles (θ_a) greater than 90°. The hydrophobic forces measured at θ_a<90° exhibit only the short-range hydrophobic forces that can be described by the single-exponential power law with decay lengths less than 2 nm. The appearance of the long-range hydrophobic forces at θ_a>90° may be attributed to the possible changes in orientation of the hydrocarbon chains. At $\theta_a \approx 90°$, the hydrocarbon chains may begin to stand-up vertically, creating a close-packed monolayer with the CH_3 groups in contact

with the aqueous phase. Presentation of an ordered array of CH_3 groups may cause a unipolar orientation of in-plane dipoles of water molecules in the vicinity. Since the adsorption of DAH^+ ions may occur in patches (or domains), the unipolar orientation may give the domains large dipole moments, which correlate with the large dipoles of the opposing surface to give rise to long-range hydrophobic forces.

Thermodynamically, cavitation should occur on or near hydrophobic surfaces whose water contact angles are greater than 90°. Therefore, the appearance of long-range hydrophobic forces at θ_a>90° may be attributed to the capillary forces associated with cavitation. Although no macroscopic cavitation has been observed during the approach cycles of direct force measurements, it is possible that microscopic cavitation may occur on the domains whose microscopic contact angles can satisfy the thermodynamic criterion. The density fluctuations caused by subcritical cavitation may be useful for explaining the origin of hydrophobic forces; however, it cannot explain the sharp increase in decay length at θ_a>90°.

3.6 References

1. Israelachvili, J. N., and Pashley, R. M., *Nature* **300,** 341, (1982).
2. Israelachvili, J. N., and Pashley, R. M., *J. Colloid Interface Sci.* **98,** 500 (1984).
3. Herder, P. C., *J. Colloid Interface Sci.* **134,** 346 (1990).
4. Kekicheff, P., Christenson, H. K., and Ninham, B. W., *Colloids Surf.* **40,** 31 (1989).
5. Parker, J. L., Yaminsky, V. V., and Claesson, P. M., *J. Phys. Chem.* **97,** 7707 (1993).
6. Pashley, R. M., Mcguiggan, P. M., Ninham, B. W., and Evans, D. F., *Science* **229,** 1088 (1985).
7. Claesson, P. M., Blom, C. E., Herder, P. C., and Ninham, B. W., *J. Colloid Interface Sci.* **114,** 234 (1986).
8. Tsao, Y. L., Yang, S. X., Evans, D. F., and Wennerstrom, H., *Langmuir* **7,** 3154 (1991).
9. Tsao, Y. L., Evans, D. F., and Wennerstrom, H., *Langmuir* **9,** 779 (1993).
10. Claesson, P. M., Christensson, H. K., *J. Phys. Chem.* **92,** 1650 (1988).
11. Christensson, H. K., Claesson, P. M., Berg, J., Herder, P. C., *J. Phys. Chem.* **93**, 1472 (1989).

12. Rabinovich, Y. I., Yoon, R.-H., *Langmuir*, **10,** 1903 (1994).

13. Rabinovich, Y. I., Guzonas, D. A., Yoon, R.-H., *Langmuir* **9,** 1168 (1993).

14. Yoon, R.-H., Ravishankar, S. A., *J. Colloid Interface Sci.* **166,** 215 (1994).

15. Zisman, W. A., *Ind. Eng. Chem.* **55,** 19 (1963).

16. Gaudin, A. M., and Fuerstenau, D. W., *Trans AIME.* **202,** 958 (1955).

17. Fuerstenau, D. W., *Trans AIME.* **208,** 1365 (1957).

18. Attard, P., *J. Phys. Chem.* **93,** 6614 (1989).

19. Podgornik, R., *J. Phys. Chem.* **91,** 5840 (1989).

20. Yaminsky, V. V., Yushchenko, V. S., Amelina, E. A., and Shchukin, E. D., *J. Colloid Interface Sci.* **96,** 301 (1983).

21. Yushchenko, V. S., Yaminsky, V. V., and Shchukin, E. D., *J. Colloid Interface Sci* **96,** 307 (1983).

22. Christensson, H. K., and Claesson, P. M., *Science* **239,** 390 (1988).

23. Yaminsky, V. V.; Ninham, B. W., *Langmuir* **9,** 3618 (1993).

24. Tabor, D., and Winterton, R. H. S., *Proc. R. Soc. London.*, **A 312**, 435 (1969).

25. Israelachvili, J. N., and Adams, G. E., *J. Chem. Soc. Faraday Trans.* **1 74,** 975 (1978).

26. Tolansky, S., "An Introduction to Interferometry", John Wiley & Sons., NewYork.

27. Chan, D. Y. C., Pashley, R. M., and White, L. R. *J. Colloid Interface Sci.* **77,** 283 (1980).

28. Smith, R.W., *Trans AIME.* **226,** 427 (1963).

29. Derajaguin, B. V. *Kolloid. Zh.*, **69,** 155 (1934).

30. Rutland, M., Waltermo, A., and Claesson, P. M., *Langmuir* **8,** 176 (1992).

31. Somasundaran, P., and Ananthapadmanabhan, K. P.," Solution Chemistry of Surfactants," Ed. Mittal, K. L., **2,** p. 777. Plenum Press. New York. 1979.

32. Flinn, D. H., Guzonas, D. A., and Yoon, R.-H., *Colloids Surf.* **87,** 163 (1994).

33. Fuerstnau, D. W., and Yamada, B. J., *AIME Trans.* **223,** 50 (1962).

34. Laskowski, J, S., and Kitchener, J. A., *J. Colloid Interface Sci.* **24,** 670 (1969).

35. Blake, T. D., and Kitchener, J. A., *J. Chem. Soc. Faraday. Trans. 1.* **68,** 1435 (1972).

36. Lee, C. Y., and McCammon, J. A., *J. Chem. Phy.* **80 (9),** 4448 (1984).

37. Marchesi, M., *Chem. Phys. Lett.* **97,** 224 (1983).

38. Anastasiou, N., Finchan, D., and Stinger, K., *J. Chem. Soc. Faraday. Trans. 1.* **79,** 1639 (1983).

39. Scott, H. L., *Chem.Phys. Lett.* **109,** 570 (1984).

40. Kjellander, R., and Marcelja, S., *Chem. Scr.* **25,** 73 (1985).

41. Christou, N. I., Whitehouse, J. S., Nicholson, D., and Parsonage, N.G., *Mol. Phys.* **55,** 397 (1985)

42. Vinogradova, O. I., *J. Colloid Interface Sci.* **169,** 306 (1995).

43. Marcelja, S., Mitchell, D. J., Ninham, B. W., and Sculley, M. J., *J. Chem. Soc. Faraday Trans. 2* **73,** 630 (1977).

44. Luzar, A., Svetina, S., and Zeks, B., *Chem. Phys. Lett.* **96,** 485 (1983).

45. Pratt, L. R., and Chandler, D. J., *J. Chem. Phys.* **67,** 3683 (1977).

46. Rao, M., Pangali, C., and Berne, B.J., *J. Chem. Phys.* **71,** 2975 (1979).

47. Eriksson, J. C., Ljunggren, S., and Claesson., P. M., *J. Chem. Soc. Faraday. Trans. 2.* **85,** 163 (1989).

48. Siepmann, J. I., McDonald, I. R., *Langmuir* **9,** 2351 (1993).

49. Delamarche, E., Michel, B., Gerber, Ch., Anselmetti, D., Guntherodt, H.-J., Wolf, H., and Ringsdorf, H., *Langmuir* **10,** 2869 (1994).

50. Miklavic, S. J., Chan, D. Y. C., White, L. R., and Healy, T. W., *J. Phys. Chem.* **98,** 9022 (1994).

51. Kjaer, K, Als-Nielsen, J., Helm, C.A., Tipperman-Krayer, P., and Möhwald, H., *J. Phys. Chem.* **93,** 3200 (1989).

52. Bain, C. D., and Whitesides, G. M., *Angew. Chem. Int. Ed. Engl.* **28,** 506 (1989).

53. Christensson, H. K., Fang, J., Ninham, B. W., and Parker, J. L., *J. Phys. Chem.* **94**, 8004 (1990).

54. Tamai, Y., Makuuchi, K., and Suzuki, M., *J. Phys. Chem.* **56,** 40 (1964).

55. Fowkes, F. M., *Ind. Chem. Eng.* **56,** 40 (1964).

56. Dann, J. R., *J. Colloid Interface Sci.*, **32,** 321 (1970).

57. Hamilton, W. C., *J. Colloid Interface Sci.*, **40,** 219 (1972).

58. Ninham, B. W., personel communication (1995).

CHAPTER 4 EFFECT OF pH ON THE HYDROPHOBIC FORCES BETWEEN DODECYLAMINE COATED MICA SURFACES

4.1 Introduction

Alkylammonium salts are widely used as hydrophobizing reagents (collectors) for minerals that are negatively charged. The hydrophobized mineral particles are then removed by air bubbles, the particle-bubble adhesion being controlled by hydrophobic interactions (1,2). Thus, the control of particle hydrophobicity is important in determining the success of flotation processes. One of the most interesting aspects of amine flotation is that it is strongly pH-dependent (3-9). For the case of floating quartz using dodecylammonium hydrochloride (DAHCl), the maximum flotation recovery is obtained over the narrow pH range of 8.0-10.3, the reasons for which have been the subject of many investigations (3-8). Gaudin and Fuerstenau (3) suggested that dodecylamine (DA) produced as a result of hydrolysis coadsorbs with dodecylammonium (DAH^+) ions on the mineral surface to form hemimicelles, which is a two-dimensional analogue of micelles in bulk solution. Somasundaran and his co-workers (6) suggested, on the other hand, that ionomolecular species ($DAH^+ \cdot DA$) adsorb on the surface, and make it more hydrophobic. The concentrations of both the DA and $DAH^+ \cdot DA$ species reach a maximum within the optimum pH range for

flotation. More recently, Laskowski and his co-workers (7,8) suggested that the adsorption of pre-precipitation complexes is responsible for the maximum flotation at pH close to the pKa (=10.6) of the surfactant. However, Laskowski considers $DAH^+ \cdot DA$ as a pre-precipitation complex.

According to the coadsorption mechanism (3), the polar head ($-NH_2$) of a DA molecule reduces the electrostatic repulsion between the polar heads ($-NH_3^+$) of neighboring DAH^+ ions, which results in an increase in the adsorbability of the charges species on quartz. The onset of the coadsorption mechanism is indicated by the sharp decrease in the negative ς-potential of quartz above pH 8. The coadsorption mechanism has two consequences; i) the adsorption of DA molecules increases the packing density of hydrocarbons, and ii) additional DAH^+ ions adsorb on the mineral surface. Both contribute to increased hydrophobicity and, hence, higher flotation recovery. Smith (10) showed that when aliphatic alcohols are added to a DAHCl solution, the pH region where maximum water contact angles are observed is extended to a significantly lower pH. The neutral alcohol molecules coadsorb on quartz at pH where there are no DA species are available, and thereby increase the hydrophobicity.

Many investigators conducted direct force measurements with mica surfaces in equilibrium with DAHCl solutions to detect hydrophobic forces not included in the DLVO theory (11,12,13). The measured hydrophobic forces (F) are usually described by an exponential function:

$$\frac{F}{R} = C_0 \exp\left\{-\frac{H}{D_0}\right\}, \qquad [1]$$

in which R is the radius of the curved mica surfaces, H the closest separation distance between the two surfaces, and C_0 and D_0 are constants. The hydrophobic forces are detectable over the separation distances of up to 15 nm, the decay length, D_0, varying in the range of 1-2 nm (11-13). When the force measurements are conducted with insoluble double-chain surfactants deposited on mica surfaces by the Langmuir-Blodgett technique, significantly stronger hydrophobic forces are observed. The hydrophobic forces can be measurable over distances of up to 100 nm (14-19). The measured forces are usually described by a double exponential function:

$$\frac{F}{R} = C_1 \exp\left\{-\frac{H}{D_1}\right\} + C_2 \exp\left\{-\frac{H}{D_2}\right\}, \qquad [2]$$

in which C_1, D_1, C_2, and D_2 have the same meaning as C_0 and D_0. The results obtained with dioctadecyldimethylammonium (DDOA) bromide (14-17) and fluorocarbon surfactants (18,19) show D_1 in the range of 1-2 nm and D_2 in the range of 10-26 nm. For the purpose of distinguishing the ranges over which hydrophobic forces are detected, the forces that can be described with Eq. [1] will be considered as short-range, while those requiring Eq. [2] as long-range. It has been shown in Chapters 3 and 4 that in the presence of small amounts of octanol and dodecanol, mica surfaces in DAHCl

solutions exhibit long-range hydrophobic forces. These results support the coadsorption mechanism, by which close-packed monolayers are formed and, as a consequence, stronger hydrophobic forces are observed.

Recently, Rutland *et al.* (12) conducted force measurements with mica in 10^{-4} M DAHCl solutions at different pHs. They showed that the hydrophobic forces become significantly stronger at pH 8-9 than at a lower pH, which was attributed to the coadsorption of DA and DAH^+ on mica. However, the hydrophobic force measured under this condition was not as long-ranged as measured with dodecanol as the coadsorbing neutral molecule. It has been shown in Chapter 3 that at $5x10^{-6}$ M DAHCl and $5x10^{-7}$ M dodecanol, two mica surfaces jump into contact at H=25 nm due to the long-range hydrophobic force with D_2=9.0 nm. The jump distance measured by Rutland *et al* (12) was only 12 nm (corrected for the thickness of adsorbed layer), which is characteristic of short-range hydrophobic forces. The reason that Rutland *et al* did not detect long-range hydrophobic forces is probably because the measurements were conducted above the point of charge reversal (p.c.r.=10^{-5} M), which is defined as the DAHCl concentration where the surface charge of mica is neutralized. Above this concentration, DAH^+ ions adsorb on mica with 'flip-flop' orientation (13,20), exposing the hydrophilic polar groups toward the aqueous phase.

It was the purpose of the present investigation to conduct direct force measurements with mica in DAHCl solutions of various concentrations and pHs. The

results are compared with the flotation data obtained by Fuerstenau (5) on quartz in order to determine the role of hydrophobic forces in flotation.

4.2 Experimental

4.2.1 Materials

Dodecylamine hydrochloride (DAHCl) obtained from Eastman Kodak was recrystallized from ethanol before use. Conductivity water was prepared by passing double distilled water through a Nanopure II water treatment unit and subsequently deaerating it under a vacuum for three hours before use. Potassium hydroxide (KOH) and hydrochloric acid (HCl) solutions were used for pH adjustments. Muscovite mica (Grade II) was obtained from Uni Mica Corp., NewYork.

4.2.2 Surface forces measurements

Direct force measurements were carried out using a Mark IV surface force apparatus (from Anutech, Pty.) designed similarly to those of Tabor and Winterton (21) and Israelachvili and Adams (22). Two thin (3-5μm) and molecularly smooth mica surfaces were silvered on one side and then glued onto silica disks with silver-side down using Epon 1004 from Shell Chemical Co. The separation distance between the two mica surfaces was measured using multiple beam interferometry technique based on the method of fringes of equal chromatic order (FECO) (23). The separation was

measured with an accuracy of ± 0.2 nm. The surface force apparatus was controlled using the SF-Scribe CV-78 software on a Macintosh computer.

In each experiment, zero separation point was determined in air, after which the mica surfaces were immersed in water. The force-distance curve obtained in Nanopure water was compared with those in the literature (11) to ensure that the mica surfaces were free of contamination. A 10^{-3} M DAHCl stock solution was prepared in Nanopure water. A requisite amount of the stock solution was then injected into a known volume of Nanopure water in the chamber to obtain a desired concentration. The measurements were made three hours after the reagent was injected with the mica surfaces separated by about 1 mm. In each series of measurements, the pull-off (or adhesion) force ($F(0)/R$) and the jump distance were also recorded. The pH of the solution was controlled by injecting requisite amounts of KOH and/or HCl solutions to the chamber, while withdrawing small volumes of the solution to monitor the pH.

4.2.3 Contact angle measurements

For contact measurements, freshly cleaved mica sheets were immersed in DAHCl solutions of different pH. After three hours of equilibration, the mica sheets were removed from the solution and blow-dried by a nitrogen jet. Water contact angles were measured using the sessile drop technique by means of a Rame-Hart goniometer.

Approximately ten measurements were made at various spots on a mica sheet and averaged.

4.3 Results

Figure 4.1 shows the force-distance curves obtained between two mica surfaces immersed in Nanopure water and in varying concentrations of DAHCl solutions at pH 5.7. The theoretical DLVO force curves, obtained using the algorithms developed by Chan *et al.* (24), are superimposed on the experimental force *vs.* distance data. The theoretical curves were calculated using the surface potential (ψ_o) and Debye length (κ^{-1}) that can best-fit the experimental data. The dispersion force was calculated using the Hamaker constant (A_{131}) of 2.2×10^{-20} J. For each concentration, the upper curve was obtained using constant charge model, while the lower curve represents the constant potential model.

The experimental data obtained in Nanopure water can be best-fit with ψ_o=-170 mV and κ^{-1}=96 nm. As shown in Fig. 4.1, the repulsive forces decrease with increasing DAHCl concentration, for which two reasons may be given. First, the charge of the mica surface is neutralized by the adsorption of DAH^+ ions on the negatively charged mica surfaces. Table 4.1 shows the changes in ψ_o at different DAHCl concentrations. Note that the mica surface is completely neutralized at 10^{-5} M

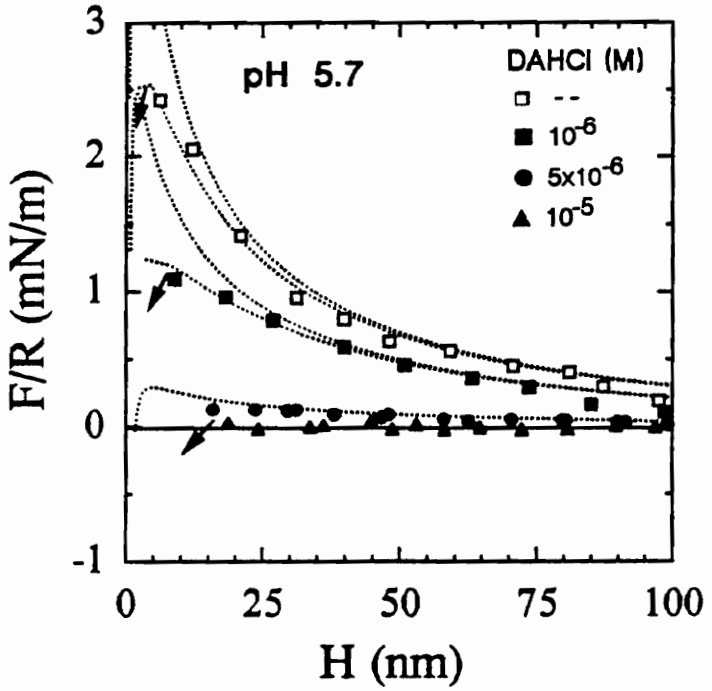

Figure 4.1. *F/R vs. H* between mica surfaces in various DAHCl solutions at pH 5.7. The upper and lower dotted curves represent the constant charge and constant potential models, respectively, of the DLVO theory obtained using A_{131}=2.2x10^{-20} J, Ψ_o=-170 mV and κ^{-1}=96.0 nm for Nanopure water; -125 mV and 76.1 nm at 10^{-6} M DAHCl; and -35 mV and 68.0 nm at 5x10^{-6} M DAHCl. The arrows represent the distance at which the two surfaces jump into contact due to attractive forces.

TABLE 4.1

Results of surface force studies with dodecylamine hydrochloride at pH 5.7.

Conc. of Amine (M)	Surface Potential (Ψ_o) (mV)	Jump Distance (nm)	Pull-off Force (mN/m) ±25	Adsorbed layer Thickness (nm)	Contact Angle (θ) (deg)
--	-170	3.0	125	--	0
$1x10^{-6}$	-125	7.0	150	0.5-0.7	30
$5x10^{-6}$	-35	14.0	225	0.5-0.7	63
$1x10^{-5}$	0	14.0	250	0.5-0.7	85
$1x10^{-4}$	60*	7.0	275	0.5-0.7	86
$5x10^{-4}$	--	--	290	0.5-0.7	88
$1x10^{-3}$	150*	5.0	325	0.5-0.7	85
$3x10^{-3}$	210*	4.0	340	0.5-0.7	83
$6x10^{-3}$	220*	-	0	2.7*	40

* from Herder [22]

DAHCl, which is referred to as point of charge reversal (p.c.r.). At higher concentrations, additional surfactant molecules adsorb on the surface with a "flip-flop" orientation (13), rendering the surface positively charged. Second, the adsorption of DAH^+ ions render the mica surface hydrophobic as evidenced by the jump occurring at longer separation distances than predicted by the DLVO theory. However, the attractive hydrophobic forces are discernible only at shorter separations ($H < 15$ nm). As shown in Table 4.1, the jump distance increases with increasing DAHCl concentration, reaching a maximum of 14 nm at 0.5-1.0x10^{-5} M DAHCl. Also shown in this table are the pull-off forces ($F(0)/R$), which represent the maximum forces measured when two mica surfaces are pulled apart after the initial contact. It has been shown that $F(0)/R = \alpha\gamma_{sl}$, α being in the range of 3-4π (15,16) and γ_{sl} the interfacial tension. The pull-off force also reaches a maximum (250 mN/m) at 0.5-1.0x10^{-5} M DAHCl, where the jump distance is maximum.

Figure 4.2 shows the effect of pH on the force-distance curves obtained at 10^{-6} M DAHCl solution. The force curves obtained in Nanopure water (pH 5.7) are shown again in this figure for comparison. At pH 5.7- 9.5, the force curves overlap with each other. All of the data obtained in this pH range can be fitted to the DLVO theory with ψ_o=-125 mV and κ^{-1}=76.1 nm, and the jump distances are the same (7.0 nm). These findings suggest that there are no significant changes in the adsorption mechanism in this pH range. At pH 10.1, however, the repulsive forces are further reduced. The

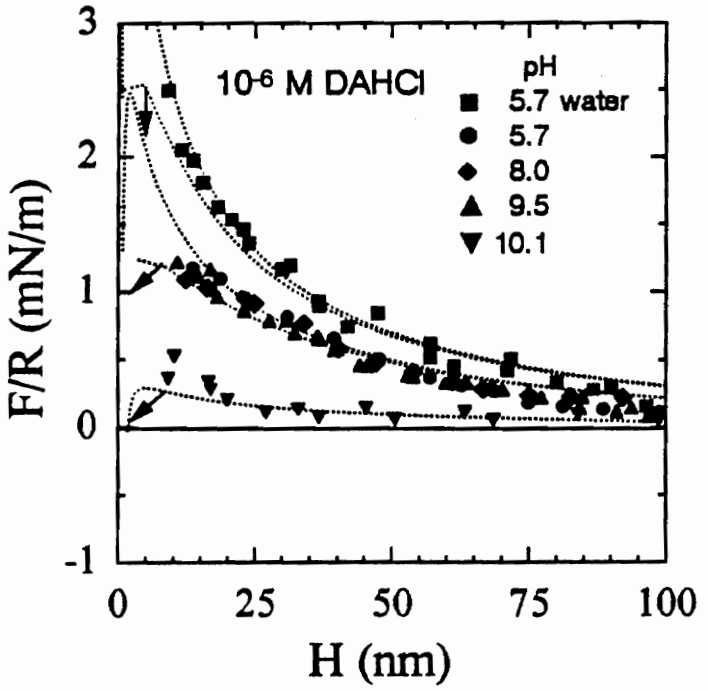

Figure 4.2. *F/R vs. H* between mica surfaces in 10^{-6} M DAHCl solutions at various pHs. The upper and lower dotted curves represent the constant charge and constant potential models, respectively, of the DLVO theory obtained using $A_{131}=2.2\text{x}10^{-20}$ J, $\Psi_o=-170$ mV and $\kappa^{-1}=96.0$ nm for Nanopure water; -125 mV and 76.1 nm at 10^{-6} M DAHCl in pH range from 5.7 to 9.5; and -35 mV and 68.0 nm at 10^{-6} M DAHCl at pH 10.1. The arrows represent the distance at which the two surfaces jump into contact due to attractive forces.

data obtained at this pH can be fitted to the DLVO theory with ψ_o=-35 mV and κ^{-1} =68 nm. The change in ψ_o from -125 mV at pH 5.7-9.5 to -35 mV at pH 10.1 indicates that additional DAH^+ ions adsorb on the mica surface at the higher pH. The increased adsorption of the DAH^+ ions can be attributed to the coadsorption of the neutral dodecylamine ($C_{12}H_{25}NH_2$ or DA) molecules and DAH^+ ions as suggested by Gaudin and Fuerstenau (3).

There is a good fit between the force data obtained at pH 10.1 and the DLVO theory at longer separation distances. However, the experimental results deviate from the theory in two aspects. First, the measured forces are more repulsive than predicted by the theory at separation distances less than approximately 20 nm. The excess repulsive forces measured at shorter separation distances are due to a steric force, the evidences for which will be presented in the following paragraph. Second, the two surfaces jump into contact at 9 nm, which is considerably larger than predicted by the theory. The jump occurs due to the attractive hydrophobic force, which is again only a short-range force with D_0 in the range of 1-2 nm. Note here that as a result of the coadsorption (or iono-molecular adsorption) mechanism, the jump occurs at a longer separation distance than at the lower pHs. Were it not for the steric repulsion, the jump could have occurred at a longer separation distance.

Shown in Figure 4.3 are the surface forces measured at varying concentrations of DAHCl at pH 10.1, where neutral amines coadsorb with DAH^+ ions on mica. The

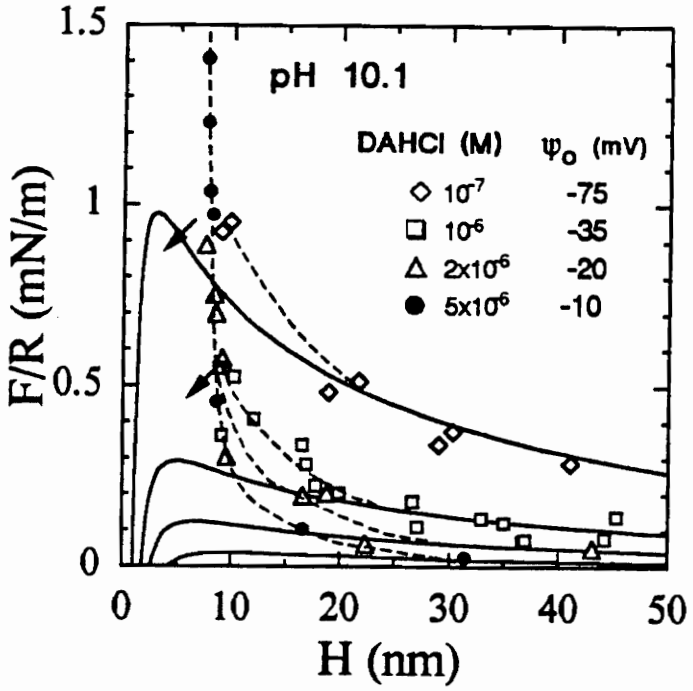

Figure 4.3. *F/R vs. H* between mica surfaces in various DAHCl solutions at pH 10.1. The upper and lower dotted curves represent the constant charge model of the DLVO theory obtained using Ψ_o=-75 mV and κ^{-1}=68.0 nm for 10^{-7} M and -35 mV and 68.1 nm at 10^{-6} , -20mV and 68.1 nm for $2x10^{-6}$ M DAHCl, and -10mV and 68.1 nm for $5x10^{-6}$ M. The theoretical DLVO curves include dispersion force calculated using A_{131}=$2.2x10^{-20}$ J. The arrows represent the distance at which the two surfaces jump into contact due to attractive forces. The dashed lines are the extraneous repulsive forces that are stronger than the DLVO forces due to steric force created by the polymeric and surface precipitates. At $5x10^{-6}$ M DAHCl, the contact thickness is about 7 nm, suggesting a thick layer (3-4 nm) of surfactant on the mica surfaces.

solid lines represent the DLVO fit of the experimental data using the constant charge model. At 10^{-7} M, the force data can be fitted to the theory with ψ_o=-75 mV and κ^{-1} =68.0 nm. The jump distance (5 nm) is slightly larger than predicted by the theory, indicating that there is a short-range hydrophobic force with D_0 less than 1 nm. Note that the forces measured at H<10 nm are considerably larger than predicted by the DLVO theory, most probably due to a steric force. At 10^{-6} M DAHCl, the force data can be fitted to the DLVO theory with ψ_o=-35 mV and κ^{-1}=68.0 nm. The decrease in the negative surface potential indicates that additional DAH^+ ions adsorb on mica as part of the coadsorption mechanism. Coadsorption of DA and DAH^+ ions allows hemimicelle formation, which gives rise to an increased hydrophobic force as evidenced by the slight increase in the jump distance to 7 nm. The data obtained at H<20 nm deviate from the DLVO curve, again due to a steric force. The deviation is more significant than at 10^{-7} M, showing that the steric repulsive force becomes stronger and longer-ranged as the concentration increases. At $2x10^{-6}$ M, the data obtained at H>30 mV can be fitted by the DLVO theory with ψ_0=-20 mV, while the those obtained at closer distances are substantially larger than predicted. No jump has been observed at this concentration, indicating that the surface is hydrophilic. At $5x10^{-6}$ M, the data obtained at larger separation distances can be fitted with ψ_0=-10 mV, but the data obtained at shorter separation distances increases sharply with decreasing separation distance. As the separation distance is reduced to 7-8 nm, the repulsive

force becomes infinite, indicating that phase-separated amines are present on the mica surface. According to the thermodynamic data available in the literature (8), dodecylamine ($C_{12}H_{25}NH_2(s)$) should precipitate out at 10^{-4} M at pH 10.1. Thus, surface precipitation has occurred at $5x10^{-6}$ M, which is 20 times lower than predicted by thermodynamics. In fact, there are evidences that the surface precipitation has occurred at $2x10^{-6}$ M. First, no jump has been observed at this concentration, most probably due to the presence of the phase-separated amine, which is hydrophilic. Second, the thickness of the monolayer is increased to 1.0-1.5 nm from 0.7 nm at 10^{-6} M DAHCl.

It is interesting that the steric forces observed at pH 10.1 resemble those measured with many water-soluble polymers adsorbed on mica (27-29). The force measurements conducted in the present work may suggest, therefore, that polymeric substances are formed before phase-separated amine is formed on the surface. The polymeric substance may be a precursor to the surface precipitation. Surprisingly, the precursor begins to form at a concentration as low as 10^{-7} M DAHCl. The polymerization of amine is consistent with Laskowski's view that the formation of the dimeric iono-molecular species, i.e., $DAH^+ \cdot DA$, should be considered as a "pre-precipitation" phenomenon (8).

Figure 4.4 compares two force curves obtained at pH 5.7 and 9.5 in the presence of $3x10^{-6}$ M DAHCl. The dotted lines represent the DLVO fit with ψ_o=-75

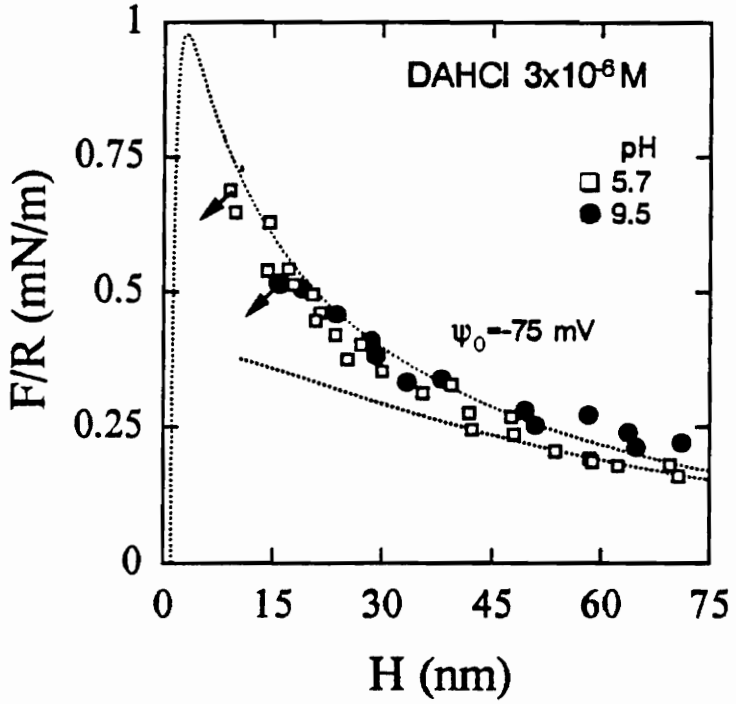

Figure 4.4. *F/R vs. H* between mica surfaces in $3x10^{-6}$ M DAHCl solutions at pH 5.7 and 9.5. The upper and lower dotted curves represent the constant charge and constant potential models, respectively, of the DLVO theory obtained using $A_{131}=2.2x10^{-20}$ J, $\Psi_o=-75$ mV and $\kappa^{-1}=68.0$ nm at $3x10^{-6}$ M DAHCl for pH 5.7 and 9.5. The arrows represent the distance at which the two surfaces jump into contact due to attractive forces. Note that the jump distance at pH 9.5 is larger than the that observed at pH 5.7. At pH 5.7, the data can be fitted only with a short-range hydrophobic force (Eq. 1) with $D_o=1.2$ nm. However, with the increase of pH from 5.7 to 9.5, it is necessary the use of the double-exponential form [Eq. 2] with $C_1=-40$ mN/m, $C_2=-0.5$ mN/m, $D_1=1.2$ nm, and $D_2=5.5$ nm, suggesting the presence of long-range hydrophobic force.

mV and κ^{-1}=68.0 nm. Note that the jump distance increases from 9 nm at pH 5.7 to 14 nm at pH 9.5, suggesting that the hydrophobic force becomes stronger at the higher pH. The increase in hydrophobic force may be attributed to the coadsorption mechanism of Gaudin and Fuerstenau (3) discussed above. However, ψ_o remains more or less constant at -75 mV at both pHs, which is atypical of the coadsorption mechanism. As shown in Figure 4.2, coadsorption of DAH^+ ions and DA molecules at 10^{-6} M DAHCl and pH 10.1 results in a substantial decrease in $-\psi_o$. Gaudin and Fuerstenau (3,5) observed sharp decrease in the negative ς-potential when coadsorption begins to take place as the pH approaches pK_b. Likewise, coadsorption of octanol and DAH^+ ion (Chapter 3; 30) and coadsorption of dodecanol and DAH^+ ion (Chapter 3) significantly decrease the negative surface potential. It is difficult to explain why the coadsorption mechanism occurring at $3x10^{-6}$ M DAHCl and pH 9.5 does not entail suppression of the negative surface potential.

Figure 4.5 shows the pull-off forces (or adhesion forces) measured at different pHs in 10^{-6} and $3x10^{-6}$ M DAHCl solutions. Also shown in this Figure are the results obtained by Rutland *et al* (12) at 10^{-4} M DAHCl. In the pH range of 5.7 and 9.5, no significant changes in the pull-off force were observed. As the pH is increased to 10.1, the pull-off force is reduced sharply to less than 25 mN/m, which may be attributed to the presence phase-separated amine on the mica surface. The precipitates may render the surface hydrophilic and create considerable roughness on the surface, both of which

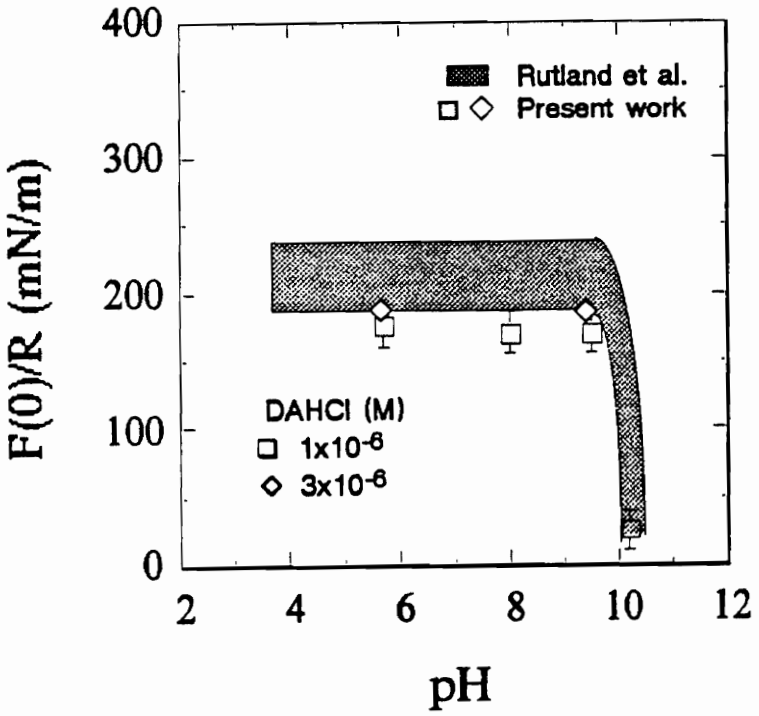

Figure 4.5. The pull-off between mica surfaces in DAHCl solutions at varying pH. *F(0)/R* represents the pull-off force needed to separate the surfaces in contact. The adhesion force values denoted by squares and diamonds are measured in the present work at 10^{-6} and $3x10^{-6}$ M DAHCl solution, respectively. The shaded region are the measurements made by Rutland *et al.* (12) at 10^{-4} M of DAHCl. Note that the pull-off forces almost remain constant in the pH range from 5.7 to 9.5 and drops dramatically with further increase to 10.1.

contribute to lowering the pull-off forces. Waltermo *et al.* [21] also observed similar results with tetraoxyethelene dodecylamine.

Shown in Figure 4.6 are the pull-off forces (*F(0)/R*) and the equilibrium water contact angles (θ) measured at pH 5.7 at various concentrations of DAHCl. Both are shown to increase rapidly with increasing DAHCl concentration. At 10^{-5} M, which is the point of charge reversal (p.c.) (Chapter 2;13), the increase in pull-off force becomes more gradual and θ stays more less constant at approximately 90°. Fuerstnau and co-workers (31) reported similar results for the adsorption of sodium dodecylsulfonate on alumina; they showed that θ does not increase above p.c.r. When DAHCl concentration is increased to above $3x10^{-3}$ M, there is a precipitous drop in the pull-off force and θ. Since this concentration is close to the critical micelle concentration (c.m.c.) of DAHCl ($1.4x10^{-2}$ M), the sudden drop in the contact angle and pull-off force may be attributed to the micellar adsorption.

The pull-off forces measured in Fig 4.6 agree well with the data reported by Herder (11) except that the point of inflection at p.c.r. ($=10^{-5}$ M) is more clearly shown in the present work. Kekicheff *et al.* (32) measured pull-off forces for the CTAB-mica system at pH 5.7. Their results also show a point of inflection at the p.c.r. ($=6x10^{-6}$ M); however, unlike the case with DAHCl, the pull-off forces measured with CTAB decrease above its p.c.r.

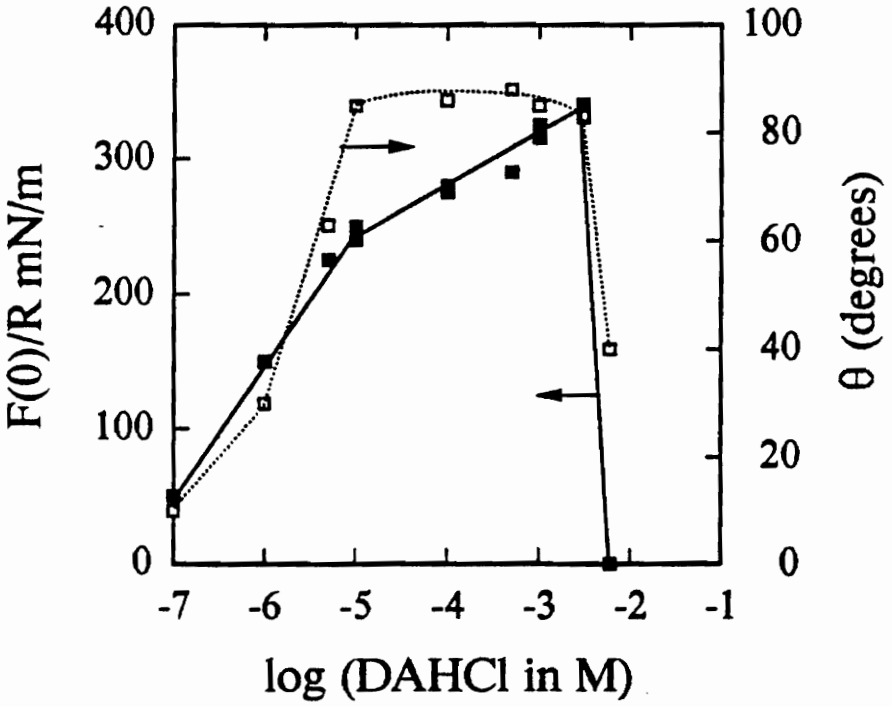

Figure 4.6. The pull-off forces and contact angle data at different concentration of DAHCl solutions at pH 5.7. A point of inflection is obtained at p.c.r. (10^{-5} M DAHCl). A sharp decrease in adhesion force and contact angle above $3x10^{-3}$ M DAHCl concentration is due to micellar adsorption at the surface.

Figure 4.7 shows the changes in pull-off force and θ at pH 10.1. The contact angle increases steadily to 88° at 10^{-5} M and levels off until the concentration reaches 10^{-4} M, where it begins to decrease. The initial increase is due to the increased packing density of hydrocarbon chains, which in turn can be attributed to the coadsorption of DAH^+ and DA species. The decrease in contact angle above 10^{-4} M is due to the formation of phase-separated amine ($C_{12}H_{25}NH_2(s)$). Thermodynamically, the precipitation should occur at 10^{-4} M.

In Figure 4.7, the pull-off force is shown to decreases with increasing DAHCl concentration. At 10^{-7} and 10^{-6} M DAHCl, the force measurements show repulsive steric forces (Figure 4.3), which have been attributed to the presence of polymeric pre-precipitation complex(es) on the surface. Therefore, the decrease in pull-off force may be attributed to an increase in the amount of these complexes with increasing concentration. As the concentration is further increased to $2x10^{-6}$ M, surface precipitation occurs as indicated by the disappearance of the pull-off force and by the increase in the thickness of the adsorbed layer (Table 4.2). Above this concentration, the mica surfaces exhibit no adhesion forces either due to the presence of the precipitates formed on the surface or of those formed in the bulk solution and transported to the surface. As shown, the surface precipitation occurs at a concentration 50-times lower than in the bulk most probably due to the concentration gradient across the solid/water interface.

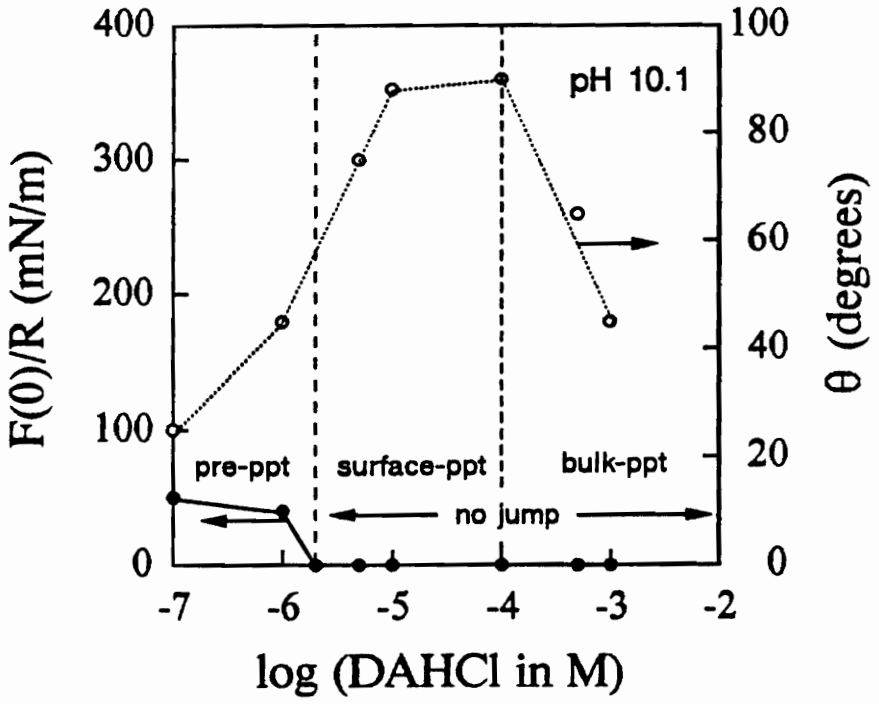

Figure 4.7. The pull-off forces and contact angle data at different concentration of DAHCl solutions at pH 10.1. The adhesion forces remain zero above $1x10^{-6}$ M DAHCl due to the adsorption of polymeric and surface precipitation species. The vertical dotted line indicates the various range of concentration in which polymeric preprecipitate, surface precipitates and bulk precipitates are formed.

TABLE 4.2

Results of surface force studies with dodecylamine hydrochloride at different pHs

pH	Conc. of Amine (M)	Surface Potential (Ψ_o) (mV)	Jump Distance (nm)	Pull-off Force (mN/m) ±25	Adsorbed layer Thickness (nm)	Contact Angle (θ) (deg)
5.7	$1x10^{-5}$	-125	7.0	170	0.5-0.7	30
8.0	$1x10^{-6}$	- 125	7.0	170	0.5-0.7	32
9.5	$1x10^{-6}$	-125	7.0	170	0.5-0.7	32
5.7	$3x10^{-6}$	-75	9.0	190	0.5-0.7	45
9.5	$3x10^{-6}$	-75	14.0	190	0.5-0.7	85
10.1	$1x10^{-7}$	-75	7.0	50	0.5	25
10.1	$1x10^{-6}$	-35	9.0	40	0.5-0.7	43
10.1	$2x10^{-6}$	-20	0.0	0	1.5-2	--
10.1	$5x10^{-6}$	-10	0.0	0	3.5-4	75

Obviously, the phase-separated amine is hydrophilic, as indicated by the drop-off in θ above 10^{-4} M DAHCl and by the zero pull-off force above $2x10^{-6}$ M DAHCl. The data shown in Figure 4.7 suggest that the pull-off force is more sensitive than θ to the presence of the hydrophilic precipitate on the surface. Note that above $2x10^{-6}$ M DAHCl, where the adhesion force is zero, the mica surfaces do not jump into contact with each other, suggesting that the surface is not hydrophobic above this concentration. However, the contact angle continues to increase until bulk precipitation occurs. It seems that contact angle is not too sensitive to the small amount of hydrophilic precipitates present on the mica surface.

4.4 Discussion

It has been shown previously that coadsorption of DAH^+ and neutral surfactant on mica results in the formation of close-packed monolayers, which in turn give rise to long-range hydrophobic forces (Chapters 2 and 3; Refs. 13 and 30). With DAHCl alone, only short-range hydrophobic forces are observed with the decay length (D_0) being 1.3 nm. The adsorption is site-specific, while the crystallographic features of the mica surface do not allow formation of closely-packed monolayer of hydrocarbon chains, which is necessary to create long-range hydrophobic forces (Chapter 3; Ref.

30). Each DAH^+ ion occupies the site vacated by the interstitial K^+ ion, which occupies 0.49 nm^2 of the surface. However, the cross-sectional area of the hydrocarbon chain is only 0.20 nm^2; therefore, the adsorption of DAH^+ ions on mica forms only a sparsely-packed monolayer. When a small amount of octanol is added to the mica/DAHCl system, however, the uncharged surfactant molecules adsorb in-between the adsorbed DAH^+ ions, thereby forming a close-packed monolayer of hydrocarbons on mica. Furthermore, the uncharged polar heads, i.e., -OH groups, reduce the electrostatic repulsion between the $-NH_3^+$ groups on the surface, which should increase the adsorption free energy of the DAH^+ ions. Thus, the presence of octanol causes additional adsorption of DAH^+ ions and results in the formation of close-packed monolayers, both of which contribute to creating long-range hydrophobic forces. The D_2 values measured in the presence of DAHCl and octanol are in the range of 4.5-6.8 nm (Chapter 2; Ref. 13). In the presence of dodecanol, D_2 becomes as large as 9.0 nm (Chapter 3; Ref. 30). It has been found that with both octanol and dodecanol the maximum decay lengths are observed when the amount of either of these neutral surfactants is only one-tenth of the DAHCl concentration. Nevertheless, the alcohol-to-DAH^+ ratio in the close-packed mixed monolayer formed on mica may be much larger than 1:10, possibly approximating 1:1. The alcohols May adsorb as iono-molecular complexes, which may have much stronger adsorbability than the DAH^+ ions, because the complex formation is an increase in the effective chain length.

The coadsorption mechanism used to explain the appearance of the long-range hydrophobic force was proposed originally by Gaudin and Fuerstenau (3). These investigators measured water contact angles (θ) on quartz in $4x10^{-5}$ M DAHCl solutions, and found that both θ and the flotability of the mineral increase sharply at pH > 8 and reach maxima at pH 10. The sharp increase was explained by the coadsorption of the neutral amine (DA), formed by *via* reaction [3], and the DAH^+ ions on quartz. In the present work, direct force measurements were conducted with mica surfaces in DAHCl solutions of varying pH and concentration. At pH 5.7, only short-range hydrophobic forces are observed with D_0 values being in the range of 1-2 nm, which are comparable with those reported in the literature (11-13). At pH 9.5, the hydrophobic force becomes stronger, as evidenced by the increase in 'jump' distance from 9 at pH 5.7 to 14 nm (Figure 4.3, Table. II). The measured forces are sufficiently strong that it is necessary to use the double-exponential function (Eq. [2]) with C_1=-40 mN/m, D_1=1.2 nm, C_2=-0.5 mN/m and D_2=5.5 nm. The appearance of the long-range hydrophobic force at pH 9.5 can be attributed to the coadsorption mechanism.

Recently, Rutland *et al.* (12) conducted direct force measurements with mica at varying pHs in the presence 10^{-4} M DAHCl. These authors also observed a stronger attractive hydrophobic force at pH 8-9 than at lower pHs, and attributed it to the coadsorption mechanism.

However, the hydrophobic force measured by these investigators is not as long-ranged as measured in the present work, because the DAHCl concentration used by Rutland *et al* (12) were above the p.c.r. ($=10^{-5}$ M), where DAH+ ions are known to form 'flip-flop' layers on mica (13). Because of the hydrophilic groups presented toward the aqueous phase, the flip-flop layer should be less hydrophobic than the mixed monolayers of DAH^+ and DA formed with normal mode of orientation.

Figure 4.6 shows that at pH 5.7 both θ and the pull-off force increase with increasing DAHCl concentration. When the concentration reaches the p.c.r., however, θ remains constant while the pull-off force increases. At this pH, the concentration of DA species is approximately 5-orders of magnitude lower than that of DAH^+ ions; therefore, the coadsorption mechanism will not occur. As the concentration is increased above p.c.r., DAH^+ ions will start adsorbing on mica with inverse orientation in-between the adsorbed DAH^+ ions that are present on the surface with normal mode of orientation (13,20). This should decrease the hydrophobicity of the mica surface. However, θ remains constant until the concentration reaches the c.m.c. The constant θ between the p.c.r and c.m.c. may be explained as follows. When a DAH^+ ion adsorbs on the surface with inverse orientation, its hydrocarbon tail (more likely the CH_3 group) will provide a shield that can minimize the electrostatic repulsion between two $-NH_3^+$ groups. This will enhance additional adsorption of DAH^+ ions with normal mode of orientation. The surfactant molecule with normal mode of

orientation will increase the hydrophobicity, while the inversely oriented species will decrease the hydrophobicity. The net result is, therefore, that the hydrophobicity remains unchanged as manifested by the θ measurements. On the other hand, the increase in pull-off force with increasing DAHCl concentration between the p.c.r. and the c.m.c. may be attributed to the decrease in the surface roughness. As additional DAH^+ ions adsorb on the mica surface above the p.c.r. owing to the shielding effect, it is necessary that some of the K^+ ions left on the mica surface be removed. This will result in an increase in the surface coverage of the flip-flop layer, which should contribute to a decrease in the surface roughness and, hence, increase the pull-off force. The sharp drop-off of both θ and the pull-off force above the c.m.c. may be attributed to the micellar adsorption, which should render the surface hydrophilic. It has been shown that the micellar adsorption increases the thickness of the adsorbed layer and the force measurement becomes hysteritic (Chapters 2 and 3; Refs 13 and 30).

Figure 4.7 shows that the adhesion force disappears completely when phase-separated amine ($C_{12}H_{25}NH_2(s)$) begins to nucleate on the surface, which should increase the surface roughness. At pH 10.1, bulk precipitation occurs at 10^{-4} M DAHCl; however, the precipitation begins on the surface at $2x10^{-6}$ M most likely due to the concentration gradient across the solid/liquid interface. It is surprising, however, that θ continues to increase above this concentration until the bulk

precipitation occurs. The decrease in θ above the concentration of bulk precipitation strongly suggests that phase-separated amine is hydrophilic. Since there are no reasons for the surface and bulk precipitates to have different surface properties, the surface precipitation should also decrease the contact angle. A possible explanation for this unexpected result may be that the surface precipitation occurs in patches, thereby leaving parts of the mica surface uncovered. Only above the concentration of bulk precipitation, the surface becomes more fully covered by the hydrophilic precipitates and θ begins to decrease as shown in Figure 4.7. The continued increase in contact angle may then be attributed to the increase in the hydrophobicity of the uncovered surface due to the coadsorption mechanism. At pH 10.1, approximately 22.7% of the surfactant molecules exist as neutral molecules, which should contribute to the formation of close-packed monolayer of mixed DAH^+ and DA species and, hence, the increased contact angle.

The direct force measurements conducted at pH 10.1 show that at $H < 20$-30 nm extraneous repulsive forces that cannot be explained by the DLVO theory are observed. A similar result was reported by Rutland *et al* (12) at pH 10.3 and 10^{-4} M DAHCl. The extraneous forces resemble the repulsive forces measured with well-defined water-soluble polymers adsorbed on mica surfaces (27-29). Since these repulsive forces are considered due to steric repulsion between polymer chains, the extraneous forces observed in the present work may also be attributed to the steric force. It is possible

that the steric force is caused by the presence of a polymeric substance, which may be formed before surface precipitation occurs. Laskowski (8) suggested that formation of the dimeric iono-molecular species, i.e., $DAH^{+}\cdot DA$, should also be considered part of the pre-precipitation phenomenon. It should be noted, however, that the formation the polymeric pre-precipitation complex should decrease the net attractive force, which must be detrimental to flotation. This observation is born out from the following results. First, the extraneous forces due to the presence of the pre-precipitation complex are repulsive as shown in Figure 4.3. Second, the adhesion forces measured at pH 10.1 are smaller than at lower pHs by an order of magnitudes as shown in Figure 4.5. Third, the repulsive steric force increases with increasing DAHCl concentration.

There are numerous reports showing good correlation between particle hydrophobicity, as represented usually by water contact angles, and floatability. In general, the higher the contact angle, the higher the flotability of the mineral in question. There are some reports, however, showing that good flotation is achieved when the contact angle is low (33-35). Thus, contact angle may not be the most ideal criterion for flotation. A better flotation criterion may be the hydrophobic force.

Figure 4.8 shows a plot of the decay length (D_1 and D_2) for the hydrophobic forces measured in the present work with the mica surfaces in equilibrium with DAHCl solutions. Also shown are the flotation recoveries of quartz and the water contact angles in $4x10^{-5}$ M DAHCl solutions as reported by Fuerstenau (5). There is an

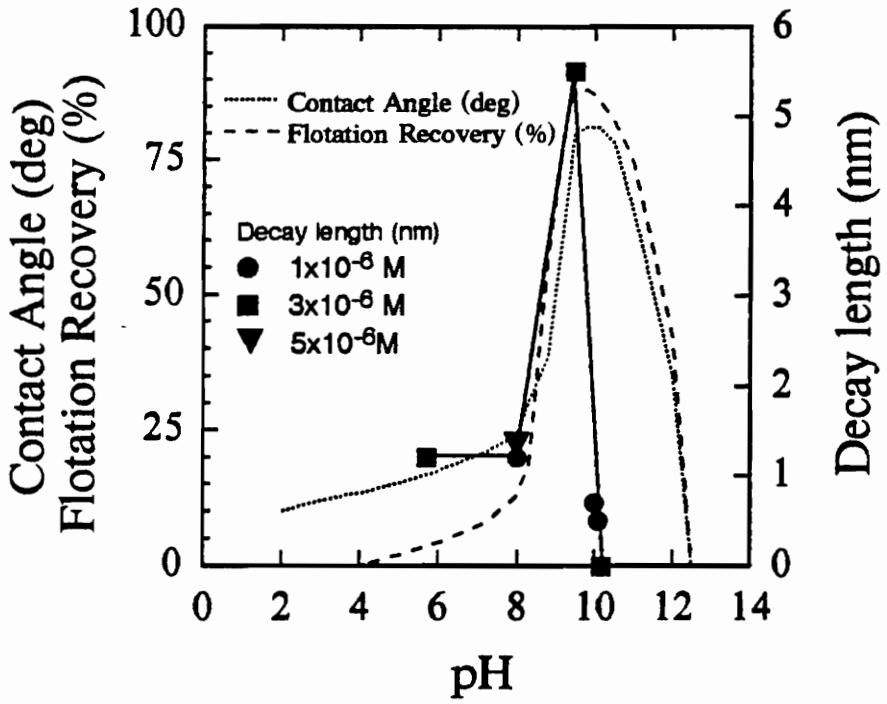

Figure 4.8. Correlation between long-range hydrophobic force parameter (D_2) measured between mica surfaces in the presence of DAHCl, contact angles obtained on quartz in the presence of $4x10^{-5}$ M DAHCl, and floatability of quartz in the presence of $4x10^{-5}$ M DAHCl. An excellent correlation between the force measurements and the flotation data suggest that long-range hydrophobic forces may be required for good flotation

excellent correlation between the data of Fuerstenau (5) and the hydrophobic force constants obtained in the resent work. As shown, the flotation recovery reaches a maximum when long-range hydrophobic forces are observed. Thus, the data shown in Figure 4.8 suggest that long-range hydrophobic force may be necessary for good flotation. The long-range hydrophobic forces can be obtained by a pH control as shown in Figure 4.8; however, one can also create long-range hydrophobic forces by increasing the surfactant concentration at lower pHs or by adding neutral surfactants such as octanol (Chapter 2; Ref. 13) and dodecanol (Chapter 3. Ref. 30).

Another evidence that long-range hydrophobic forces are needed for flotation was also given in Chapter 2 and by Yoon and Ravishankar (13). They showed that at pH 5.7 the flotation recovery of silica is only 20% in 10^{-5} M DAHCl solution. In a solution containing both octanol and DAHCl, however, the flotation recovery was increased to 95%, which can be attributed to the appearance of the long-range hydrophobic force. The direct force measurements conducted with mica in a solution containing $5x10^{-7}$ M octanol and $5x10^{-6}$ M DAHCl gave a long-range hydrophobic force with D_2=6.8 nm. The appearance of the long-range hydrophobic force has been attributed to the coadsorption mechanism in the same manner as discussed for the DAHCl solution in alkaline solutions.

Although mica and quartz are different substrates, there have been close correlations between the surface force measurements conducted with mica and the set

of data, such as contact angle, flotation and ς-potentials, obtained with quartz. The coadsorption mechanism discussed in the foregoing paragraphs seems to apply to both minerals. One reason that the coadsorption mechanism plays an important role in the adsorption of DAH^+ ions on mica is that each surfactant molecule occupies 0.49 nm^2 of the surface vacated by the K^+ ion, while each hydrocarbon chain occupies 0.21 nm^2 in a close-packed monolayer. Thus, the geometric constraints of the mica surface makes it difficult to form a close-packed monolayer without the coadsorption mechanism. For the case of quartz, however, each hydroxyl group occupies only 0.234 nm^2 of the surface (36). Therefore, formation of a close-packed monolayer may not be as difficult as with mica. Nevertheless, not all of the crystallographically possible silanol sites may be charges in alkaline solutions. Healy and White (37) showed that the surface charge density on silica is substantially lower than those on other minerals such as goethite, hematite, alumina and rutile. Therefore, the quartz surface may also have rooms to accommodate neutral molecules to exhibit the coadsorption mechanism. Even if there are enough charge sites available to form a close-packed monolayer, the presence of neutral molecules will greatly enhance the formation of close-packed monolayers by the coadsorption mechanism.

4.5 Conclusions

Direct force measurements have conducted with mica surfaces in DAHCl solutions of varying concentrations and pHs. At $3x10^{-6}$ M and pH 5.7, where the surfactant is in ionized form, i.e., dodecylammonium (DAH^+) ions, only short-range hydrophobic forces with decay length (D_0) of 1.3 nm are measured. The weak hydrophobic forces observed at low pH can be attributed to the difficulty in forming close-packed monolayers on the mica surface. At pH 9.5, where appreciable amount of neutral dodecylamine (DA) is formed as a result of hydrolysis, long-range hydrophobic forces with decay length as large as 5.5 nm are observed. The appearance of the long-range hydrophobic force may be attributed to the coadsorption of DAH^+ and DA on the mica surface, which increases the packing density of hydrocarbon chains on the surface.

The force measurements have been conducted as a function of DAHCl concentration at pH 10.1, which is very close to its pK_a (=10.6). The results showed that the repulsive force decreases with increasing concentration due to increased charge neutralization and hydrophobic force. However, the mica surfaces do not jump into contact when the concentration is above $2x10^{-6}$ M, where phase-separated amine is precipitated on the surface. This concentration is 50-times lower than the concentration where amine precipitation occurs in the bulk solution. That no jump occurs above this

concentration suggests that the precipitate renders the surface hydrophilic. However, contact angle continues to increase beyond the concentration where the surface precipitation occurs, which may be explained by the possibility that the surface precipitation occurs in patches leaving parts of the hydrophobic surface available for three-phase contact. As the surfactant concentration is increased above 10^{-4} M, bulk precipitation occurs and the contact angle decreases. At concentrations below $2x10^{-6}$ M, the repulsive forces that cannot be explained by the DLVO theory are observed at separation distances below 20-30 nm. The force curves pertaining to the extraneous repulsive forces resemble those observed with water-soluble polymers on mica. Therefore, the extraneous repulsive forces may be attributed to the steric repulsion caused by preprecipitation complex(es) which may be in polymeric form.

The decay lengths measured in the present work at 10^{-6}, $3x10^{-6}$ and $5x10^{-6}$ M DAHCl have been plotted as a function of pH and compared with the flotation and contact angle data obtained by Fuerstenau at $4x10^{-5}$ M DAHCl. The pH at which maximum contact angle and flotation recovery are obtained correspond to the pH where long-range hydrophobic force is observed due to the coadsorption mechanism. The excellent correlation between the force measurements and the flotation data suggest that long-range hydrophobic forces may be required for good flotation.

4.6 References

1. Yoon, R.-H., Plenary paper presented at the XVII International Mineral Processing Congress. September 23-28, Dresden, Germany; *Aufbereitungs-technik.* **32,** 474 (1991).
2. Yordan, J., Ph.D. Thesis, Dept. of Mining Eng. Virginia Polytechnic Institute and State University, (1989).
3. Gaudin, A.M., and Fuerstenau, D. W., *Trans AIME.* **202,** 958 (1955).
4. de Bruyn, P. L., *Mining Engg. Trans SME.* **292,** 291 (1955).
5. Fuerstenau, D. W., *Trans AIME.* **208,** 1365 (1957).
6. Somasundaran, P., and Ananthapadmanabhan, K.P.," Solution Chemistry of Surfactants," Ed. Mittal, K. L., **2,** p. 777. Plenum Press. New York. 1979.
7. Laskowski, J.S., Vurdela, R.M., and Liu, Q., *Proc. 16 th Int. Mineral Processing Congress.* (Ed. K.S. Eric Forssberg) 10a, 703 (1988).
8. Laskowski, J.S., "Challenges in Mineral Processing" Ch.2, 15 (1989).
9. Novich, B.E., and Ring, T.A., *Langmuir* **1,** 701 (1985).
10. Smith, R. W., *Trans AIME.* **226,** 427 (1963).
11. Herder, P.C., *J. Colloid Interface Sci.* **134,** 346 (1990).
12. Rutland, M., Waltermo, A., and Claesson, P.M., *Langmuir* **8,** 176 (1992).

13. Yoon, R.-H., and Ravishankar, S. A., *J. Colloid Interface Sci.* **166,** 215 (1994).

14. Pashley, R.M., McGuiggan, P.M., Ninham, B.W. and Evans, D.F., *Science* **229,** 1088 (1985).

15. Parker, J.L., Cho, D.L., and Claesson , P.M., *J. Phys. Chem.* **93,** 6121 (1989).

16. Tsao, Y, Yang, S.X., Evans, D.F..and Wennerstrom, H., *Langmuir* **7,** 3154 (1991).

17. Christenson, H.K., Fang, J., Ninham, B. W., Parker, J.L., *J. Phys. Chem.* **94,** 8004 (1990).

18. Claesson, P.M., and Christenson, H.K., *J. Phys. Chem.* **92,** 1650 (1988).

19. Christenson, H.K., Claesson, P.M., Berg, J., Herder, P.M., *J. Phys. Chem.* **93,** 1472 (1989).

20. Chen, Y.L., Chen, S., Frank, C., and Israelachvili, J.N., *J. Colloid Interface Sci.* **153,** 244 (1992).

21. Tabor, D., and Winterton, R.H.S., *Proc. R. Soc. London,* A **312,** 435, (1969).

22. Israelachvili, J.N., and Adams, G.E., *J. Chem. Soc., Faraday Trans. 1* **74,** 975 (1978).

23. Tolanski, S., *An Introduction to Interferometry* 2nd Ed. John Wiley. (1973).

24. Chan, D.Y.C., Pashley, R.M., and White, L.R., *J. Colloid Interface Sci.* **77,** 283 (1980).

25. Johnson, K.L., Kendall, K., and Roberts.A.D., *Proc. R. Soc London A* **324,** 301 (1971).

26. Muller, V.M, Yushchenko, V.S., Derjaguin,B.V., *J. Colloid Interface Sci.* **77,** 283 (1980).

27. Claesson, P. M., and Ninham, B. W., *Langmuir* **8,** 1406 (1992).

28. Luckham, P. F., and Klein, J., *J. Chem. Soc., Faraday Trans. 1* **80,** 865 (1984).

29. Malmsten, M., and Claesson, P. M., *Langmuir* **7,** 988 (1991).

30. Ravishankar, S. A., and Yoon, R.-H., To be published.

31. Wakamatsu, T., and Fuerstenau, D. W., *Trans AIME,* **254,** 123 (1973).

32. Kekicheff. P., Christenson, H. K., and Ninham, B.W. *Colloids Surf.* **40,** 31 (1989).

33. Iwasaki, I., Cooke, S. R. B., and Kim, Y. S., *Trans AIME*, **223,** 113 (1962).

34. Lai, R. W. M., and Smith, R. W., *Trans AIME*, **235,** 413 (1966).

35. Finch, J. A., and Smith, R. W., *Trans IMM.* **81,** C213 (1972).

36. Iler. K. R., "The Colloid Chemistry of Silica and Silicates" NewYork. (1955).

37. Healy, T. W., White, L. R., *Adv. Colloid and Interface Science* **9,** 303 (1978).

CHAPTER 5: CONCLUSIONS

The major findings of the present investigation are summarized as follows:

1) Mica surfaces in dodecylammonium chloride (DAHCl) solutions at pH 5.7 exhibit relatively "short-range" hydrophobic forces with decay lengths in the 1-2 nm range, which are constant with the results reported in the literature by other investigators. That only short-range hydrophobic forces are observed can be attributed to the geometrical constraints of the mica surface that cannot allow formation of close-packed monolayers of single chain cationic surfactants.

2) In the presence of small amount of neutral surfactants such as octanol, the mica surfaces exhibit long-range hydrophobic forces with decay lengths as large as 4.5 nm. Appearance of the long-range hydrophobic force can be explained by the coadsorption mechanism of Gaudin and Fuerstenau, which suggests that hemimicelles are formed on the surface. The hemimicellization represents a patch-wise adsorption process, in which the free energy of adsorption becomes maximum when hydrocarbon chains form clusters.

3) When dodecanol is used as a coadsorbing neutral surfactant, even longer-range hydrophobic hydrophobic forces are observed with the decay lengths becoming as large as 9.0 nm. The longer-chain alcohols may result in the formation of larger hemimicelles, in which hydrocarbon chains are more closely packed and the hydrocarbon chains display a higher degree of ordering.

4) The coadsorption mechanism have two important consequences; i) hydrocarbon chains will have a higher packing density, and ii) additional dodecylammonium (DAH^+) ions adsorb on the mica surface, both contributing to the increase in hydrophobic force. The additional adsorption of the DAH^+ ions can be attributed to the hydrocarbon chain association and a decreased electrostatic repulsion between the polar heads of the neighboring cationic species. Evidence for the additional DAH^+ ion adsorption is given by the decrease in negative surface potential of the mica surface in the presence of octanol and dodecanol.

5) The floatability of silica in DAHCl solutions of pH 5.7 increases substantially in the presence of octanol, which can be attributed to the long-range hydrophobic forces created as a result of the coadsorption mechanism.

6) Mica surfaces in equilibrium with a $3x10^{-6}$ M DAHCl solutions exhibit a long-range hydrophobic force with a decay length of 5.5 nm when the pH is raised to 9.5. The appearance of the long-range hydrophobic force can be attributed to the coadsorption of DAH^+ ions and the neutral dodecylamine (DA) molecules on mica. The latter is produced as a result of hydrolysis, and its concentration reaches a maximum at pH close to its *pKa* (=10.6).

7) Appearance of the long-range hydrophobic force at pH 9.5 may be related to the maximum flotation of quartz observed at the same pH. The close correlation between the pH of long-range hydrophobic force and the maximum flotation of quartz suggest that long-range hydrophobic force is required for good flotation.

8) At pH 10.1, the mica surfaces in DAHCl solutions do not jump into contact and the adhesion forces become zero at concentrations above $2x10^{-6}$ M. Furthermore, the thickness of the adsorbed layer is significantly increased. These findings suggest that phase-separated amine is formed above this concentration, which is 50-times lower than the concentration (10^{-4} M) for bulk precipitation.

9) That mica surfaces do not jump into contact above $2x10^{-6}$ M indicates that the surface precipitation renders the mica surface hydrophilic. However, the water contact angle continues to increase above this concentration, which suggests that surface precipitation occurs in patches leaving parts of the hydrophobic surface available for three-phase contact. The contact angle decreases sharply above 10^{-4} M, indicating that phase-separated amine is hydrophilic.

10) At 10.1, which is very close to the pK_a of DAHCl, mica surfaces exhibit non-DLVO repulsive forces that resemble those measured in water-soluble polymers adsorbed on mica. Therefore, the extraneous repulsive forces may be attributed to the steric repulsion caused by pre-precipitation complexes which may be in polymeric form.

11) The decay lengths of the hydrophobic forces measured in the present work and reported in the literature have been plotted vs. advancing contact angles (θ_a). The result show that the decay length increases sharply at θ_a>90°.

12) The appearance of the long-range hydrophobic forces at θ_a>90° may be attributed to the possible changes in orientation of the hydrocarbon chains. There are

evidences that the hydrocarbon chains of the adsorbs species begin to stand-up vertically at $\theta_a \approx 90°$, forming a close-packed monolayer with the CH_3 groups in contact with the aqueous phase. That CH_3 groups are more hydrophobic may provide an explanation for the appearance of the long-range hydrophobic force at $\theta_a > 90°$.

13) Presentation of an ordered array of CH_3 groups toward the aqueous phase may cause a unipolar orientation of in-plane dipoles of water molecules in the vicinity. Since the adsorption of DAH^+ ions may occur in patches (or domains), the unipolar orientation may give the domains large dipole moments (or possibly charges), which in turn correlate with the large dipoles of the opposing surface to give rise to long-range hydrophobic forces.

14) Thermodynamically, cavitation should occur on or near hydrophobic surfaces whose water contact angles are greater than 90°. Therefore, the appearance of long-range hydrophobic forces at $\theta_a > 90°$ may also be attributed to the cavitation mechanism. However, no one has yet observed *macroscopic cavities* during the approach cycles of force measurements possibly because of the large activation energies involved. It is possible, nevertheless, that *microscopic cavitation* could occur on the hydrophobic domains, which is occupied by close-packed hydrocarbons, and whose microscopic contact angles can satisfy the thermodynamic criterion for cavitation.

15) The subcritical cavitation due to density fluctuations may be useful for explaining the origin of hydrophobic forces; however, it cannot explain the appearance of long-range hydrophobic force at $\theta_a > 90°$ because the theory predicts monotonical changes in hydrophobic force with contact angle.

CHAPTER 6 RECOMMENDATIONS FOR FUTURE RESEARCH

The following areas of research are recommended based on the present study:

1) The origin of hydrophobic force is one of the most debated issues in the direct force measurements literature. It has been proposed in the present study that the long-range hydrophobic force measured between amine coated monolayer is due to the molecular ordering of hydrocarbon chains as a result of coadsorption of nonionic alcohol molecules. The coadsorption of neutral alcohol molecules may produce weel ordered hydrocarbon domains which in turn may correlate electrostatically with those of the opposing surface to give rise to long-range hydrophobic forces. Preliminary studies on the mixed monolayers using FTIR and AFM studies indicated that ordering takes place as a result of coadsorption. More systematic investigations are needed using FTIR and AFM to show the changes in hydrocarbon ordering and morphology of the monolayer with DAHCl in the presence of long-chain alcohols of different chain lengths and correlate these results with the appearance of long-range hydrophobic forces in the present work.

2) It has been shown in the present study that the long-range hydrophobic force can be measured by coadsorbing dodecanol even when they are 50 times lower than the DAHCl concentration. In spite of low bulk concentration, it is possible

that the surface concentration of dodecanol may be comparable to the adsorbed dodecylammonium ions due to coadsorption mechanism. It will be interesting to conduct some adsorption studies to find out the amount of dodecylammonium ions and long-chain alcohol molecules at the surface. For this purpose, a radio active long-chain alcohol, labeled with O^{18} atom, will be used as the coadsorbing agent. By counting the surface radio activity, it should be possible to find out adsorption density of alcohol molecules on the surface. Knowing the total adsorption density of the hydrocarbons, one can find out the adsorption density of alcohol and dodecylammonium ions. This may give some idea about the role of long-chain alcohol in forming hydrocarbon domains.

3) Long-range hydrophobic forces measured between insoluble surfactant coated monolayers increase in the presence of gas molecules in the water interlayer. It has been suggested that the presence of gas molecules may enhance the cavitation between the hydrophobic surfaces, which is considered to occur between hydrophobic surfaces with $\theta_a > 90°$. However, it is not clear if gas molecules have the same effect on short-range hydrophobic forces measured between surfaces with θ_a less than 90°. Therefore, it would be interesting to investigate the role soluble gases, such as argon in water, on hydrophobic forces between mica surfaces coated with amine and amine/alcohol monolayers.

4) The results presented in this work were mainly between symmetrically hydrophobized surfaces with soluble amine surfactant. However, in order to study the bubble-particle interaction, it is important obtain the hydrophobic force parameters for asymmetric interaction. In order to obtain this information two types of studies are needed; one, involving direct force measurements between a hydrophobic solid and a negatively charged hydrophilic solid such as silica in the presence of amine and the other using a very recently developed direct force measurement technique between a bubble and a silica particle in the presence of amine.

VITAE

Ravishankar was born in Salem, a small town in the southern part of India. He completed his high school in 1978 and his college degree from Roorkee University in 1983. He then enrolled himself at Indian Institute of Technology, Kanpur for a masters programme in Metallurgical engineering. After finishing his masters program in 1985, he worked for the Tata Research Development and Design Center, Pune, a leading private R & D research organization in India, for four years. In Fall 1990, he enrolled in a Ph.D program at Virginia Polytechnic Institute and State University, Blacksburg. Virginia.

He has to his credit seven journal publications and two additional papers which are to be published shortly. He won the Hargopal memorial award for academic excellence during his masters programme and Outstanding graduate student award during his Ph.D programme. He has accepted an offer as a Scientist, R & D Division, at Nord Technical Center, Jeffersonville, GA.